東京大學

地震研究所彙報

第27號　第1～4册

昭和24年1～12月

目　次

論文及報告　　頁

1. 彈性波發生の問題における境界條件（英文）……佐藤泰夫 1
2. 粒狀物體を傳はる彈性波の理論（I）（英文）……高橋健人・佐藤泰夫 11
3. 地球內部の溫度分布について（英文）……武者力 17
4. 有珠火山地變地域における地磁氣測量（英文）……越川善明 21
5. 地震斷層の運動（其一）（福井斷層及び其他）（英文）……那須信治 27
6. 油壺に於ける地殼變動の觀測　第二報（英文）……萩原武雄・笠原常重・松沢一平 35
7. 油壺に於ける地殼變動の觀測　第三報（英文）……萩原武雄・笠原常重・松沢一平 39
8. 四國足摺岬の花崗岩類（II）（英文）……森本良平 45
9. 地震動の尾部について（其の4）（英文）……表俊一郎 49
10. 關東大地震による横濱市內の震害分布（英文）……表俊一郎 57
11. 横濱市內の震害分布と地盤との關係（英文）……表俊一郎 63
12. 振り振子を應用した低域濾波器による地震波の研究（英文）……秋間哲夫 69
13. 土地の脈動の傳播に關する研究（英文）……池上良平・岸上多彦 75
14. 脈動による建物の振動について（英文）……池上良平 81
15. 建築土木材料の內部摩擦係數の測定（其の一）（英文）……下鶴大輔 85
16. 實在建物の振動實診結果（英文）……金井清・田中貞二・鈴木富三郎 91
17. 非木造建物の震害と地盤の性質との關係（英文）……金井清 97
18. 土壤層の彈性的性質に關する野外測定（其の一）（英文）……那須信治 101
19. 最近の磐山火山爆發の調査概報（英文）……村山毅平・森本良平・津屋弘逵 107
20. 新潟縣磐山火山噴氣孔で採集された水酸化硫酸アルミニユム鑛物（英文）……津屋弘逵・市村俊明・白井俊明 115
21. 磐山火山の 1949 年の小活動（英文）……佐久間修・水上武 117
22. 有珠火山の最近の活動（III）　爆發的噴火の期間に發生した地震（英文）水上武 123
23. 有珠火山の最近の活動（IV）　熔岩丘の成長に伴つた地震（英文）……水上武 129
24. 北海道有珠昭和新山の噴氣孔ガス及び昇華物（英文）……津屋弘逵・白井俊明 135
25. 米代川にそう一部水準路線の測量（第二報）（邦文）……宮村攝三・岡田惇 141

所　報

本彙報ハ年4回（但シ第1號ヨリ第6號マデハ不定期ニ，第7號ハ3冊トシテ發行セリ），彙報別冊ハ不定期ニ發行ス．

本彙報掲載ノ論文及ビ報告ノ内容ニ關シテハ著者ノミニ其責任アルモノトス．

本彙報ニ關スル照會通信ハ東京大學地震研究所長ヘ宛テラレタシ．

The Bulletin is published quarterly. (Vols. I-VI were published at irregular intervals and Vol. VII consisted of three parts.)
Supplementary Volume is published at irregular interval.

The authors of the papers alone are responsible for the statements and opinions contained in their respective papers.

All communications relating to this Bulletin should be addressed to the Director of the Earthquake Research Institute, Tokyo University.

1. *Boundary Conditions in the Problem of Generation of Elastic Waves.*

By Yasuo SATÔ,

Earthquake Research Institute.

(Read Dec. 17, 1946.—Received Feb. 14, 1947.)

The problem of generation of elastic waves attracted the interest of many seismologists in our country, and a number of excellent papers are published[1]. But in these works, boundary conditions are not without some restriction. In this paper we will take up this point and show how to remove this restriction and give the boundary condition in a most general form.

The equation of motion of the elastic solid in spherical polar coordinates (R, θ, φ) are written in the following form.....

$$\begin{cases} \rho\dfrac{\partial^2 u}{\partial t^2}=(\lambda+2\mu)\dfrac{\partial\Delta}{\partial R}-\dfrac{2\mu}{R\sin\theta}\dfrac{\partial}{\partial\theta}(\omega_\varphi\sin\theta)+\dfrac{2\mu}{R\sin\theta}\dfrac{\partial\omega_\theta}{\partial\varphi} \\ \rho\dfrac{\partial^2 v}{\partial t^2}=(\lambda+2\mu)\dfrac{1}{R}\dfrac{\partial\Delta}{\partial\theta}-\dfrac{2\mu}{R\sin\theta}\dfrac{\partial\omega_R}{\partial\varphi}+\dfrac{2\mu}{R}\dfrac{\partial(R\omega_\varphi)}{\partial R} \\ \rho\dfrac{\partial^2 w}{\partial t^2}=(\lambda+2\mu)\dfrac{1}{R\sin\theta}\dfrac{\partial\Delta}{\partial\varphi}-\dfrac{2\mu}{R}\dfrac{\partial(R\omega_\theta)}{\partial R}+\dfrac{2\mu}{R}\dfrac{\partial\omega_R}{\partial\theta} \end{cases} \quad \cdots\cdots(1)$$

where

ρ ..... density

λ, μ ..... Lamé's elastic constants

u, v, w .. radial, colatitudinal and azimuthal components of displacement

ω_R, ω_θ, ω_φ .. components of rotation

Δ ..... volume dilatation

If we denote the displacement vector by $\mathfrak{D}$, we can write

$$\mathfrak{D}={}_0\mathfrak{D}+{}_1\mathfrak{D}+{}_2\mathfrak{D} \quad \cdots\cdots(2)$$

---

1) K. SEZAWA, *Bull, Earthq. Res. Inst.*, **2** (1927). **17**; **10** (1932), 299. *Sindôgaku* (1932) 653.

H. KAWASUMI, *Bull. Earthq. Res.*, **11** (1933), 403.

H. KAWASUMI and R. YOSHIYAMA, *Disin*, **7** (1935), 367.

W. INOUE, *Bull. Earthq. Res. Inst.*, **14** (1936), 582; **15** (1937), 90, 674, 686, 956; **16** (1938), 597.

S. SYÔNO, *Geophys. Mag.*, **9** (1935) 285; **12** (1937) 83; **13** (1938) 1.

where

$$\begin{cases} {}_0\mathfrak{D}=\text{grad}\,\Phi \\ {}_1\mathfrak{D}=\text{rot}\,({}_1\Psi,\ 0,\ 0) \\ {}_2\mathfrak{D}=\text{rot rot}\,({}_2\Psi,\ 0,\ 0) \end{cases} \quad \cdots\cdots(3)$$

Using these notations we can write the solutions of the equations of motion as follows (omitting the time factor $\exp(ipt)$) :—

$$\begin{cases} \Phi=f(hR)\bar{P}_n^m(\cos\theta)(A\cos m\varphi+A'\sin m\varphi) \\ {}_1\Psi=Rg(kR)\bar{P}_n^m(\cos\theta)(B\cos m\varphi+B'\sin m\varphi) \\ {}_2\Psi=Rg(kR)\bar{P}_n^m(\cos\theta)(C\cos m\varphi+C'\sin m\varphi) \end{cases} \quad \cdots\cdots(4)$$

where $\begin{cases} \bar{P}_n^m(\cos\theta)\cdots\cdots\text{associated Legendre function by Ferrer's definition} \\ f(hR)=(hR)^{-\frac{1}{2}}H^{(2)}_{n+1/2}(hR) \\ g(kR)=(kR)^{-\frac{1}{2}}H^{(2)}_{n+1/2}(kR) \\ h^2=p^2\rho/(\lambda+2\mu),\quad k^2=p^2\rho/\mu \end{cases} \quad \cdots\cdots(5)$

From (2), (3) and (4), we get

$$\begin{cases} u=\left\{A\dfrac{df}{dR}+C\dfrac{n(n+1)}{R}g\right\}\bar{P}_n^m(\cos\theta)\cos m\varphi \\ \quad+\left\{A'\dfrac{df}{dR}+C'\dfrac{n(n+1)}{R}g\right\}\bar{P}_n^m(\cos\theta)\sin m\varphi \\ v=\left[\left\{A\dfrac{f}{R}+C\dfrac{1}{R}\dfrac{d(Rg)}{dR}\right\}\dfrac{d}{d\theta}\bar{P}_n^m(\cos\theta)+B'mg\dfrac{1}{\sin\theta}\bar{P}_n^m(\cos\theta)\right]\cos m\varphi \\ \quad+\left[\left\{A'\dfrac{f}{R}+C'\dfrac{1}{R}\dfrac{d(Rg)}{dR}\right\}\dfrac{d}{d\theta}\bar{P}_n^m(\cos\theta)-Bmg\dfrac{1}{\sin\theta}\bar{P}_n^m(\cos\theta)\right]\sin m\varphi \\ w=\left[m\left\{A'\dfrac{f}{R}+C'\dfrac{1}{R}\dfrac{d(Rg)}{dR}\right\}\dfrac{1}{\sin\theta}\bar{P}_n^m(\cos\theta)-Bg\dfrac{d}{d\theta}\bar{P}_n^m(\cos\theta)\right]\cos m\varphi \\ \quad+\left[-m\left\{A\dfrac{f}{R}+C\dfrac{1}{R}\dfrac{d(Rg)}{dR}\right\}\dfrac{1}{\sin\theta}\bar{P}_n^m(\cos\theta)-B'g\dfrac{d}{d\theta}\bar{P}_n^m(\cos\theta)\right]\sin m\varphi \end{cases} \quad (6)$$

Now, putting

$$\begin{cases} \mathfrak{A}\equiv A\dfrac{df}{dR}+C\dfrac{n(n+1)}{R}g, & \mathfrak{A}'\equiv A'\dfrac{df}{dR}+C'\dfrac{n(n+1)}{R}g \\ \mathfrak{C}\equiv A\dfrac{f}{R}+C\dfrac{1}{R}\dfrac{d(Rg)}{dR}, & \mathfrak{C}'\equiv A'\dfrac{f}{R}+C'\dfrac{1}{R}\dfrac{d(Rg)}{dR} \\ \mathfrak{B}\equiv Bg, & \mathfrak{B}'\equiv B'g \end{cases} \quad \cdots\cdots(7)$$

we obtain

$$\begin{cases} u=\mathfrak{A}\,P_n^m\cdot\cos m\varphi+\mathfrak{A}'\,P_n^m\cdot\sin m\varphi \\ v=\left[\mathfrak{C}\dfrac{d}{d\theta}P_n^m\cdot+\mathfrak{B}'m\dfrac{1}{\sin\theta}P_n^m\right]\cos m\varphi \\ \quad+\left[\mathfrak{C}'\dfrac{d}{d\theta}P_n^m-\mathfrak{B}'m\dfrac{1}{\sin\theta}P_n^m\right]\sin m\varphi \\ w=\left[\mathfrak{C}'m\dfrac{1}{\sin\theta}P_n^m-\mathfrak{B}\dfrac{d}{d\theta}P_n^m\right]\cos m\varphi \\ \quad+\left[-\mathfrak{C}m\dfrac{1}{\sin\theta}P_n^m-\mathfrak{B}'\dfrac{d}{d\theta}P_n^m\right]\sin m\varphi \end{cases} \quad\cdots\cdots(8)$$

where P_n^m means $\bar{P}_n^m(\cos\theta)$.

Hitherto, the boundary-value problems, in which the displacements are given on the spherical surface $R=a$, have, on account of the forms of expressions in (8), always been introduced in the following scheme[2].

$$\begin{cases} u=D\cdot\bar{P}_n^m(\cos\theta)\cdot\cos m\varphi \\ v=w=0 \end{cases} \quad\cdots\cdots(9)$$

or

$$\begin{cases} u=0 \\ v=Em\dfrac{1}{\sin\theta}\bar{P}_n^m(\cos\theta)\cdot\cos m\varphi \\ w=-Em\dfrac{d}{d\theta}\bar{P}_n^m(\cos\theta)\cdot\sin m\varphi \end{cases} \quad\cdots\cdots(10)$$

But these are very unsatisfactory, because in the expression (9) v and w are both zero, and in (10) v and w must satisfy some definite relation, which made us unable to give v and w both arbitrarily. This fact is clearly pointed out by Mr. S. Honma in his initial-value problem[3]. In this paper we will study how to remove this defect, and give the displacement u, v and w all arbitrary on the spherical surface $R=a$.

Now, we assume

$$u=U(\theta,\varphi),\quad v=V(\theta,\varphi),\quad w=W(\theta,\varphi) \quad\cdots\cdots(11)$$

on the surface $R=a$ and will show that the coefficients A, A', B, B', C, C'

2) S. Syôno, *loc. cit.* (1) second paper.
H. Kawasumi and R. Yoshiyama, *loc. cit.*
W. Inoue, *loc. cit.*
S. Honma, *Kensin Ziho*, **12** (1942), 106.

3) *loc, cit.* (2)

are uniquely determined, if certain conditions are satisfied which enable us the following treatment.

First, expand $U(\theta, \varphi)$, $V(\theta, \varphi)$, $W(\theta, \varphi)$ into Fourier series

$$\begin{cases} U(\theta,\varphi)=\sum_m U^m(\cos\theta)\cos m\varphi+\sum_m U^{m'}(\cos\theta)\sin m\varphi \\ V(\theta,\varphi)=\sum V^m(\cos\theta)\cos m\varphi+\sum V^{m'}(\cos\theta)\sin m\varphi \\ W(\theta,\varphi)=\sum W^m(\cos\theta)\cos m\varphi+\sum W^{m'}(\cos\theta)\sin m\varphi \end{cases} \quad \cdots\cdots(12)$$

Comparing the expressions (12) with the generalized forms of (8) (in which $\mathfrak{A}$, $\mathfrak{A}'$ etc. are respectively replaced by $\sum_m\sum_n \mathfrak{A}_n^m$, $\sum_m\sum_n \mathfrak{A}_n^{m'}$, etc. and equating the corresponding right hand sides of the two sets of equations respectively, we have

$$\begin{cases} \sum_n \mathfrak{A}_n^m P_n^m = U^m(\cos\theta) & \cdots\cdots(13\cdot1) \\ \sum \mathfrak{A}_n^{m'} P_n^m = U^{m'}(\cos\theta) & \cdots\cdots(13\cdot2) \\ \sum\left(\mathfrak{C}_n^m \dfrac{d}{d\theta}P_n^m+\mathfrak{B}_n^{m'} m\dfrac{1}{\sin\theta}P_n^m\right)=V^m(\cos\theta) & \cdots\cdots(13\cdot3) \\ \sum\left(\mathfrak{C}_n^{m'} \dfrac{d}{d\theta}P_n^m-\mathfrak{B}_n^m m\dfrac{1}{\sin\theta}P_n^m\right)=V^{m'}(\cos\theta) & \cdots\cdots(13\cdot4) \\ \sum\left(\mathfrak{C}_n^{m'} m\dfrac{1}{\sin\theta}P_n^m-\mathfrak{B}_n^m \dfrac{d}{d\theta}P_n^m\right)=W^m(\cos\theta) & \cdots\cdots(13\cdot5) \\ \sum\left(-\mathfrak{C}_n^m m\dfrac{1}{\sin\theta}P_n^m-\mathfrak{B}_n^{m'} \dfrac{d}{d\theta}P_n^m\right)=W^{m'}(\cos\theta) & \cdots\cdots(13\cdot6) \end{cases}$$

$\mathfrak{A}_n^m$ and $\mathfrak{A}_n^{m'}$ are directly obtained from (13.1) and (13.2) by using the orthogonality of P_n^m functions.

$$\begin{cases} \mathfrak{A}_n^m=\dfrac{2n+1}{2}\dfrac{(n-m)!}{(n+m)!}\displaystyle\int_{-1}^{1} U^m(\cos\theta)\,\bar{P}_n^m(\cos\theta)\,d(\cos\theta) \\ \mathfrak{A}_n^{m'}=\dfrac{2n+1}{2}\dfrac{(n-m)!}{(n+m)!}\displaystyle\int_{-1}^{1} U^{m'}(\cos\theta)\,\bar{P}_n^m(\cos\theta)\,d(\cos\theta) \end{cases} \quad \cdots\cdots(14)$$

Next, we will consider the other unknowns. $\mathfrak{C}_n^m$ and $\mathfrak{B}_n^{m'}$ are involved only in (13.3) and (13.6), and $\mathfrak{C}_n^{m'}$ and $\mathfrak{B}_n^m$ in (13.4) and (13.5). So, we will at first take up (13.4) and (13.5).

Multiplying $\sin\theta$ on both sides of (13.5) and then operating $\dfrac{d}{d\theta}$, we get

$$\sum_n \left(\mathfrak{C}_n^{m'} m \frac{d}{d\theta} P_n^m - \mathfrak{B}_n^m \frac{d}{d\theta} \left\{ \sin\theta \frac{d}{d\theta} P_n^m \right\} \right) = \frac{d}{d\theta} \{ \sin\theta W^m \} \quad \text{.....(15)}$$

Then multiplying $-m$ on the expression (13.4) and adding to (15)

$$\sum \mathfrak{B}_n^m \left(-\frac{d}{d\theta} \left\{ \sin\theta \frac{d}{d\theta} P_n^m \right\} + m^2 \frac{1}{\sin\theta} P_n^m \right) = \frac{d}{d\theta} \{ \sin\theta W^m \} - mV^m$$

or

$$\sum -\mathfrak{B}_n^m \sin\theta \left(\frac{d^2}{d\theta^2} P_n^m + \cot\theta \frac{d}{d\theta} P_n^m - m^2 \frac{1}{\sin^2\theta} P_n^m \right)$$

$$= \frac{d}{d\theta} \{ \sin\theta W^m \} - mV^m \quad \text{.....(16)}$$

On the other hand, associated Legendre function P_n^m satisfies the following differential equation with respect to θ

$$\frac{d^2}{d\theta^2} \bar{P}_n^m(\cos\theta) + \cot\theta \frac{d}{d\theta} \bar{P}_n^m(\cos\theta) + \left\{ n(n+1) - \frac{m^2}{\sin^2\theta} \right\} \bar{P}_n^m(\cos\theta) = 0 \text{...(17)}$$

Introducing (17) into (16), and dividing both sides by $\sin\theta$, we get

$$\sum n(n+1) \mathfrak{B}_n^m P_n^m = \frac{1}{\sin\theta} \frac{d}{d\theta} \{ \sin\theta W^m \} - mV^m \quad \text{.....(18)}$$

From this expression we can easily determine $\mathfrak{B}_n^m$, as we determined $\mathfrak{A}_n^m$ from (13.1). Namely,

$$\mathfrak{B}_n^m = \frac{2n+1}{2n(n+1)} \frac{(n-m)!}{(n+m)!} \int_{-1}^{1} \left[\frac{1}{\sin\theta} \frac{d}{d\theta} \{ \sin\theta W^m(\cos\theta) \} \right.$$

$$\left. - mV^{m'}(\cos\theta) \right] \cdot \bar{P}_n^m(\cos\theta) \, d(\cos\theta) \quad \text{.....(19)}$$

By the similar manner we may get $\mathfrak{C}_n^{m'}$. The result is as follows:

$$\mathfrak{C}_n^{m'} = -\frac{2n+1}{2n(n+1)} \frac{(n-m)!}{(n+m)!} \int_{-1}^{1} \left[\frac{1}{\sin\theta} \frac{d}{d\theta} \{ \sin\theta V^{m'}(\cos\theta) \} \right.$$

$$\left. - mW^m(\cos\theta) \right] \cdot \bar{P}_n^m(\cos\theta) \, d(\cos\theta) \quad \text{.....(20)}$$

Using the above solutions we can obtain $\mathfrak{B}_n^{m'}$, $\mathfrak{C}_n^m$ easily; if we substitute $\mathfrak{C}_n^m$, $-\mathfrak{B}_n^{m'}$ and V^m, $-W^{m'}$ in place of $\mathfrak{C}_n^{m'}$, $\mathfrak{B}_n^m$ and $V^{m'}$, W^m respectively, then the expression (13.4) changes to (13.3), and (13.5) to (13.6). Therefore the unknowns $\mathfrak{B}_n^{m'}$, $\mathfrak{C}_n^m$ are at once obtained from the expressions (19) and (20) by applying the above substitution.

$$\mathfrak{B}_n^{m'} = \frac{2n+1}{2n(n+1)} \frac{(n-m)!}{(n+m)!} \int_{-1}^{1} \left[\frac{1}{\sin\theta} \frac{d}{d\theta} \{ \sin\theta W^{m'}(\cos\theta) \} \right.$$

$$\left. + mV^m(\cos\theta) \right] \cdot \bar{P}_n^m(\cos\theta) \, d(\cos\theta) \quad \text{.....(21)}$$

$$\mathfrak{C}_n^m=\frac{2n+1}{2n(n+1)}\frac{(n-m)!}{(n+m)!}\int_{-1}^{1}\left[\frac{1}{\sin\theta}\frac{d}{d\theta}\{\sin\theta V^m(\cos\theta)\}\right.$$
$$\left.+mW^{m'}(\cos\theta)\right]\cdot\bar{P}_n^m(\cos\theta)d(\cos\theta) \quad \cdots\cdots(22)$$

Thus the quantities $\mathfrak{A}_n^m$, $\mathfrak{A}_n^{m'}$ etc. are all solved explicitly. And the next step to be taken is to obtain A_n^m, $A_n^{m'}$ etc. But this is very simple.

Solving (7) with respect to A, A' etc. we have at once

$$\begin{cases} A=\left\{\frac{1}{R}\frac{d(Rg)}{dR}\mathfrak{A}-\frac{n(n+1)}{R}g\mathfrak{C}\right\}\Big/D \\ A'=\left\{\frac{1}{R}\frac{d(Rg)}{dR}\mathfrak{A}'-\frac{n(n+1)}{R}g\mathfrak{C}'\right\}\Big/D \\ C=\left\{-\frac{f}{R}\mathfrak{A}+\frac{df}{dR}\mathfrak{C}\right\}\Big/D \\ C'=\left\{-\frac{f}{R}\mathfrak{A}'+\frac{df}{dR}\mathfrak{C}'\right\}\Big/D \\ B=\frac{1}{g}\mathfrak{B} \\ B'=\frac{1}{g}\mathfrak{B}' \end{cases} \quad \cdots\cdots(23)$$

where

$$D=\begin{vmatrix} \frac{df}{dR} & \frac{n(n+1)}{R} \\ \frac{f}{R} & \frac{1}{R}\frac{d(Rg)}{dR} \end{vmatrix} \quad \cdots\cdots(24)$$

and all R_s' involved in the above expressions are substituted by a after the differentiation is performed. (The affixes m and n are abridged for brevity.)

In this way, the values of A, A' etc. are uniquely determined when we give the values of u, v, w on the spherical surface by the expression (11), so long as the operations so far performed are permissible. This fact means that the boundary-value problem given on the spherical surface is completely solved.

Initial-value problem in the theory of elastic waves, studied by Mr. S. Honma, is in its essential part, equivalent to the above problem. If the initial displacements are given by

$$u_0=U_0(R,\theta,\varphi),\quad v_0=V_0(R,\theta,\varphi),\quad w_0=W_0(R,\theta,\varphi) \quad \cdots\cdots(25)$$

and the functions U_0, V_0, W_0 are expressed by the integral form such as

$$U_0(R,\theta,\varphi)=\int F(R;s)U(s;\theta,\varphi)ds \quad \cdots\cdots(26)$$

which are uniformly convergent with respect to R, then we may treat the integrand by nearly equal manner with U^m, $U^{m'}$ etc. of (13) and integrate with respect to s.

In the potential theory there are two types of problems; one is that of Dirichlet and the other is that of Neumann. In the former case potential is given on some closed surface, and in the latter, normal derivative is given. In the theory of elastic waves, however, it has little meaning to give displacement potential on the surfaces. In the above theory so far shown, displacement components were given on the spherical surface, that is to say the first derivatives of potential were given. Therefore, this problem corresponds to that of Neumann. But another type of problem is possible; that is to give normal components of stresses on the closed surface. This is a particular subject which has no corresponding one in the potential theory, and because of the important position of "forces" in the field of mechanics this is a subject of great interest.

The stress components are given by

$$\begin{cases} T_{RR}=\lambda\Delta\mathfrak{D}+2\mu\dfrac{\partial u}{\partial R} \\ T_{R\theta}=\mu\left\{R\dfrac{\partial}{\partial R}\left(\dfrac{v}{R}\right)+\dfrac{1}{R}\dfrac{\partial v}{\partial\theta}\right\} \\ T_{R\varphi}=\mu\left\{\dfrac{1}{R\sin\theta}\dfrac{\partial u}{\partial\varphi}+R\dfrac{\partial}{\partial R}\left(\dfrac{w}{R}\right)\right\} \end{cases} \quad \cdots\cdots(27)$$

From (2), (3) and (5) we get the following relation:—

$$n(n+1)\frac{\Psi}{R^2}=\frac{\partial^2\Psi}{\partial R^2}+k^2\Psi \quad \cdots\cdots(28)$$

where Ψ is ${}_1\Psi$ or ${}_2\Psi$ as already defined in (3).
Introducing (4) and (28) into (27), we get

$$\begin{cases} T_{RR}=\mathfrak{D}P_n^m\cdot\cos m\varphi+\mathfrak{D}'P_n^m\cdot\sin m\varphi \\ T_{R\theta}=\left[\mathfrak{F}\dfrac{d}{d\theta}P_n^m+\mathfrak{E}m\dfrac{1}{\sin\theta}P_n^m\right]\cos m\varphi \\ \qquad +\left[\mathfrak{F}'\dfrac{d}{d\theta}P_n^m-\mathfrak{E}m\dfrac{1}{\sin\theta}P_n^m\right]\sin m\varphi \\ T_{R\varphi}=\left[\mathfrak{F}'m\dfrac{1}{\sin\theta}P_n^m-\mathfrak{E}\dfrac{d}{d\theta}P_n^m\right]\cos m\varphi \\ \qquad +\left[-\mathfrak{F}m\dfrac{1}{\sin\theta}P_n^m-\mathfrak{E}'\dfrac{d}{d\theta}P_n^m\right]\sin m\varphi \end{cases} \quad \cdots\cdots(29)$$

where
$$\begin{cases} \mathfrak{D} = A\left\{-\lambda h^2 f + 2\mu \dfrac{d^2 f}{dR^2}\right\} + C \cdot 2\mu n(n+1) \dfrac{d}{dR}\left(\dfrac{g}{R}\right) \\ \mathfrak{D}' = A'\{ \quad '' \quad \} + C' \cdot \quad '' \\ \mathfrak{F} = \mu\left\{A \cdot 2 \dfrac{d}{dR}\left(\dfrac{f}{R}\right) + C \cdot \left(2 \dfrac{d}{dR}\left(\dfrac{1}{R} \dfrac{d(Rg)}{dR}\right) + k^2 g\right)\right\} \\ \mathfrak{F}' = \mu\{A' \cdot \quad '' \quad + C' \cdot \quad ''\} \\ \mathfrak{E} = B \cdot R \dfrac{d}{dR}\left(\dfrac{g}{R}\right) \\ \mathfrak{E}' = B' \cdot \quad '' \end{cases} \quad \ldots\ldots(30)$$

Now the forms of the equations (29) is completely similar to (8) provided $\mathfrak{A}$, $\mathfrak{A}'$, $\mathfrak{B}$, $\mathfrak{B}'$, $\mathfrak{C}$, $\mathfrak{C}'$ are interchanged by $\mathfrak{D}$, $\mathfrak{D}'$, $\mathfrak{E}$, $\mathfrak{E}'$, $\mathfrak{F}$, $\mathfrak{F}'$ respectively. Therefore the problem, in which the normal components of stress are given on the surface $R=a$, is theoretically equivalent with the former case. The only difference existing in the two cases is that the equations which determine $\mathfrak{A}$, $\mathfrak{A}'$ etc. (equations (7)) and $\mathfrak{D}$, $\mathfrak{D}'$ etc. (equations (30)) have not the same coefficients. After getting $\mathfrak{D}$, $\mathfrak{D}'$ etc. by the application of expressions (14), (19), (20), (21) and (22) we may solve the linear equations (30), and obtain A, A' etc. as follows :—

$$\begin{cases} A = \mu\left\{\mathfrak{D}\left(2 \dfrac{d}{dR}\left(\dfrac{1}{R} \dfrac{d(Rg)}{dR}\right) + k^2 g\right) - \mathfrak{F} \cdot 2n(n+1) \dfrac{d}{dR}\left(\dfrac{g}{R}\right)\right\} \Big/ E \\ A' = \mu\{\mathfrak{D}'(\quad '' \quad)- \mathfrak{F}' \cdot \quad '' \quad \} / E \\ C = \left\{-\mathfrak{D} \cdot \mu \dfrac{d}{dR}\left(\dfrac{f}{R}\right) + \mathfrak{F}\left(-\lambda h^2 f + 2\mu \dfrac{d^2 f}{dR^2}\right)\right\} \Big/ E \\ C' = \{-\mathfrak{D}' \cdot \quad '' \quad + \mathfrak{F}'(\quad '' \quad)\} / E \\ B = \mathfrak{E}/R \dfrac{d}{dR}\left(\dfrac{R}{g}\right) \\ B' = \mathfrak{E}'/ \quad '' \end{cases} \quad \ldots\ldots(31)$$

where
$$E = \begin{vmatrix} -\lambda h^2 f + 2\mu \dfrac{d^2 f}{dR^2} & 2\mu n(n+1) \dfrac{d}{dR}\left(\dfrac{g}{R}\right) \\ \mu 2 \dfrac{d}{dR}\left(\dfrac{f}{R}\right) & \mu\left(2 \dfrac{d}{dR}\left(\dfrac{1}{R} \dfrac{d(Rg)}{dR}\right) + k^2 g\right) \end{vmatrix} \quad \ldots\ldots(32)$$

and after carrying out the differentiation, all $R's$ are replaced by a.

In this paper we have studied the problem of the generation of elastic waves, in which the boundary conditions on the spherical surface are given,

in most general forms; and showed the solutions explicitly. Thus the previous defect pointed out by Mr. S. Honma, in boundary—or initial—value problem, is excluded altogether.

In concluding this paper, the writer wishes to express sincere thanks to Dr. H. Kawasumi and Mr. S. Honma for the valuable advices and suggestions throughout this study.

2. *On the Theory of Elastic Waves in Granular Substance. I.*

By Takehito TAKAHASHI, Seijô High School
and
Yasuo SATÔ, Earthquake Research Institute.

(Read Oct. 19, 1948.—Received Oct. 6, 1949.)

Elastic waves are propagated in sand with only 1/3 of their velocity in rock. We tried here to explain this property by a simple structural model. Though many problems are left untouched, we at least succeeded to gain some fundamental formulæ.

1. *One-dimensional model.* Consider a large number of elastic spheres of radius r and mass m pressing each other on a straight-line. In equilibrium, each sphere suffers equal pressure from both sides due to elastic deformation, which we could write $P(\alpha)$, where $\alpha=2r-a$ and $a=X_{n+1}-X_n$, X_n being the coordinate of the center of gravity of the nth sphere. Owing to small displacements, X_n changes to X_n+x_n. If we write $\Delta\alpha_n$ and ΔP_n for the variations between nth and $(n+1)$th spheres,

$$-\Delta\alpha_n=x_{n+1}-x_n, \quad \cdots\cdots(1)$$

$$\Delta P_n=P_n-P=k\Delta\alpha_n, \ (k=dP/d\alpha). \quad \cdots\cdots(2)$$

Neglecting higher orders, we may consider that the center of gravity of the sphere always coincides with its geometrical center. Then we can write down the equation of motion of the n th sphere

$$\begin{aligned} m\ddot{x}_n &= -P_n+P_{n+1}=-k(\Delta\alpha_n-\Delta\alpha_{n+1}) \\ &= -k\{(x_n-x_{n+1})-(x_{n-1}-x_n)\}. \quad \cdots\cdots(3) \end{aligned}$$

Under Born-von Kármán's boundary condition, (3) is easily solved, putting

$$x_n=A\exp\{2\pi i(\sigma X_n-\nu t)\}, \quad \cdots\cdots(4)$$

where σ means wave number, that is, inverse of wave length. In our case σa must be very small, so that we can neglect its higher orders. Substituting (4) in (3), $m\ddot{x}_n+4\pi^2a^2\sigma^2kx_n=0$.

Hence for the velocity $v_0=\nu/\sigma=a\sqrt{(k/m)}=2r\sqrt{(k/m)}$ $\cdots\cdots(5)$

To determine k, we could adopt the formula gained statically by Hertz[1].

$$P=(3\pi\vartheta)^{-1}(2r)^{\frac{1}{2}}\alpha^{\frac{3}{2}}, \qquad \vartheta=(\lambda+2\mu)/4\pi\mu(\lambda+\mu) \quad \cdots\cdots(6)$$

Hence $$k=dP/d\alpha=(1/\pi\vartheta)\sqrt{(r\alpha/2)} \quad \cdots\cdots(7)$$

Putting (7) in (5), if ρ means the density,

$$v_0^2=(3/\pi^2\vartheta\rho)\sqrt{(\alpha/2r)}. \quad \cdots\cdots(8)$$

When $\lambda=\mu$, (8) is expressed as

$$v_0/v_p \fallingdotseq 0.921(\alpha/2r)^{\frac{1}{4}}, \quad \cdots\cdots(9)$$

where $$v_p^2=(\lambda+2\mu)/\rho=3\mu/\rho.$$

If we eliminate α from (6) and (9), we know v_0 is proportional to $P^{1/6}$.

Similar results were already gained by K. Iida[2].

2. *Three-dimensional model.* Imagine that centers of spheres form a space lattice in equilibrium, and pressures are the same at all contact points.

Let vector R_0 indicate the center of a sphere in question. If n is the number of its neighboring spheres, vectors connecting their centers R_j with the center R_0 are expressed as

$$\pm a t_j=R_{\pm j}-R_0, \quad |t_j|=1, \quad (j=1, 2, \cdots\cdots n/2). \quad \cdots\cdots(1)$$

Assuming that the direction of the pressure coincides with t_j,

$$\Delta P_j=t_j\cdot k\,\Delta\alpha_j \fallingdotseq -k(\mathfrak{r}_j-\mathfrak{r}_0,\ t_j)\,t_j. \quad \cdots\cdots(2)$$

where $\mathfrak{r}_j$ is the displacement of the center of the j th neighboring sphere.

Neglecting other forces we get the equation of motion

$$m\ddot{\mathfrak{r}}_0=k\sum_{\pm j}(\mathfrak{r}_j-\mathfrak{r}_0, t_j)t_j=k\sum_j(\mathfrak{r}_j+\mathfrak{r}_{-j}-2\mathfrak{r}_0, t_j)t_j. \quad \cdots\cdots(3)$$

We put $$\mathfrak{r}_j=\mathfrak{A}\exp\{2\pi i(\sigma R_j-\nu t)\}, \quad \cdots\cdots(4)$$

where $\nu/|\sigma|=v$ and $\sigma=|\sigma|s$, $|s|=1$ means the wave number vector.

Now $|\sigma|$ being very small, (3) becomes

$$m\ddot{\mathfrak{r}}_0+4\pi^2a^2\sigma k\sum(st_j)^2(\mathfrak{r}_0t_j)t_j=0, \quad \cdots\cdots(5)$$

or $$(v/v_0)^2\mathfrak{A}-\sum(\mathfrak{A}t_j)(st_j)^2t_j=0. \quad \cdots\cdots(6)$$

From (6) secular equation for $(v/v_0)^2$ may be immediately obtained. We can solve this third order equation assuming lattice structure. But this is uninteresting, for, although its three roots depend on the propa-

(1) LOVE, "*Theory of Elasticity.*" p. 200.

(2) K. IIDA, *Bull. E. R. I.*, **16** (1938) 131, **17** (1939) 782.

gating direction, we practically observe only two sorts of velocities—longitudinal and transversal, which should be the consequence of irregular overlapping of so many fundamental lattices considered above. We will deal with this problem in the next section.

Here, treating approximately as a continuous substance, we will determine apparent elastic constants of our model.

Modifying (5) into

$$m\ddot{\tau}_0 - ka^2\sigma^2\nu^{-2}\sum(st_j)^2(\ddot{\tau}_0 t_j)\,t_j = 0,$$

We get by integration

$$m(\dot{\tau}_0)^2 - ka^2\nu^{-2}\sum(st_j)^2(\dot{\tau}_0 t_j)^2 = 0. \quad \cdots\cdots(7)$$

If ϵ is the energy per one sphere ($=m\dot{\tau}_0^2/2$), and the components of τ_0, s and t_j are (u_1, u_2, u_3), (s_1, s_2, s_3) and (t_{j1}, t_{j2}, t_{j3}) respectively, (7) becomes

$$2\varepsilon/m = (v_0/v)^2\sum(s_1t_{1j} + s_2t_{2j} + s_3t_{3j})^2(\dot{u}_1t_{1j} + \dot{u}_2t_{2j} + \dot{u}_3t_{3j})^2. \quad \cdots\cdots(8)$$

Considering (4), we can under continuity assumption define strain components $x_1 \cdots\cdots x_6$ as follows

$$\left.\begin{aligned} x_1 &= -s_1\dot{u}_1/v, \quad x_2 = -s_2\dot{u}_2/v, \quad \cdots\cdots \\ x_4 &= -s_2\dot{u}_3/v - s_3\dot{u}_2/v, \cdots\cdots \end{aligned}\right\} \cdots\cdots(9)$$

Hence (8) becomes

$$2\varepsilon/mv_0^2 = \sum(x_1t_{j1}^2 + x_2t_{j2}^2 + x_3t_{j3}^2 + x_4t_{j2}t_{j3} + x_5t_{j3}t_{j1} + x_6t_{j1}t_{j2})^2. \quad \cdots\cdots(10)$$

If ρ^* is apparent density, ρ^*/m means the number of spheres per unit volume. Then according to the theory of elasticity

$$2\varepsilon\rho^*/m = (x_1c_1 + x_2c_2 + x_4c_4 + x_4c_4 + x_5c_5 + x_6c_6)^3, \quad \cdots\cdots(11)$$

where the right side is written symbolically—c_ic_j means elastic constant c_{ij} if developed.

Comparing (10) with (11), we get

$$c_{\kappa\iota} = \rho^*v_0^3\sum_i\tau_\kappa\tau_\iota \quad \cdots\cdots(12)$$

where

$$\tau_1 = t_{i1}^3, \quad \tau_2 = t_{i2}^3, \quad \tau_3 = t_{i3}^3,$$
$$\tau_4 = t_{i2}t_{i3}, \quad \tau_5 = t_{i3}t_{i1}, \quad \tau_6 = t_{i1}t_{i2}.$$

We know immediately that Cauchy's relations are satisfied, which is also natural seeing that the assumption of central force is made.

From (12) important formulæ are gained. Thus

$$\left.\begin{aligned} c_{12} + c_{13} + c_{23} &= c_{44} + c_{55} + c_{66}, \\ c_{11} + c_{22} + c_{33} &= (n/2)\rho^*v_0^3 - 2(c_{12} + c_{13} + c_{23}). \end{aligned}\right\} \cdots\cdots(13)$$

3. ***Elastic constants of an aggregate of aeolotropic bodies, when regarded as if the whole were an isotrope.*** Suppose an aggregate of many small bodies of one kind. Their crystal axes are arranged in all directions, and in their average we should like to treat the aggregate as an isotrope.

We write strain components x_i and elastic constants c_{ij} in matrices

$$x=\begin{pmatrix} x_1 \\ \vdots \\ x_6 \end{pmatrix}, \qquad C=\begin{pmatrix} c_{11}\cdots\cdots c_{16} \\ \ddots\cdots\cdots \\ c_{65}\cdots\cdots c_{66} \end{pmatrix} \quad \cdots\cdots(1)$$

Then the energy per unit volume may be expressed as

$$2E=x^*Cx, \quad \cdots\cdots(2)$$

where x^* means the transposed matrix of x.

The direction of each crystal axis determines the rotation r from fixed position, so we write E^r and x^r in (2) to show their rotated position. If $V(r)$ means the representation of rotation group in terms of x, we may write

$$x^r=V(r)x. \quad \cdots\cdots(3)$$

Then $$2E^r=x^{*r}Cx^r=x^*(V^*(r)CV(r))x. \quad \cdots\cdots(4)$$

We define the energy E_0 of the resulted isotrope as the average of all E^r, that is

$$2E^0=x^*C^0x=2(1/\Omega)\int E^r d\Omega. \quad \cdots\cdots(5)$$

where Ω means the volume of the parameter space of rotation r.

From (5) and (6)

$$C^0=(1/\Omega)\int V^*(r)CV(r)d\Omega. \quad \cdots\cdots(6)$$

Now our problem becomes clear—being given C, to determine C^0.

To make use of the theory of representations, we must first decompose the matrix $V(r)$. This will be done by transforming $V(r)$ with a constant matrix T

$$U(r)=T^{-1}V(r)T, \qquad U^*(r)=U(r)^{-1}. \quad \cdots\cdots(7)$$

If we put $$C^{0r}=T^*C^0T, \qquad C^r=T^*CT, \quad \cdots\cdots(8)$$

we get from (6) and (7)

$$C^{0r}=(1/\Omega)\int U(r)^*C^rU(r)d\Omega. \quad \cdots\cdots(9)$$

As x is a symmetric tensor of rank 2, $U(r)$ must be decomposed into two irreducible parts of 1st and 5th order. Then, from the well

known lemma of Schur concerning irreducible representations, we know at last that (9) is a diagonal matrix, and its diagonal elements are

$$c_{11}^{0T}=c_{11}^{T},\quad 5c_{jj}^{0T}=\{c_{22}^{T}+c_{33}^{T}+c_{44}^{T}+c_{55}^{T}+c_{66}^{T}\}\ (j\geqq 2). \quad \cdots\cdots(10)$$

Thus we must only know T to determine C^0.

In the space of homogeneous polynomials, solid spherical harmonics are the bases of irreducible representation of rotation group. To the representation of 5th order corresponds spherical function of order 2. Adding to them an invariant $(x^2+y^2+z^2)$, T will mean the transformation from these six functions to the components of the symmetric tensor, x^2, y^2, z^2, $2yz$, $2zx$, $2xy$. To calculate T is then an easy task.

Finally we calculated c_{jj}^{T} from the second equation of (8), and putting them in (10), we got c_{jj}^{0T}. Determination of C^0 was the consequent result of the first equation of (8) written in the following form

$$C^0=(T^*)^{-1}C^{0T}T^{-1}. \quad \cdots\cdots (11)$$

The obtained C^0 is a symmetric matrix, and the components except the followings. are all zeros.

$$c_{11}^0=c_{22}^0=c_{33}^0=(3/15)(c_{11}+c_{22}+c_{33})+(2/15)(c_{23}+c_{31}+c_{12})+(4/15)(c_{44}+c_{55}+c_{66}),$$

$$c_{23}^0=c_{31}^0=c_{12}^0=(1/15)(\quad ,,\quad)+(4/15)(\quad ,,\quad)-(2/15)(\quad ,,\quad),$$

$$c_{44}^0=c_{55}^0=c_{66}^0=(1/2)(c_{11}^0-c_{12}^0). \quad \cdots\cdots (12)$$

From this result C^0 can be interpreted as the tensor of elastic constants of an isotrope, as we expected.

Application of this section is not restricted to the granular structure only, but here we will not go further.

4. *Conclusions.* Applying the last section to our case, that is, if we substitute 2-(13) in 3-(12), we get immediately

$$c_{12}^0=(n/30)\rho^* v_0^2,\qquad c_{11}^0=(n/10)\rho^* v_0^2=3c_{12}^0 \quad \cdots\cdots(1)$$

c_{11}^0 and c_{12}^0 depend only on the number of neighboring spheres, and not on lattice structure. This is a remarkable fact. (Equation (1) could also be gained by directly averaging 2. (3).)

Then the velocities of elastic waves are

$$v_p^*=\sqrt{(c_{11}^0/\rho^*)}=v_0\sqrt{(n/10)},\quad v_s^*=\sqrt{\{(c_{11}^0-c_{12}^0)/2\rho^*\}}=v_p^*/\sqrt{3}. \quad \cdots(2)$$

These are the desired results.

To consult with experimental data, a slight deformation should be made on the expression of v_0. We define statical pressure P_0 as the force per unit area acting perpendicular on the plane imagined in the granular aggregate. Consider a polyhedron wrapping a sphere made up

of tangential planes at contact points, and replace its surface area with that of the equivoluminal sphere. Then P_0 may be expressed as

$$P_0=(nP/4\pi r^2)(\rho^*/\rho)^{2/3} \quad \cdots\cdots(3)$$

From (2) and (3)

$$v_p^*=0.930\,\varepsilon_n(P_0/\rho)^{1/6}\cdot v_p^{2/3},\quad \varepsilon_n=(n/10)^{1/3}(\rho^*/\rho)^{-1/9} \quad \cdots\cdots(4)$$

Values of ε_n are shown in Table I. We compared the results with K. Iida's experiments[3], assuming temporarily $P_0=\rho^* gh$, the coincidence was somewhat satisfactory with sand but not so good in case of lead and rubber, and the remarkable change due to porosity $(=1-\rho^*/\rho)$ could not be well explained.

An example of the numerical calculation is in Tab. II, which we think proves qualitative correctness of our theory.

For the results in this paper, so also for the faults, if any, one of the authors, Takahashi, is responsible.

Table I. Values of ε_n.

n	6	8	10
ρ^*/ρ	.52	.60	.70
ε_n	.90	.90	1.04

Values of ρ^*/ρ due to L. C. Graton and H. J. Frazer are quoted in Iida's paper.

Table II. Wave-velocities in a Sand, when $\rho=2.7$ g/cm^3, $v_p=5000$ m/sec. and $\varepsilon_n=1$.

p_0 bar	.001	.01	1	100	1000
v_p^* m/sec	157	230	497	1070	1570
v_s^* "	91	133	287	618	907

(3) K. Iida, *loc. cit.*

3. *A Note on the Temperature-Distribution within the Earth.*

By Tsuneji RIKITAKE,

Earthquake Research Institute.

(Read Sept. 20, 1949.—Received Oct. 20, 1949.)

In spite of the recent development of researches on the earth's interior, few studies have been carried out concerning the temperature-distribution within the earth. The main difficulty of this problem is due to the fact that we cannot get sufficient data by which we presume the distribution from the physical standpoint. L. H. Adams[1] and H. Jeffreys[2] discussed the cooling of the earth under some assumptions. On account of the ambiguities of various quantities included, however, their results seem to be probable solutions for this problem. E. C. Bullard[3] also made a similar study along the line of Jeffreys' treatment. Meanwhile, B. Gutenberg[4] proposed a different distribution.

Recently, H. P. Coster[5] measured changes in electrical conductivity of rocks at high temperatures and, with the aid of the theory of lattice defect of ionic crystal, presumed considerable increase in electrical conductivity at the depth of several hundred kilometers in the earth. On the other hand, the writer[6] obtained an approximate distribution of the electrical conductivity in the earth's interior from the standpoint of electromagnetic induction theory which has been developed by S. Chapman,[7] A. T. Price,[8] B. N. Lahiri[9] and others. Studying electromagnetic induction by S_D (solar daily disturbance variation), bay-type disturbance, variation connected with solar eruption and sudden commencement of magnetic storm

1) L. H. ADAMS, *Washington Acad. Jour.*, **14** (1924) 459.
2) H. JEEFFREYS, *The Earth.* Cambridge (1924), p. 79.
3) E. C. BULLARD, *M. N. R. A. S. Geophys. Suppl.*, **4** (1939) 534.
4) B. GUTENBERG, *Physics of the Earth* VII. *Internal Constitution of the Earth.* 1st. ed. p. 153.
5) H. P. COSTER, *M. N. R. A. S. Geophys. Suppl.*, **5** (1949) 193.
6) T. RIKITAKE, Reported to *Intern. Ass. Terr. Mag. Electr. Oslo Assembly*, Aug. 1948.
7) S. CHAPMAN, *Trans. Roy. Soc. London* A **218** (1919) 1.
8) S. CHAPMAN and A. T. PRICE, *Trans. Roy. Soc. London*, A, **229** (1930) 427.
9) B. N. LAHIRI and A. T. PRICE, *Trans. Roy. Soc. London*, A, **237** (1939) 509.

together with S_q (solar diurnal variation on quiet days) and D_{st} (average main phase of magnetic storm), the writer concluded, as shown in Fig. 1, that the conductivity increases discontinuously below the depth of 400 *km* amounting to the order of 10^{-12} *e. m. u.* while the outer layer seems to be almost non-conducting, its conductivity amounting to only 10^{-15} *e. m. u.* near the earth's surface. On the basis of the conductivity-distribution thus obtained, the writer will presume the temperature-distribution in the earth in a similar way with Coster's study.

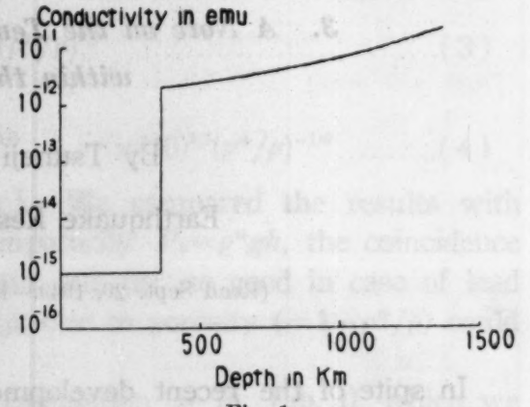

Fig. 1.

According to T. Nagata[10], the electrical conductivity of igneous rocks at high temperature satisfies approximately the equation

$$\sigma = Ae^{-B/T} \quad \cdots\cdots(1)$$

as well as obtained by Coster, where A and B are constant. T denotes the absolute temperature. According to the theory of electric conduction in ionic crystal[11], B is interpreted as

$$B = \epsilon/k = \frac{1}{k}\left(\frac{1}{2}w_0 + v_0\right) \quad \cdots\cdots(2)$$

where k, w_0 and v_0 denote respectively Boltzmann's constant, energy required to make a lattice defect at zero temperature and activation energy at zero temperature. Thus we may regard the main part of electric conduction in rocks as due to the motion of ions in ionic crystals.

On logarithmically differentiating, we get from (1)

$$\frac{\partial \log \sigma}{\partial p} = -\frac{1}{kT}\frac{\partial \epsilon}{\partial p} + \frac{\partial \log A}{\partial p} \quad \cdots\cdots(3)$$

where the second term of the right may be neglected except at very high temperature. Further, we write

$$\frac{\partial \epsilon}{\partial p} = -\epsilon\chi\frac{\partial \log \epsilon}{\partial \log V} \quad \cdots\cdots(4)$$

where χ and V denote respectively the compressibility and the volume of unit mass.

---

10) T. NAGATA, *Bull. Earthq. Res. Inst.*, **15** (1937) 663.

11) N. F. MOTT and R. W. GURNEY, *Electronic Processes in Ionic Crystals*. Oxford, 1940.

Hence, we have

$$\frac{\partial \log \sigma}{\partial p} = \frac{\chi \epsilon}{kT} \frac{\partial \log \epsilon}{\partial \log V} \quad \cdots\cdots(5)$$

$\partial \log \epsilon / \partial \log V$ is thought to be about the same for all substances and

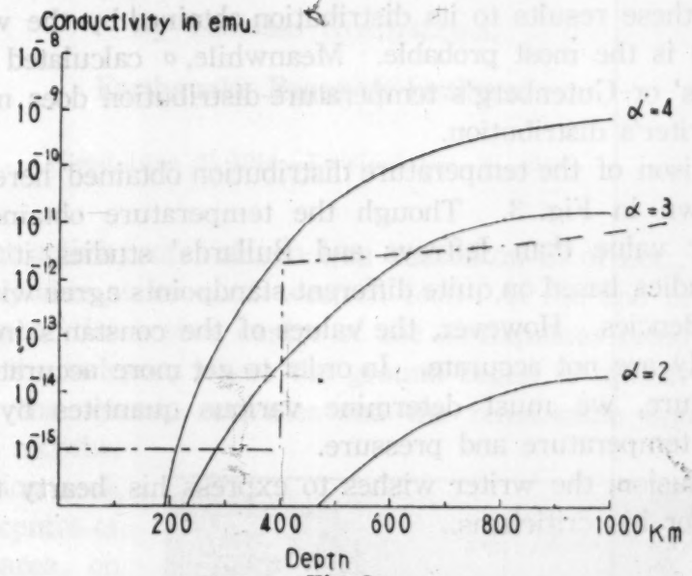

Fig. 2.

takes a value of about -2 from the standpoint of theoretical physics. From (4). we get

$$\epsilon = \epsilon_0 e^{-\chi p \frac{\partial \log \epsilon}{\partial \log V}} \quad \cdots\cdots(6)$$

where ϵ_0 denotes ϵ at zero pressure. Putting $\chi = 0.7 \times 10^{-12}$ *cgs* and $\epsilon_0 = 2.3$ *eV* as taken by Coster, ϵ is obtainable for given pressure. Strictly speaking, χ depends on pressure. But it may be assumed that χ does not depend on pressure for rough estimation.

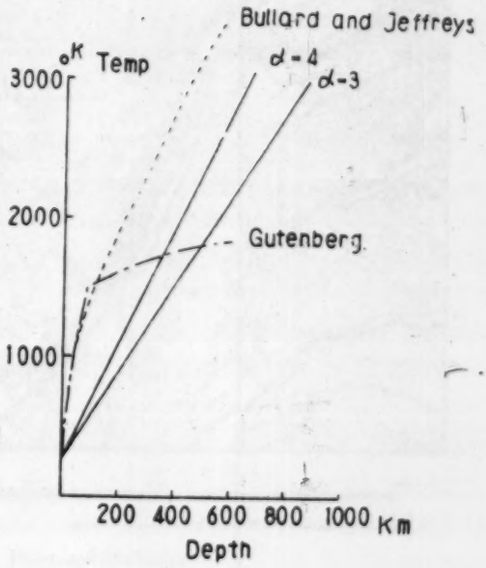

Fig. 3.

Next, giving 10^5 *ohm*$^{-1}$ *cm*$^{-1}$ to A as obtained from Nagata's and Coster's experiments, we get σ from (1) and (2) for zero pressure and any temperature. As to the temperature-distribution within the earth, the simplest expression

$$T=273+\alpha x$$

is assumed for the first time, where x denotes the depth and α is a constant. Then, taking into consideration the pressure-distribution obtained by K. E. Bullen[12], σ is reduced to the value that corresponds to the actual pressure. As shown in Fig. 2, σ is calculated for $\alpha=2$, 3 and 4° K/km. Comparing these results to its distribution obtained by the writer, we see $\alpha=3°$ K/km is the most probable. Meanwhile, σ calculated from Jeffreys and Bullards' or Gutenberg's temperature-distribution does not agree well with the writer's distribution.

Comparison of the temperature distribution obtained here to the other ones is shown in Fig. 3. Though the temperature obtained here takes rather lower value than Jeffreys and Bullards' studies, it is of interest that two studies based on quite different standpoints agree with each other in their tendencies. However, the values of the constants included in the present study are not accurate. In order to get more accurate distribution of temperature, we must determine various quantites by experiments under high temperature and pressure.

In conclusion, the writer wishes to express his hearty thanks to Dr. T. Nagata for his criticisms.

12) K. E. Bullen, *Bull. Seism. Soc. Amer.*, **30** (1940), 246.

4. *Magnetic Survey in the Area of Topographical Deformation of Volcano Usu.*

By Yoshiaki KOSHIKAWA,

Earthquake Research Institute.

(Read June 20, 1944.—Received Dec. 30, 1949.)

The present activity of Volcano Usu started on 27 of Dec., 1943, with numerous earthquakes at its north-western foot. At the end of February in 1944, however, the active centre of the earthquakes removed to the eastern foot of the volcano, where the ground began to upheave simultaneously. After the seismic activities and the remarkable upheaval had lasted for six months, the first explosion took place near the centre of the upheaved area, on 23 of June, 1944.[1]

Fig. 1

The magnetic survey with the Askania magnetometer of Schmidt type was carried out by the present author in the upheaved area, during the period from 11 to 23 of April. 1944. Along the road running from north to south through the area, the relative intensities of the vertical component (Z) of geomagnetic field were measured at 100 stations within the distance of about 7km.. The standard station. where the measurements were repeated twice a day, morning and evening, was placed about 3 km south-

wards the upheaved centre (the station No. 3). At many other stations, the measurements were repeated two or three times during this period. [Fig. 1.]

The scale value (S) and the temperature coefficient (k) of the magnetometer used here are as follows,

$S=43.5^{\gamma}$ per 1 scale division,

$k=2.77^{\gamma}$ per 1°C.

To all observed values at every station, the temperature correction according to $k=2.77^{\gamma}/°$, and the correction of daily variation of general geomagnetic field basing on the observation of the Mitsui Geophysical Observatory, Izu Peninsula, were applied. Thus, all measured intensities of Z were reduced to the values of 21st 12h of April, whereas the values of 16th and 17th of April at some stations just measured greatly deviate from their mean values, as indicated in Fig. 2. Fortunately, at the stations No. 29 and No. 87. Dr. Nagata's absolute measurements were carried out, and it is much indebted to his kindness that these values could be plotted in the same illustration figure. Such a magnetic intensity variation seems to be correlated with the volcanic or seismic activities, because sensible earthquakes took place frequently between 14th and 17th of April and the most intense one occurred at 20h 25m of 15th of April, when our survey was being carried out. The intensity of this earthquake was II degree of the C. M. O. intensity scale of Japan at Date-Monbetsu about 8 km southwards the upheaved centre.

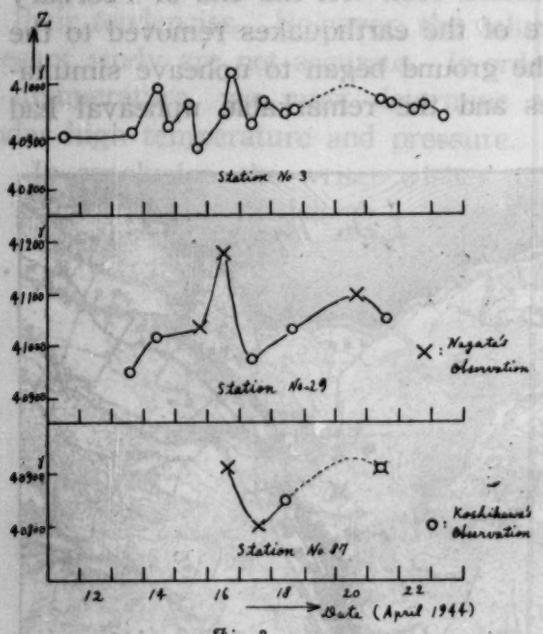

Fig. 2

Taking into account the above mentioned variation of Z, the mean value of Z of each station was calculated, and thus the magnetic profile as indicated in Fig. 3 (a) was obtained. Basing on this magnetic profile, confirming the subterranean mass distribution, Tsuboi-Nagata's analytical method was used.[3]

If the intensity of magnetization of the subterranean mass is represented as

$$J(\xi)=\sum_m a_m \cos m\xi+\sum_m b_m \sin m\xi,$$

the magnetic anomaly due to this mass will be written as in the form,

$$Z(x)=\sum_m \alpha_m \cos mx+\sum_m \beta_m \sin mx.$$

Thus, there exist the relations

$$a_m=\frac{e^{md}}{2\pi m}(\alpha_m \sin\theta-\beta_m \cos\theta)$$

$$b_m=\frac{e^{md}}{2\pi m}(\alpha_m \cos\theta+\beta_m \sin\theta),\quad (m\geqq 1),$$

where, d is the depth of a plane where the subterranean mass is condensed, and θ denotes the dip angle of magnetization.

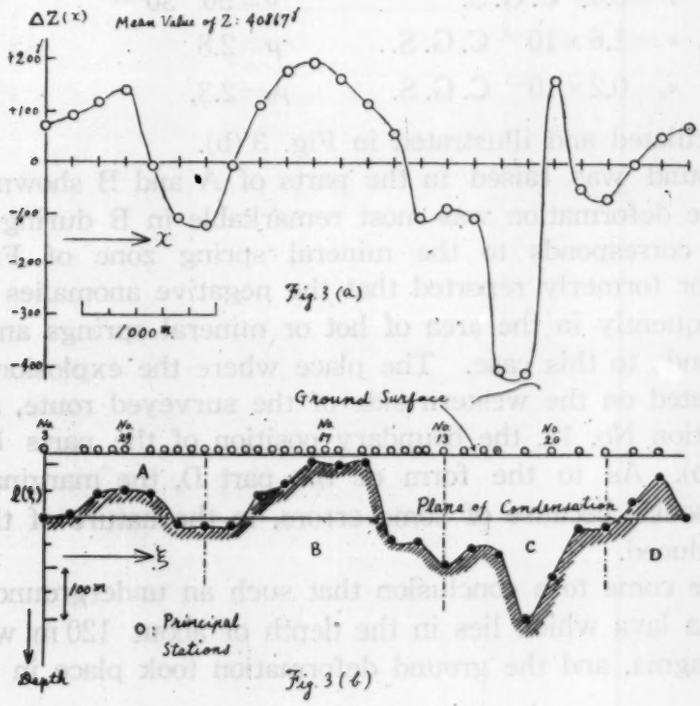

By means of Fourier analysis of the magnetic profile, α_m and β_m are known, then a_m and b_m can be calculated by assuming d. And

$$J(\xi)=(\kappa\rho-\kappa_0\rho_0)F\cdot l(\xi),$$

where κ and κ_0 denote the magnetic susceptibilities of lower mass and of superficial layer respectively, whereas ρ and ρ_0 are the densities of them. F is the total intensity of general magnetic field, and $l(\xi)$ displays the elevation of the subterranean mass above the condensed plane.

The present author, assuming the various values of d, calculated $J(\xi)$, whereas, if d is larger than 200 m, Fourier coefficients (a_m, b_m) of higher order become very large, and $J(\xi)$ profile seems, therefore, unreasonable. On the other hand, the susceptibility of the subterranean mass must be larger than 9×10^{-3} C. G. S., if d is smaller than 50 m, because the maximum l is smaller than or equal to d. It is difficult to obtain such a value in ordinary rocks. Its largest value is about 7.5×10^{-3} C. G. S. even in basic rocks. Hence, 120 m was adopted as the intermediate value of d.

Comparing the normative magnetite of the somma lava of this volcano and with that of other volcanoes (Mt. Fuji, Mt. Asama, etc.),[3][4] and refering to Y. Harada's observation in the vicinity of the Lake Toya,[5] only about 1 km. from this area, 1.6×10^{-3} C. G. S. was selected as the most suitable value of κ. Then, adopting the following values

$$F=0.49 \text{ C. G. S.} \qquad \theta=56^\circ\ 30'^{[6]}$$
$$\kappa=1.6\times10^{-3} \text{ C. G. S.} \qquad \rho=2.8$$
$$\kappa_0=0.2\times10^{-3} \text{ C. G. S.} \qquad \rho_0=2.3,$$

$l(\xi)$ was calculated and illustrated in Fig. 3 (b).

The ground was raised in the parts of A and B shown in the Fig. 3 (b), and the deformation was most remarkable in B during this period. The part C corresponds to the mineral spring zone of Fukaba. The present author formerly reported that the negative anomalies of Z were observed frequently in the area of hot or mineral springs and the part C just corresponds to this case. The place where the explosion took place later is situated on the western side of the surveyed route, about 500 m from the station No. 13, the boundary position of the parts B and C in the Fig. 3 (b). As to the form of the part D, the marginal part, it is difficult to discuss, because of some errors, in the nature of this analysis, will be introduced.

Thus, we come to a conclusion that such an underground basic rock as the somma lava which lies in the depth of about 120 m was elevated by active magma, and the ground deformation took place in the parts of A and B.

In conclusion, the writer wishes to express his sincere thanks to Professors Ch. Tsuboi and T. Nagata who gave him kind advices.

Literatures

(1) T. Minakami: Recent Activities of Volcano Usu (I), Bulletin of the Earthquake Research Institute.
Vol. 25, Nos. 1~4, 1947.

(2) T. Nagata: Magnetic Anomalies and the Corresponding Subterranean Structure.
Proc. Imp. Acad. Tokyo, Vol. XIV.

(3) K. Yagi: Petrological Studies on Syowa-Sinzan, Usu Volcano, Hokkaido, Japan.
Journal of the Jap. Assoc. of Mineralog., Petrolog. and Econom. Geolog.
Vol. 33, No. 1, 1949.

(4) T. Nagata: Some Physical Properties of Volcanic Rocks.
"Zisin" (Jour. Seism. Soc. Japan), Vol. 12, No. 3, 1940.

(5) Y. Harada: Magnetic Anomalies around the Lake of Toya.
"Zisin" Vol. 15, No. 4, 1943.

(6) Bulletin of the Hydrographic Department, Imperial Navy, Vol. VIII. 1936.

5. *Block Movement along the Seismic Fault (1).* (*Fukui Fault and Others*)

By Nobuji NASU,

Earthquake Research Institute.

(Read Oct. 19, 1949—Received Nov. 30, 1949.)

A noteworthy fact in the topographical changes at the time of the Fukui earthquake of 1948 was the occurrence of an invisible, or intrinsic fault which could be detected only by means of the precise surveys[1]. As this fault occurred across the lowland, the Fukui Plain, the boundary of the land-blocks which moved at the time of the earthquake could not be traced clearly as in the cases of the seismic faults which appeared in the past earthquakes. With the naked eye no direct evidence of the relative movement of the land-blocks was observed on the ground, but the movement was remarkable as was revealed by the surveys. So far as determined on the land, the fault, with its northern extension terminating near the coast-line of the Japan Sea, extended over a distance of 25 km., taking a direction N. 20°W.–S. 20°E. in its northern part and N. 7°W.–S. 7°E. in the southern. There were uplift and subsidence of the ground. In general, the former was on the eastern side of the fault and the latter was on the western side of it. As the direct measurement of the horizontal shift of this fault was impossible, the shift was estimated in the manner as will be described in the following paragraph.

Estimation of the horizontal displacement. The horizontal displacement of the land-blocks along the fault has been made clear by means of the triangulation survey carried out by the Geographical Survey Bureau after the present earthquake (Fig. 1). However, the shifts of the points as determined by this survey are only relative, since the survey had not yet been carried outside the seismic region to establish the absolute movement. As to the horizontal displacements, the data have been already made public (Table I).

It will be seen that excepting Funayose, the directions of the shifts

1) T. NAGATA and A. OKADA; N. NASU, S. KAWASHIMA; Geographical Survey Bureau; K. MUTO, T. OKUDA; *Advanced Report Fukui Earthq., March 1949.*

of the triangulation points are nearly parallel with the trend of the faults. Strictly speaking, the deviations of the direction from this trend range

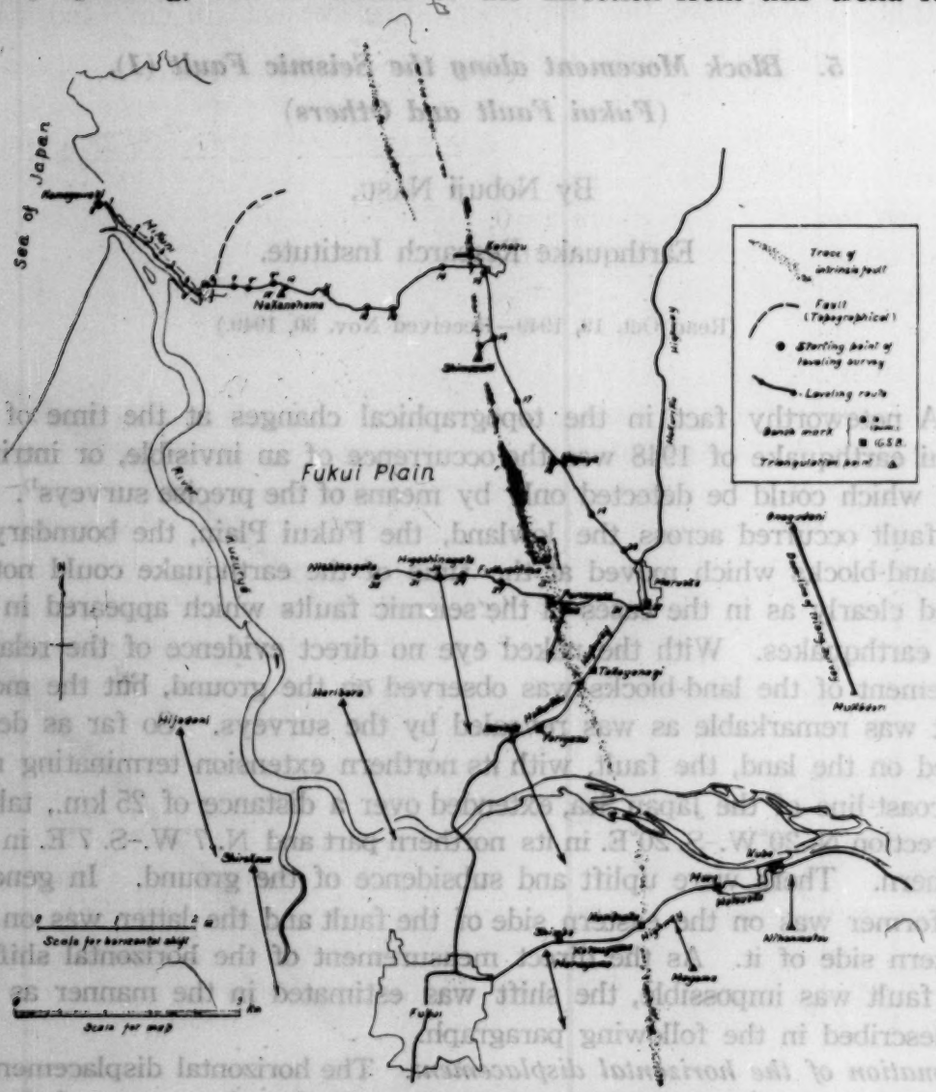

Fig. 1. Resurveyed route of leveling and the horizontal displacement of the triangulation point.

between 3" and 7" in the area lying north of the Katsuyama Highway and between 7" and 15" in the area south of the same highway. The deviation at Funayose showed a maximum of 39". This might be resulted from the complicated movement of the ground lying in a zone of sliding between land-blocks.

Taking five points, Higashinagata and others, which lie on the western side of the fault and to the north of the Katsuyama Highway just men-

tioned, the components of the displacement parallel to the fault were calculated and plotted against the distance of the point measured from the fault (Fig. 2). Let y be the component displacement (in cm.) and x the distance (in km.). Then, the relation between these quantities may be expressed by

$$y=203e^{-0.025x},$$

Hence, on the fault line where $x=0$, the horizontal displacement of the western side becomes as 203 cm. in a southerly direction. As there is no triangulation points of which displacement was determined by the survey, the movement of the eastern side of the faults is uncertain, but this much is true that the eastern side of the same fault has slipped in a direction opposite to that of the western side. If so, the land which lay between the base-line of survey[2] and the fault must have moved relatively to this base-line. Further, if the rate of

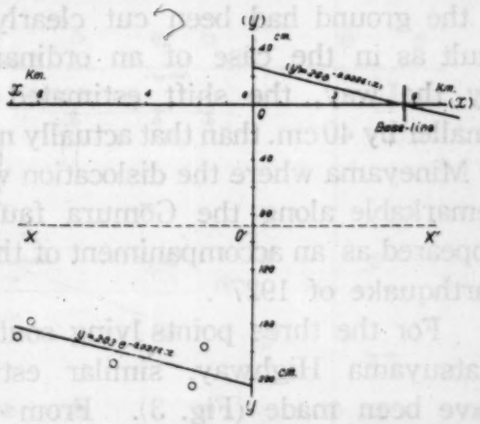

Fig. 2. Horizonal shift of of the northern part of the Fukui fault.

Table I. Horizontal displacement of the triangulation point.

Triangulation point (order)	Horizontal displacement			
	N. S.—comp.	E. W.—comp.	Resultant	Direction
	cm.	cm.		
Mukōdori (II)	0	0	End points of base-line of survey.	
Onagadani (III)	0	0		
			cm.	
Higashinagata (III)	−200	+47	205	166° 47′
Hijadani (III)	−160	+50	168	162 39
Kanado (Yoriyasu) (III)	−163	+70	177	156 46
Shirokawa (III)	−154	+35	158	167 12
Haribara (III)	−173	+73	188	157 7
Funayose (IV)	−65	−22	76	198 42
Nihonmatsu (IV)	+62	0	62	0 0
Mayama (IV)	+62	−25	67	338 2
Maruyama (IV)	+92	+25	95	164 48

N. S.—component : (+) towards N., (−) towards S.
E. W.—component : (+) towards E., (−) towards W.
Angle is measured from the north in clockwise direction.

2) The line is nearly parallel to the fault, the distance between them is 5.7 km.

decrease of the displacement with increasing distance from the fault was the same as that on the western side, the displacement of the eastern side relative to the base-line was as much as 26 cm. Thus, a horizontal shift of about 230 cm. would have been observed, if the ground had been cut clearly by the fault as in the case of an ordinary fault. By the way, the shift estimated here is smaller by 40 cm. than that actually measured at Mineyama where the dislocation was most remarkable along the Gōmura fault which appeared as an accompaniment of the Tango earthquake of 1927[3].

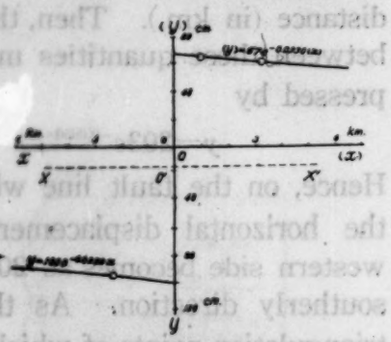

Fig. 3. Horizontal shift of the southern part of the Fukui fault.

For the three points lying south of the Katsuyama Highway, similar estimations have been made (Fig. 3). From the two points situated to the east of the fault we have

$$(y)=67e^{-0.0235(x)},$$

where (y) and (x) denotes the northward displacement and the distance from the fault measured eastwards. For the point lying on the western side of the same fault we have

$$y=100e^{-0.0235x}.$$

Hence, the horizontal shift becomes as 167 cm. in the southern part of the fault. If both sides of the fault had slipped to an equal extent in the opposite directions as actually revealed to be the absolute displacement in the Tango district[4], the movement of the fault may be illustrated by the same curves, but refering to new axes XOX′ in Figs. 2 and 3. The estimations given above are helpful in determining the amount of the relative movement of the fault, especially when the direct measurement is impossible as in the case of the Fukui fault.

Resurvey of the land-level. By means of the leveling survey made along the route as shown in Fig. 1, the changes in land-level undergone by the seismic area during about one year following the last survey were studied. The resurvey was completed in 12 days from July 22 to August 2, 1949. In the area north and east of the River Kuzuryū, the survey started from Komegawaki (bench mark of the Hydrographic Bureau) of which elevation was assumed to be unchanged as was in the last year, while in the area

3) A. IMAMURA, *Theoretical and Applied Seismology*, p. 212, 1937.
4) A. IMAMURA, *loc. cit.*

south of the Katsuyama Highway, the bench mark at Kubo in Matsuoka (No. 5254, GSB) was assumed to be steady. The instrument and the accuracy of the survey[5] were the same as those in the last survey. The changes as determined by the present survey are shown in Fig. 4.

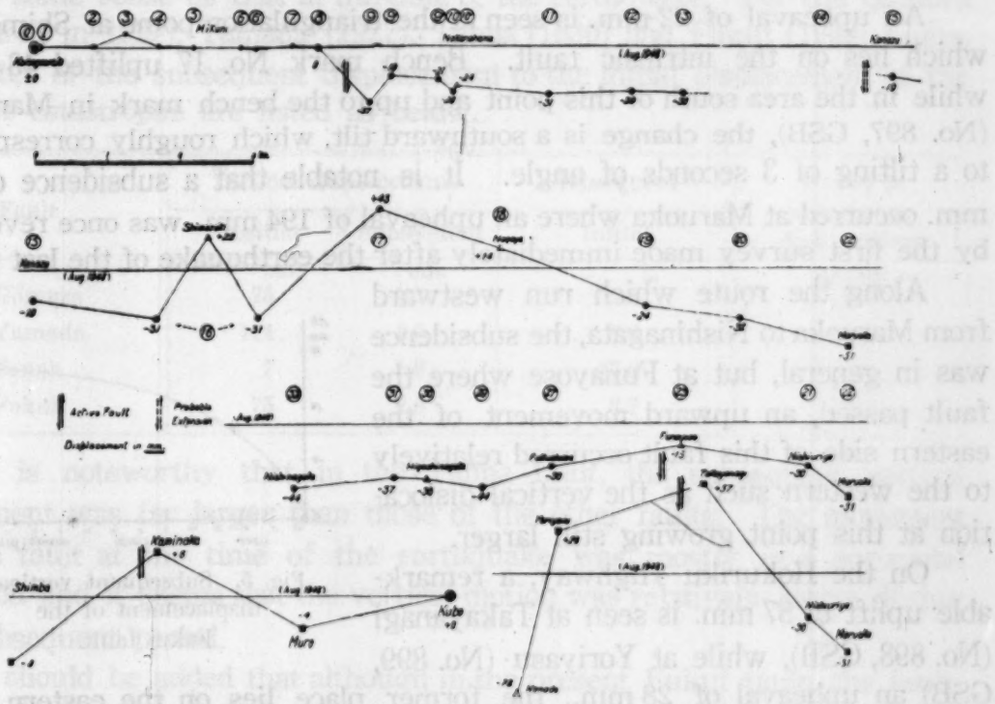

Fig. 4. Resurvey of the land-level in July 1949.

It will be seen that along the route between Komegawaki and bench mark No. 8, there can be seen practically no change. Although in this figure, a change of 10 mm. is seen at bench mark No. 3, the change is insignificant, because it was merely due to some artificial causes. However, a remarkable change has been revealed between bench marks Nos. 8 and 9 such that a general depression can be seen along the route between the latter bench mark and that No. 16. The change is in the same downward sense, similar to that experienced at the time of the main shock. The geologic map shows that this subsided area is of the alluvial formation. From the topographical point of view, a fault is drawn along the boundary of this alluvium and the diluvium on the side of Mikuni. By the survey, a vertical but relative movement of the land-blocks along this fault was proved to be still continued up to present. Hence, this fault is evidently active.

5) N. Nasu, S. Kawashima, loc. cit.

As bench mark No. 14 was unfortunately missed, the post-seismic movement of the northern part of the intrinsic fault is uncertain. However, a gap seems to exist in the amounts of changes undergone by bench marks Nos. 13 and 15; the depression at the latter point is rather smaller.

An upheaval of 22 mm. is seen at the triangulation point at Shimozeki which lies on the intrinsic fault. Bench mark No. 17 uplifted 43 mm., while in the area south of this point and up to the bench mark in Maruoka (No. 897, GSB), the change is a southward tilt, which roughly corresponds to a tilting of 3 seconds of angle. It is notable that a subsidence of 51 mm. occurred at Maruoka where an upheaval of 194 mm. was once revealed by the first survey made immediately after the earthquake of the last year.

Along the route which run westward from Maruoka to Nishinagata, the subsidence was in general, but at Funayose where the fault passed, an upward movement of the eastern side of this fault occurred relatively to the western such as the vertical dislocation at this point growing still larger.

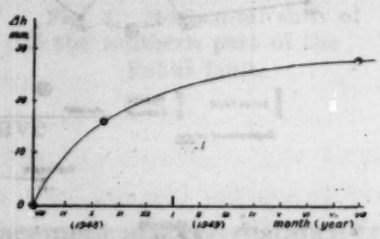

Fig. 5. Subsequent vertical displacement of the Fukui fault.

On the Hokuriku Highway, a remarkable uplift of 57 mm. is seen at Takayanagi (No. 898, GSB), while at Yoriyasu (No. 899, GSB) an upheaval of 28 mm., the former place lies on the eastern (uplifted) side of the fault and the latter on the western (subsided) side. It must be remembered that the fault was most pronounced near Takayanagi, the relative vertical displacement which occurred between bench marks at these two places was determined to be 755 mm. by the first post-seismic survey[6]. Since then this vertical dislocation was increased by 28 mm. This vertical displacement, however, gradually decelerated with time as shown in Fig. 5. A similar fact has been already pointed out by C. Tsuboi for the seismic faults in the Tango and Izu districts.

An increase of the vertical displacement of the same kind which occurred subsequently can be seen also in the southern part of the fault traversing the leveling route between Kaminaka (No. 5256) and Shimbo (No. 5257). There is an increase of 14 mm. of the relative height of the bench marks at these places during these ten months.

Subsequent displacement along the fault. From the experience gained in the past and the recent earthquakes, the following fact has been found as to the vertical displacement of the seismic fault. In general, most of the

6) N. NASU and also T. NAGATA, A. OKADA, see 1).

7) C. TSUBOI, *Japanese Journ. Astro. Geophy.*, **10** (1932—33).

vertical displacement occurred at the time of the main earthquakes, while the remaining displacement occurred subsequently during several months or years. So far as known at present, the subsequent displacement was in the same sense as that at the time of the earthquake. For the Gōmura (appeared in 1927), Yamada (1927), Tanna (1930) and Fukui (1948) faults, the rates of the subsequent displacement to the initial displacement at the time of catastrophe are listed as below.

Fault	Vertical displacement		Subsequent / Initial	Period of subsequent displacement
	Initial	Subsequent		
	cm.	cm.	%	month
Gōmura	75	1.7	2.3	39
Yamada	114	3.0	2.6	39
Tanna	7	1.9	37.0	8
Fukui	75	2.8	3.7	12

It is noteworthy that in the Tanna fault, the subsequent vertical movement was far larger than those of the other faults. The movement of this fault at the time of the earthquake was mostly in a horizontal direction and it seems that the vertical motion was relatively active during the subsequent period.

It should be added that although in the present Fukui fault, the fault-line itself was intercepted to the naked eye, the crustal deformations undergone by both sides of the fault showed no particularly different characters when they were compared with the case of the clearly traceable seismic fault. We have experienced that there exists a new kind of the seismic fault which is called the intrinsic seismic fault as mentioned in this paper.

After the dissolution of the Special Investigation Committee of the Fukui Earthquake in March, 1949, the study of the post-seismic topographical changes was made personally by the writer with the Fund for Scientific Research of the Ministry of Education. To establish the general character of the seismic fault, the study will be extended further to the faults which made their appearances at the past great earthquakes.

6. *Observations of the Deformation of the Earth's Surface at Aburatsubo, Miura Peninsula. Part II.*

By Takahiro HAGIWARA, Tsuneji RIKITAKE, Keichi KASAHARA and Juhei YAMADA,

Earthquake Research Institute.

(Read March 29, 1949.—Received Apr. 20, 1949.)

1. In the previous paper[1], the writers reported briefly the outline of the observation at Aburatsubo, which was commenced since the beginning of 1948. Periodic deformation of the earth's surface was remarkably observed there, being as shown, for example, in Photo. 1. The deformation

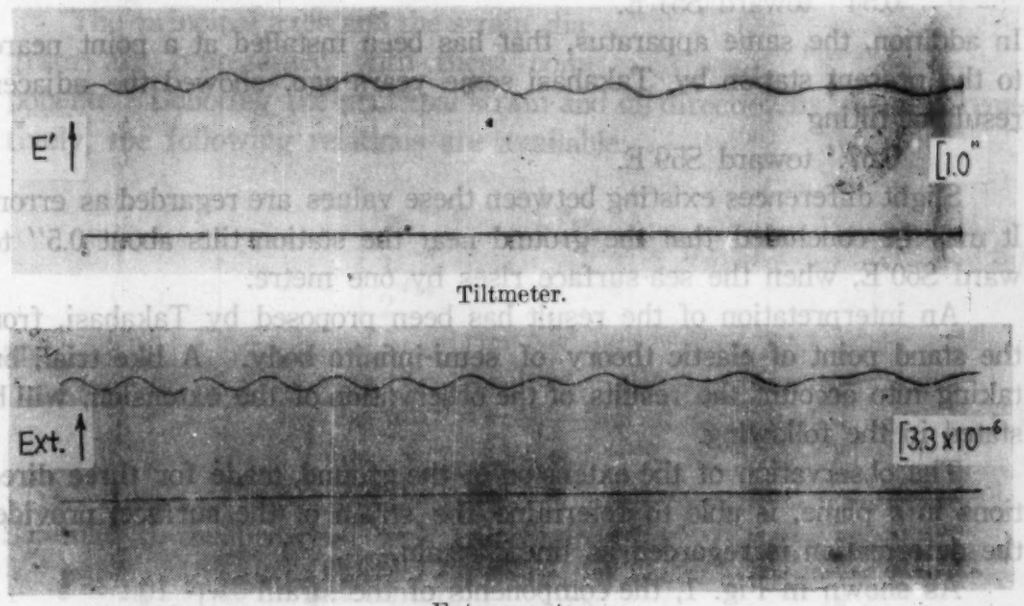

Tiltmeter.

Extensometer

Photo. 1.

was considered to be due to the variation of the load of sea-water, because the records showed remarkable parallelism between the mode of variation of the ocean tide and extension as well as the tilting of the earth's surface. As already pointed out by R. Takahasi[2], there can be no other causes of such deformation.

1) T. HAGIWARA, T. RIKITAKE and J. YAMADA, *Bull. Earthq. Res. Inst.*, **26** (1948), 23.
2) R. TAKAHASI, *Bull. Earthq. Res. Inst.*, **6** (1929), 86.

2. As already stated, the observation is made for the tilting in two components and for the extension in three directions. It would be sufficient to determine the mode of the deformation in horizontal plane by these observation, if the deformation be regarded as infinitesimal.

As to the tilting, the mode is represented with the direction and the amount of maximum tilting. A pair of water-tube tiltmeters records the tilting amounting to

0.04″ downward to the direction S′ (S22°W)

and

0.51″ downward to the direction E′ (E9°S),

when the sea-surface rises by one metre. Hence the resultant tilting is

0.53″ downward to S64°E,

when the sea-surface rises by one metre. While, the observation with the Ishimoto's all-silica tiltmeters record the resultant tilting

0.54″ toward S51°E.

In addition, the same apparatus, that has been installed at a point nearer to the present station by Takahasi some years ago, showed the adjacent resultant tilting

0.67″ toward S59°E.

Slight differences existing between these values are regarded as errors. It may be concluded that the ground near the station tilts about 0.5″ toward S60°E, when the sea-surface rises by one metre.

An interpretation of the result has been proposed by Takahasi, from the stand point of elastic theory of semi-infinite body. A like trial, but taking into account the results of the observation of the extension, will be stated in the following.

The observation of the extension of the ground, made for three directions in a plane, is able to determine the strain of the surface, provided the deformation is regarded as linear strain.

As shown in Fig. 1, the components of the strain are denoted by e_{xx}, e_{yy}, and e_{xy}. The extension in any direction i will be given, then, by

$$e_i = e_{xx}l^2 + e_{yy}m^2 + e_{xy}lm, \quad \cdots\cdots\cdots(1)$$

where l and m denote the direction cosines of the direction i, taken to the x, y axes. Substituting in l, m the actual values of the direction of N′S′, E′W′, and $8m$ component (which, for the brevity, are named as 1, 2, 3, respectively), we can obtain the components of the strain as the solutions of the next equations,

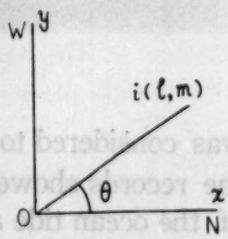

Fig. 1.

$$\left.\begin{aligned} e_{xx} &= 0.5858e_1 - 0.1967e_2 + 0.6111e_3, \\ e_{yy} &= 0.1981e_1 + 1.0397e_2 - 0.2399e_3, \\ e_{xy} &= -1.348e_1 - 0.0642e_2 + 1.412e_3. \end{aligned}\right\} \quad \cdots\cdots(2)$$

According to the observation with the extensometers, we get,

$$\left.\begin{aligned} e_1 &= 0.07 \times 10^{-6} \\ e_2 &= 1.44 \times 10^{-6} \\ e_3 &= 0.94 \times 10^{-6} \end{aligned}\right\} \quad \cdots\cdots(3)$$

for the rise of the sea-surface by one metre, which mode can be seen in Fig. 2. Therefore, the components of the strain become

$$\left.\begin{aligned} e_{xx} &= 0.33 \times 10^{-6} \\ e_{yy} &= 1.35 \times 10^{-6} \\ e_{xy} &= 1.09 \times 10^{-6}. \end{aligned}\right\} \quad \cdots\cdots(4)$$

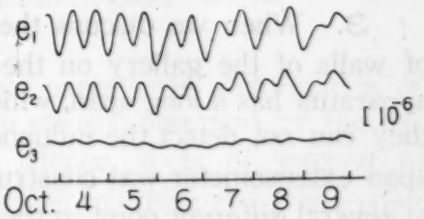

Fig. 2.

The principal axes and the strain diagram are represented with these components. Denoting the principal strain and its direction by e and θ respectively, the following relations are available,

$$\begin{vmatrix} e_{xx} - e & \frac{1}{2}e_{xy} \\ \frac{1}{2}e_{xy} & e_{yy} - e \end{vmatrix} = 0 \quad \cdots\cdots(5)$$

and

$$\tan\theta = -\frac{e_{xx} - e}{\frac{1}{2}e_{xy}}. \quad \cdots\cdots(6)$$

Solving (5), the principal axes are obtained as

$$\left.\begin{aligned} e &= 1.61 \times 10^{-6} \quad \text{(maximum)} \\ &\quad 0.07 \times 10^{-6} \quad \text{(minimum).} \end{aligned}\right\} \quad \cdots(7)$$

The strain ellipse is calculated from (1) as shown in Fig. 3.

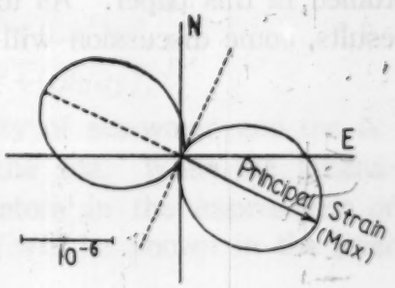

Fig. 3.

It must be noticed that one of the principal axes (maximum) lies in nearly the same direction with that of the maximum tilting, given in the later paragraph. This fact is quite suggestible, though the discussion of its physical meaning will be postponed.

Succeeding to the horizontal extensometers, a vertical one was installed in the same station. The observation with it revealed also an interesting result. It detects the contraction of the ground, when the sea-surface rises, that is,

$$e_{zz} = -1.53 \times 10^{-6} \quad \text{(by one metre rise of sea-surface)} \quad \cdots\cdots\cdots(8)$$

With the aid of (4), the volume dilatation is calculated, amounting to only

$$D = e_{xx} + e_{yy} + e_{zz} = 0.15 \times 10^{-6}, \quad \cdots\cdots\cdots\cdots\cdots\cdots(9)$$

which is regarded as to be zero. This result should be taken into account when we discuss the phenomena theoretically.

3. When we discuss the deformation, the influence of the existence of walls of the gallery on the deformation should be considered. As the apparatus has a long span, which is comparable to the length of the gallery, they can not detect the influence by themselves. For this reason, a short-span extensometer was constructed, and a series of observation were made at several different point in the gallery, in the same direction with one of the long-span apparatus. The observation was made for one or two weeks at each point, and the observed amplitudes was compared with that of the long-span extensometers. Numbers written in Fig. 4 shows the ratio of the both amplitudes, its situation in the figure and the direction of the bar representing the place and the direction where the observation was made. As can be seen in the figure, the irregularity of the amplitudes is not so clear in the gallery, and we may ignore the effect of the cavity due to the gallery, in the present case.

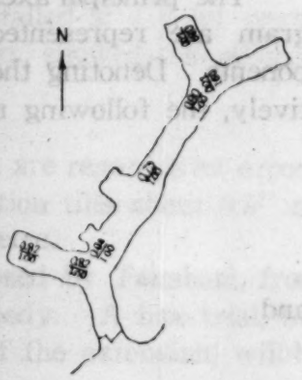

Fig. 4.

4. The mode of periodic deformation of the earth's surface has been studied in this paper. As to the theoretical interpretation of the observed results, some discussion will be made in the following paper.

7. *Observations of the Deformation of the Earth's Surface at Aburatsubo, Miura Peninsula. Part III.*

By Takahiro HAGIWARA, Tsuneji RIKITAKE, Keichi KASAHARA and Juhei YAMADA,
Earthquake Research Institute.

(Read March 29, 1949.—Received Oct. 20, 1949.)

1. As already described in the previous paper[1], the deformation of the earth's surface caused by ocean-tide is clearly observed by the extensometers as well as by the tiltmeters. Hence, it is of interest to study how well the deformation may be explained from the stand-point of the theory of elasticity. The deformation due to ocean-tide, which was observed hitherto only by tiltmeters, was usually interpreted as that of the surface of isotropic and semi-infinite solid under surface tractions. R. Takahasi[2], who observed the tilting motion at the same place, also treated the problem along the above-mentioned line. In the first place, the writers will attempt to interpret the problem with the similar method.

2. It was hitherto considered that when the surface of sea upheaves as high as Δh, the increase of the vertical component of the pressure on the sea-bottom was only effective to the deformation of the earth's surface. It should be borne in mind, however, that there occur the horizontal components in the event of inclined bottom. If we define the increase of the vertical component, the horizontal component to the direction x and y by P_1, P_2 and P_3 respectively, we obtain

$$\left.\begin{aligned} P_1 &= \rho g \Delta h / \sqrt{1+(\partial h/\partial x)^2+(\partial h/\partial y)^2}, \\ P_2 &= -\rho g \Delta h (\partial h/\partial x) / \sqrt{1+(\partial h/\partial x)^2+(\partial h/\partial y)^2}, \\ P_3 &= -\rho g \Delta h (\partial h/\partial y) / \sqrt{1+(\partial h/\partial x)^2+(\partial h/\partial y)^2}, \end{aligned}\right\} \quad \cdots\cdots\cdots(1)$$

where ρ and g denote respectively the density of sea-water and the acceleration of gravity and h is the depth of the sea. When the inclination of the sea-bottom is small, the denominators in the expressions of (1) are regarded as to be equal to unity. As will be shown in the later

1) T. HAGIWARA, T. RIKITAKE, K. KASAHARA and J. YAMADA, *Bull. Earthq. Res. Inst.*, **27** (1949), 35.

2) R. TAKAHASI, *Bull. Earthq. Res. Inst.*, **6** (1929), 86.

paragraph, the horizontal forces acting on the bottom become appreciable in the case of extension or contraction though they can be neglected in the treatment of tilting.

The forces P_1, P_2 and P_3 acting at a point $(x, y, z=0)$ on the surface of semi-infinite elastic body cause some deformations which are easily calculated with the aid of elasticity-theory. The displacements in x, y and z directions due to respective forces are given by

$$\left.\begin{aligned} u_1&=\frac{P_1}{4\pi\mu}\frac{zx}{R^3}-\frac{P_1}{4\pi(\lambda+\mu)}\frac{x}{R(R+z)}\\ v_1&=\frac{P_1}{4\pi\mu}\frac{yz}{R^3}-\frac{P_1}{4\pi(\lambda+\mu)}\frac{y}{R(R+z)}\\ w_1&=\frac{P_1}{4\pi\mu}\frac{z^2}{R^3}+\frac{P_1}{4\pi\mu}\frac{\lambda+2\mu}{\lambda+\mu}\frac{1}{R} \end{aligned}\right\}\quad\text{,}\qquad\text{.....(2)}$$

$$\left.\begin{aligned} u_2&=\frac{P_2}{4\pi\mu}\left(\frac{1}{R}+\frac{x^2}{R^3}\right)+\frac{P_2}{4\pi(\lambda+\mu)}\left\{\frac{1}{R+z}-\frac{x^2}{R(R+z)^2}\right\}\\ v_2&=\frac{P_2}{4\pi\mu}\frac{xy}{R^3}-\frac{P_2}{4\pi(\lambda+\mu)}\frac{xy}{R(R+z)^2}\\ w_2&=\frac{P_2}{4\pi\mu}\frac{zx}{R^3}+\frac{P_2}{4\pi(\lambda+\mu)}\frac{x}{R(R+z)} \end{aligned}\right\}\quad\text{,}\qquad\text{.....(3)}$$

$$\left.\begin{aligned} u_3&=\frac{P_3}{4\pi\mu}\frac{xy}{R^3}-\frac{P_3}{4\pi(\lambda+\mu)}\frac{xy}{R(R+z)^2}\\ v_3&=\frac{P_3}{4\pi\mu}\left(\frac{1}{R}+\frac{y^2}{R^3}\right)+\frac{P_3}{4\pi(\lambda+\mu)}\left\{\frac{1}{R+z}-\frac{y^2}{R(R+z)^2}\right\}\\ w_3&=\frac{P_3}{4\pi\mu}\frac{yz}{R^3}+\frac{P_3}{4\pi(\lambda+\mu)}\frac{y}{R(R+z)} \end{aligned}\right\}\quad\text{,}\qquad\text{.....(4)}$$

where $$R^2=x^2+y^2+z^2$$

and z is taken to be positive inwards. Hence, the extension, the tilting in x direction and the extension in z direction due to the respective forces become as follows:

$$\left.\begin{aligned} \left(\frac{\partial u_1}{\partial x}\right)_0&=\frac{P_1}{4\pi(\lambda+\mu)}\frac{x^2-y^2}{r^4}\\ \left(\frac{\partial w_1}{\partial x}\right)_0&=-\frac{P_1}{4\pi\mu}\frac{\lambda+2\mu}{\lambda+\mu}\frac{x}{r^3}\\ \left(\frac{\partial w_1}{\partial z}\right)_0&=0 \end{aligned}\right\}\quad\text{,}\qquad\text{.....(5)}$$

$$\left.\begin{aligned}
\left(\frac{\partial u_2}{\partial x}\right)_0 &= \frac{P_2}{4\pi\mu}\frac{x(r^2-3x^2)}{r^5} - \frac{P_2}{4\pi(\lambda+\mu)}\frac{3xy^2}{r^5}, \\
\left(\frac{\partial w_2}{\partial x}\right)_0 &= -\frac{P_2}{4\pi(\lambda+\mu)}\frac{x^2-y^2}{r^4}, \\
\left(\frac{\partial w_2}{\partial z}\right)_0 &= \frac{P_2}{4\pi\mu}\frac{\lambda}{\lambda+\mu}\frac{x}{r^3},
\end{aligned}\right\} \quad \cdots\cdots(6)$$

$$\left.\begin{aligned}
\left(\frac{\partial u_3}{\partial x}\right)_0 &= \frac{P_3}{4\pi\mu}\frac{\lambda}{\lambda+\mu}\frac{y(r^2-3x^2)}{r^5}, \\
\left(\frac{\partial w_3}{\partial x}\right)_0 &= -\frac{P_3}{4\pi(\lambda+\mu)}\frac{2xy}{r^4}, \\
\left(\frac{\partial w_3}{\partial z}\right)_0 &= \frac{P_3}{4\pi\mu}\frac{\lambda}{\lambda+\mu}\frac{y}{r^3},
\end{aligned}\right\} \quad \cdots\cdots(7)$$

where $r^2=x^2+y^2$.

The suffix denotes the quantities at the surface.

In the next place, the strain-components are obtained by integrating the expressions (5), (6), and (7) with respect to the actual distribution of land and sea. In the practice, the integrations are carried out with a similar method with that of topographical correction of the torsion-balance[3].

3. Assuming that the surface of sea-water upheaves uniformly, the tilting to the direction E 9° S was obtained as shown in Figs. 1 and 2. In the figures, the effect of the sea-water integrated from the observing-point to the respective distance is taken as the ordinates. The effect of the horizontal forces are so small that the scale in Fig. 2 is taken to be ten times larger than that in Fig. 1. In order to explain the observed tilting, it has

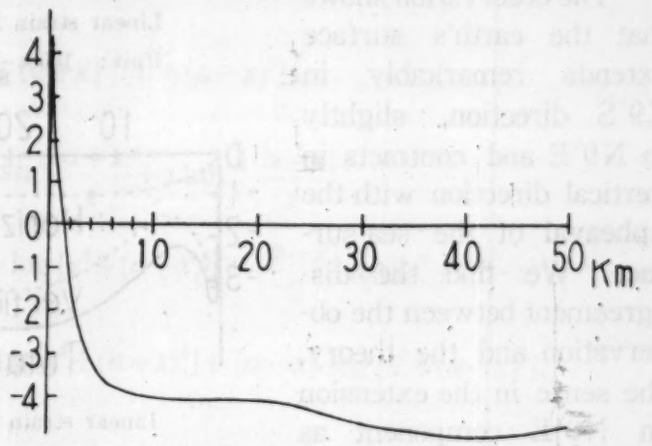

Fig. 1.
Tilting in the direction E 9°S due to the vertical force.
Unit: $100\times\frac{\kappa}{4\pi\mu}\frac{\lambda+2\mu}{\lambda+\mu}\rho g\Delta h$

3) P_2 and P_3 are obtained by making the differences of the depths which are read on the chart. The writers express their hearty thanks to Dr. K. Suda, the Chief of the Hydrographic Bureau, for his kindness of putting the necessary charts at the writers' disposal.

to be assumed that only the water within the range of 100—200 m is effective, the conclusion being the same with Takahasi's one.

On the other hand, assuming $\lambda=\mu$, the extension to E 9° S, and N 9° E was calculated as shown in Figs. 3 and 4. The contribution of the horizontal forces are considerable as seen in the figures. The extension to the vertical direction is also shown in Fig. 5 in which the contribution of the vertical force does not exist.

The observation shows that the earth's surface extends remarkably in E9°S direction, slightly in N9°E and contracts in vertical direction with the upheaval of the sea-surface. We find the disagreement between the observation and the theory, the sense in the extension in N9°E component as well as in vertical one being reversed and their relative magnitude considerably differing each other.

It was found out, thus, that the state of the earth's surface must have a com-

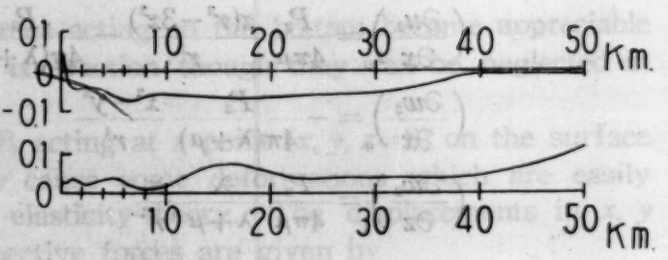

Fig. 2.
Upper: Tilt in the direction E 9°S due to the horizontal force in the same direction.
Lower: Tilt in the direction N 9°E, due to the horizontal force in the perpendicular direction.
Unit: $100\times\frac{\kappa}{4\pi(\lambda+\mu)}\rho g\Delta h$

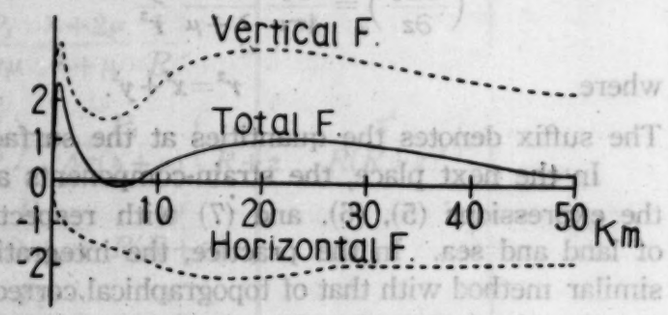

Fig. 3.
Linear strain in the direction E9°S.
Unit: $100\times\frac{\kappa}{8\pi\mu}\rho g\Delta h$

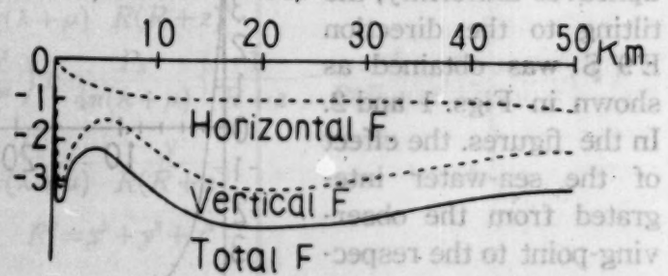

Fig. 4.
Linear strain in the direction N 9°E.
Unit: $100\times\frac{\kappa}{8\pi\mu}\rho g\Delta h$

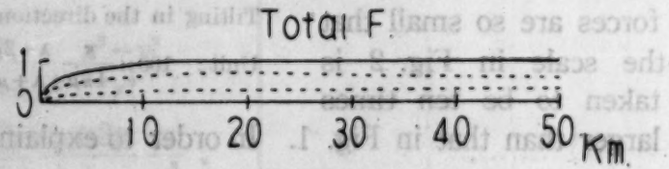

Fig. 5.
Linear strain in the vertical direction.
Unit: $100\times\frac{\kappa}{8\pi\mu}\rho g\Delta h$

plicated structure which is considered to be far from the simple one such as semi-infinite elastic solid. However, it is of great difficulty to decide an adequate model of the earth's surface with which we can satisfactorily explain the observed deformations.

4. We shall next examine the influences of the topography around the observing point. For this purpose, the elastic deformation of a body, the section of which is shown in Fig. 6, were studied in an approximate method, where normal pressure acting on the surface except the raised part. As a result of two dimensional treatment, it was proved without any serious errors that the deformation nearly agrees with that of semi-infinite body under the same traction, provided the height of the raised part is small in proportion to its breadth.

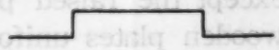

Fig. 6.

If it is supposed that the pressure $-Q$ acts on the surface, which is taken as $z=0$, except the region $-a<x<a$, the x and z components of the displacement of the body are respectively given by

$$u=\frac{Q}{2\pi(\lambda+\mu)}\left\{(a+x)\tan^{-1}\frac{a+x}{z}+|a-x|\tan^{-1}\frac{|a-x|}{z}\right.$$
$$\left.-\frac{z}{2}\log[z^2+(a+x)^2][z^2+(a-x)^2]\right\}$$
$$+\frac{Q}{4\pi\mu}z\log[z^2+(a+x)^2][z^2+(a-x)^2]$$
$$w=-\frac{Q}{2\pi(\lambda+\mu)}\left\{z\tan^{-1}\frac{a+x}{z}+z\tan^{-1}\frac{|a-x|}{z}\right.$$
$$\left.+\frac{a+x}{2}\log[z^2+(a+x)^2]+\frac{|a-x|}{2}\log[z^2+(a-x)^2]\right\}$$
$$-\frac{Q}{4\pi\mu}\{(a+x)\log[z^2+(a+x)^2]+|a-x|\log[z^2+(a-x)^2]\}.$$

Hence, we get at $z=0$

$$u_0=0,$$
$$w_0=-\frac{Q}{2\pi\mu}\frac{\lambda+2\mu}{\lambda+\mu}\{(a+x)\log(a+x)+|a-x|\log|a-x|\}.$$

At $x=0$, it becomes

$$w_{00}=-\frac{Q}{\pi\mu}\frac{\lambda+2\mu}{\lambda+\mu}a\log a.$$

The relative deformation is shown in Fig. 7 in an arbitrary scale. In order to check the above-mentioned theory, an experiment was made by use of agar-agar. An agar-agar model of suitable size, having the cross-section as shown in Fig. 6, was prepared. The surface, except the raised part, was pressed by wooden plates uniformly. Many marks, written on the side of the agar-agar, were photographed and the displacement of the marks were read off from the photograph. As shown in Fig. 8, the relative deformation agrees within limits of errors of the experiment with the theoretically calculated one.

Fig. 7.

Fig. 8.

Summarizing the theoretical and experimental studies described in this section, we are able to say approximately that the deformation in the raised part agrees with that of semi-infinite body under the same pressure. Hence, we may be able to conclude that the actual topography around the observing point approximately satisfies the condition of plain surface and the influence of the topography is small. And the conclusion obtained in the foregoing section will not be seriously affected by the topography.

5. In summary, the deformations due to the tidal load are so complicated that the explanation is not possible by the simple theory in which the earth is treated as a semi-infinite elastic body. A more complete interpretation of the observed results will be made after measuring the distribution of the deformation at various places nearer to the present observing point.

8. *A Petrological Note on the Granitic Rocks near the Cape Ashizuri, Shikoku Island, Japan (II).*

By Ryōhei MORIMOTO,

Earthquake Research Institute.

(Read Sept. 16, 1947—Received Nov. 30, 1949.)

(2) BIOTITE-QUARTZ-MONZONITE (continued):

These porphyritic microperthite[7], 1–2 cm in its dia., are so prominent in this place, that the rock has an extreme persemic appearance, and other constituents such as biotite[8], oligoclase and quartz occur interstitially.

Oligoclase (An 12–17 %) is subordinately prominent in this part; it forms general mass of the rock with quartz, and sometimes it reaches up to 5 mm or more in dia., dirty sericitized cores and lamellar twinning are common in these plagioclase.

The mass of this monzonite is characterized not only by these conspicuous porphyritic microperthite, but also by those in the matrix of the rock. Thus, according to the degree of development of these perthite in the rock, rock facies locally or partially changes from monzonitic granite or quartz-monzonite to the quartz-syenite principally of microperthitic felspar with biotite or green amphibole and interstitial quartz. Near the contact with the hornfels exposed along the high way south of Ohama, the rock becomes siliceous; conspicuous myrmekitic quartz are formed in the peripheries of microperthitic crystals which interfere with neighbouring large quartz grains, and the perthitic felspar in this place does not grow so large as in the above-mentioned porphyritic monzonite. The oligoclase often graduates in its margin into perthitic felspar. Fluorite is found with sepia brown biotite[9], and the pleochroic haloes around zircon enclosures are remarkable in the biotite of the monzonite. At the very contact with the hornfels, the rock facies of the monzonite becomes fine grained; myrmekitic and micrographic textures are developed.

Under the microscope, these porphyritic microperthite are not homo-

---

7) α_D=1.518, β_D=1.522, γ_D=1.525.

8) γ_D=1.666-7, X=Cream yellow (28), Y=Old gold (36), Z=Harzel brown (54)*, X<Y<Z.

9) γ_D=1.667, X=Cream yellow (28), Y=Bronze (38), Z=Sepia (37)* X<Y<Z.

* These numbers are due to WADA's colour chert.

geneous single crystals; large twinned crystals are always composed of several individuals whose orientation are slightly different each other, and the septa between these individual grains consists of relic formed quartz and oligoclase, as shown diagramatically in Fig. 5. It is dangerous to interpret how the mineral grew, judging only from its textural relation observed in thin slices. These microperthite, however, seem to have been formed not at an earlier stage of consolidation of the rock as a phenocryst, but it might have been formed *in situ* at a later stage as a kind of porphyroblast, having included or replaced the earlier formed minerals such as oligoclase, quartz, etc.. If we consider the hypothetic constituents of this monzonite from which all of these perthitic felspar, or of the introduced material that might have converted earlier formed plagioclase to the present microperthite, are removed away, then the biotite-granite or biotite-quartz-diorite principally of oligoclase, quartz with biotite or with or without microcline may be reserved, and the hypothetic pre-existed rock may contain porphyritic large crystals of oligoclase. Postulate that into such hypothetic biotite-granite or biotite-quartz-diorite, alkaline solution capable of forming these perthite or of converting soda-lime felspar to these perthite were immersed *in situ*, the present quartz-monzonite might be formed. And according to the grade of 'alkali-zufuhr,' various rock facies as actually observed in the granitic rock might have appeared. Such a hypothesis of alkali-metasomatism will reasonably explain the petrogenesis of this igneous mass at least as one of the many alternatives. And this postulated pre-existed biotite-granite or biotite-quartz-diorite may be suggested by petrographic features of the remarkable xenoliths in the monzonite that are thought to have been derived from more basic rocks such as gabbro. diabase or diorite whose petrographic characters are quite similar to those of so-called basic xenoliths commonly found in granitic rocks.

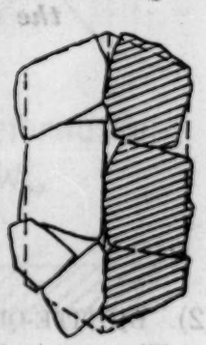

Fig. 5.
(×10)

(3) QUARTZ-SYENITE:

Quartz-syenite composed principally of perthitic felspar with biotite or amphibole and interstitial quartz is exposed areally in the vicinity of Oto and Isa. Boundary between this felspathic syenite and the monzonite could not be traced during his stay there.

Scanty mafic constituents are orange yellow biotite[10] and dull green

10) γ_D=1.673, X=Orange (51), Y=English Red (52), Z=Vndyke Brown (55).

amphibole[11], and the latter intends to take the place of the former in the more felspathic portions. Both minerals often intimately associate with each other to form the clots among the perthitic felspar. Peripheral zone of these amphibole often graduate to the more bluish fringe of lower birefringence. The rock consists mainly of microperthitic felspar (Fig. 6). In this rock also, the large crystals of soda-lime felspar up to about 5mm in diametre are often found among the general mass of microperthitic felspar, 1–2mm in diametres. They usually indicate gradual zoning from sodic oligoclase in cores to albite further to microperthite in margin. In the larger crystals of these microperthitic felspar, central portion of the crystals are clear albite and graduates to microperthitic margin. The smaller crystals, in the other hand, consist essentially of microperthite. The textural relation between those two kinds of felspar is quite reciprocal, compared with the case of "rapakivi granite." As the minor constituents, sphene is most predominant, zircon, fluorite. calcite, iron ore, allanite are succeeding.

Fig. 6. Microperthitic felspar forming the principal portion of the quartz-syenite exposed along the road side west of Isa. Microphoto., analyzer being inserted. (RM 47040359).

The fine grained facies of this felspathic rock are exposed along the road-side west of the tribe of Isa, where the dark bluish green inclusions of rounded or subangular shape are frequently found. They are various in their size, from microscopic dimension to megascopic up to several centimeters in diametres. These inclusions show, in general, the same mineral assemblage with that of the surrounding host rock, and are often considerably rich in coloured minerals. Some are rich in yellowish brown biotite[12], some contain considerable greenish amphibole, and there are also intermediate rock varieties. Detailed description and discussion on the origin of these inclusions will be mentioned in later pages. These inclusions, however, are the same in their origin as the xenoliths remarkedly found in the syenite exposed at the road-cutting between Oto and Isa (Fig. 3–4). Some of them might have been derived from the pre-existing volcanic

11) X=Old Gold (36), Y=Grape Green (161), Z=Dull Viridian Green (145), $c \wedge Z \fallingdotseq 20°$

12) γ_D=1.664, X=Ochraceous Salmon (44), Y, Z=Orange Rufous (45).

rocks and might have been affected by the host rock or by some agencies related to the host rock. And the original rock of these inclusions cannot be found in this vicinity. Blastoporphyritic dirty calcic plagioclase are commonly found in these inclusions. At the very contact with these inclusions, the syenite often changes sharply into aplitic film comparatively rich in quartz.

Through the microscopic observation on the quartz-monzonite and the quartz-syenite, general trend may be considered in the paragenic relation between coloured minerals and the felspathic constituents; sepia brown biotite are associated with the oligoclase in the monzonitic facies, orange yellow biotite with dull greenish amphibole are associated with the partially microperthitic felspar in which clear albite cores are still reserved. In the more felspathic rock composed principally of microperthite, greenish pyroxene appears.

(4) BASIC INCLUSIONS IN THE QUARTZ-MONZONITE:

One of the remarkable petrographic features of this igneous mass is the common occurrence of basic xenoliths as well as that of syenite. They are resembled in many respects to so-called basic inclusions commonly found in contaminated granitic rocks. The most representative type of this rock is exposed along the curved road 500 m west of Matsuo. The similar rock is also exposed at the seashore south of Isa. And the more melanocratic varieties are found as subangular xenoliths, about 50 cm or more in dia., in the porphyritic biotite-quartz-monzonite exposed at the road side 500 m south of Shirobae, western side of the peninsula. On these basic inclusions[13], it may be unnecessary to describe in detail here, for these rocks have been much debated by petrologists. The only thing to be discriminated from basic xenoliths in granite for these inclusions is the perthitic felspar permeating in these xenoliths. The blastoporphyritic calcic plagioclase are characteristic to these rocks (Fig. 7). (To be continued).

Fig. 7. Blastoporphyritic plagioclase in basic xenolith. Microphotographed analyzer being inserted. (RM 47040464)

13) This ajective "basic" must be discussed from the petrogenetical standpoint. Here, it is conveniently used.

9. *On the Coda Waves of Earthquake Motions. (Part 4.)*

By Syun'itiro OMOTE,

Earthquake Research Institute.

(Read Feb. 15, 1940. — Received Nov. 30, 1949.)

Chapter 5. Periodgram Analysis of Coda Oscillations.

§ 18. In the preceding Chapters[1] studies have been made on the coda oscillations of 53 earthquakes, and their predominant periods have been determined from the curves of the successive one minute means of the periods of coda oscillations. In the present Chapter, with a view of establishing more definitely the periodicities in coda oscillations, a method of periodgram analysis has been resorted to.

The amplitudes of coda waves measured at equal intervals of time have been represented by the sequence $u_0, u_1, \ldots\ldots$. To test the existence in sequence of a periodicity with the period extending over p consecutive terms of the sequence, we will write down the $u's$ in order in horizontal lines, each of which will contain p $u's$. Seen vertically the completed diagram will be found to contain p columns and n rows. We will add up the terms in the individual vertical columns, and denote the sums by $U_0, U_1, \ldots\ldots, U_{p-1}$. Then, dividing these sums by n, we obtain the means $N_0, N_1, \ldots\ldots, N_{p-1}$ of the values of u in the individual columns. If the tentative period p should fall near the actual period of the oscillations, the difference between the greatest and the smallest numbers of the sequence $N_0, \ldots\ldots, N_{p-1}$ would have a large value. This difference we call "the amplitude" of the sequence $N_0, \ldots\ldots, N_{p-1}$ corresponding to the trial period p. Taking p as abscissa and the amplitude as ordinate, we get the periodgram for the trial period p.

§ 19. In the neighbourhood of the true period p, when the trial period is not a whole number of the unit of time but is, say, $p+0.5$, for the purpose of finding out the amplitude of that trial period, T. Whittaker[2] suggested modifying the arragement of $u's$ slightly so that terms in the same phase might be found in the same vertical column. But according to his method a u in the second row is not exactly in the same phase as that of the first row in the same vertical column, the difference of the

1) S. OMOTE, *Bull. Earthq. Res. Inst.*, **21** (1943) 458, **22** (1944), 140, **23** (1945), 47.

2) E. T. WHITTAKER and G. ROBINSON, "The Calculus of Observations." (1926), 343.

two being by no means small, especially when p is smaller than 5.[3]

In such a case, two classes of $u's$ must be distinguished in one vertical column, and the sums of each class of $u's$ must be worked out separately; the sum of the $u's$ in odd rows, and the sum of the $u's$ in even rows. Thus we get two sequences of $N's$, namely, N odd's and N even's. If we denote by $\mathfrak{N}_{od}$ and $\mathfrak{N}_{ev}$ the amplitudes of the two respective sequences, the amplitude for the trial period $p+0.5$ can be given more accurately by $\mathfrak{N}=\mathfrak{N}_{od}+\mathfrak{N}_{ev}$. For the convenience of calculation the author suggests the following manner of arrangement of $u's$ to give the amplitude for the trial period $p+0.5$:

$$
\begin{array}{llllllll}
u_0, & u_1, & \cdots\cdots & u_{p-1}, & u_p, & u_{p+1}, & \cdots\cdots & u_{2p-1}, \quad u_{2p} \\
u_{2p+1}, & u_{2p+2}, & \cdots\cdots & u_{3p}, & u_{3p+1}, & u_{3p+2}, & \cdots\cdots & u_{4p}, \quad u_{4p+1} \\
\cdots\cdots & & & & & & & \\
\cdots\cdots & & & & & & & \\
u_{2(m-1)p+m-1}, & \cdots\cdots & u_{(2m-1)p+m-2}, & u_{(2m-1)p+m-1}, & u_{(2m-1)p+m}, & \cdots\cdots & u_{(2m)p+m-1}. &
\end{array}
$$

Sums.	U_0,	U_1,	.....	U_{p-1},	U_p,	U_{p+1},	.....	U_{2p-1}, U_{2p}
1/m of $U's$.	M_0,	M_1,	.....	M_{p-1},	M_p,	M_{p+1},	.....	M_{2p-1}, M_{2p}

The $u's$ are to be written in horizontal rows of $2\times(p+0.5)$ terms each, and terms in vertical columns are to be added up, yielding the sums $U_0, \cdots\cdots, U_{p-1}, U_p, \cdots\cdots, U_{2p-1}, U_{2p}$. Divinding these sums by m (which is a number of horizontal rows) we obtain the means $M_0, \cdots\cdots, M_{p-1}, M_p, \cdots\cdots, M_{2p-1}, M_{2p}$ of the values of $u's$ in the individual columns.

Table I.

Earthquake that the periodgram analysis was executed and its portions in which the analysis was made.

Earthq. No.	Date	Epicenter	Epicentral distance	Portions studied
			km	m m m m
16	1925 III 31	Siwoyasaki	259	6~ 7, 8~10
20	1936 II 21	Kôti-Yamato	391	11~13
54	1941 XII 17	Kagi	2230	22~29, 30~37
36	1938 V 20	Celebes	4500	42~44, 52~53
37	1938 V 13	New Guinea	4600	55~56, 80~83, 102~103
49	1937 XII 23	Mexico	11600	80~83
51	1937 VI 21	Peru	14900	69~75, 123~126
52	1936 VII 13	Chili	16800	64~70, 78~81, 138~141

3) S. OMOTE, *Special Bulletin of the Earthq. Res. Inst.*, No. 7 (1949), 7.

If we denote by $\mathfrak{M}_1$, and $\mathfrak{M}_2$ the amplitudes of the two sequences M_0, ..., M_{p-1} and M_p, ..., M_{2p} respectively, the most reasonable amplitude for the trial period $p+0.5$ will be given by $\mathfrak{M}=\mathfrak{M}_1+\mathfrak{M}_2$.

§ 20. In this manner periodgrams have been prepared for the eight selected earthquakes (Table I), two of which had epicentral distances less than 1,000 km, one about 2,000 km, two others about 4,000 km, and the remaining three exceeding 10,000 km. The amplitude for each trial period

Table II.

Amplitudes $\mathfrak{M}$ for respective trial period p of each portions.

Earthq. No.	No. 16		No. 20	No. 54		No. 36		No. 37			No. 49	No. 51		No. 52		
Portion / p	6 ~ 7	8 ~ 10	11 ~ 13	22 ~ 29	30 ~ 37	42 ~ 44	52 ~ 53	55 ~ 56	80 ~ 83	102 ~ 103	80 ~ 83	69 ~ 75	123 ~ 130	64 ~ 70	78 ~ 81	138 ~ 141
5	64.5	103.8	117.6	8.4									0.34			
6	115.2	84.9	69.6	6.6	5.3								1.01			
6.5		168.2														
7	89.3	118.9	298.6	11.6	7.1								0.29			
7.5		77.0	222.7		19.3											
8	221.7	363.8	148.9	13.5	17.4								1.19			
8.5		130.1		65.3	14.2											
9	125.4	131 8	83.8	40.3	23.5								1.23			
9.5				115.8	46.2											
10	113.7	101.8	153.1	118.4	47.5			27.4					0.94	15.8	9.1	
10.5				88.6	39.7											
11	80.7	89.4	139.4	70.1	15.9								0.95			
11.5					10.7											
12	130.3	109.9		57.3	23.9	106.4	77.0	24.0	16.7	9.6	34.9		1.23	11.2	10.1	19.3
12.5					23.4											
13				9.1	16.6	140.8	58.3	27.5	22.1	10.5	31.5		0.62			
13.5					18.9											
14			178.6	15.6	8.7	193.8	149.7	44.4	29.2	25.6	27.7	16.7	3.55	63.4	21.3	29.3
15			144.6	45.3	15.6	141.0	100.8	73.8	18.3	32.1	37.8	17.7	4.20	57.2	36.8	45.9
15.5												42.0		128.9	22.5	
16			92.5	91.4		117.1	64.3	51.3	72.7	32.9	158.2	46.3	10.03	133.0	28.7	115.6
16.5												59.2	5.20	60.5	70.8	
17			157.1			111.0	100.7	17.6	38.2	34.7	130.7	66.9	3.37	89.0	123.6	58.8
17.5												52.0			54.2	
18				22.6		215.3	122.2	19.2	32.1	21.2	112.5	94.6	3.49	397.1	40.8	
18.5												44.9			92.7	
19			136.9			264.4	175.3	31.4	45.8	10.5	33.3	17.9	2.57	141.0	108.7	36.6
19.5															90.9	
20			186.9			256.1	106.9	63.5	38.5	7.8	18.0	18.5		90.9	58.0	31.3
21						273.7	71.0	50.2	81.3	10.5	58.6	65.5		212.2		
22						125.0	33.2	49.3	22.0		61.1	23.7		117.6		
23												26.4				

will be seen in Table II. The curves for the periodgrams will be reproduced in Figs. 1~16. Generally speaking, the periods obtained from periodgram analysis have been found to coincide fairly well with the

Fig. 1.
No. 16 (Siwoya-Saki) 6 min~7 min.

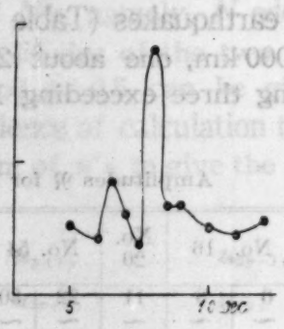

Fig. 2.
No. 16 (Siwoya-Saki) 8 min~10 min.

predominant periods determined in the preceding chapters from the curves of successive one minute means of periods of the respective earthquakes.

With regard to some figures two peaks are seen in a curve. For instance Celebes earthquake (Figs. 6, 7) has two peaks at 14 sec. and 19 or 20 sec. New Guinea earthquake (Figs. 8, 9 and

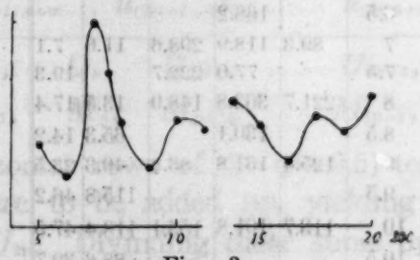

Fig. 3.
No. 20 (Kôti-Yamato)
11 min~13 min.

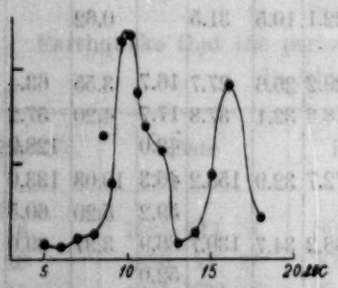

Fig. 4.
No. 54 (Kagi) 22 min~29 min.

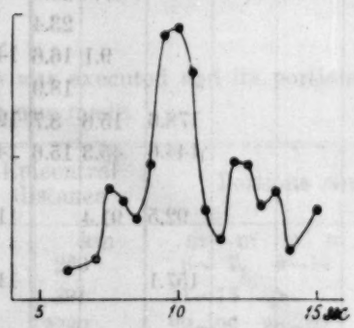

Fig. 5.
No. 54 (Kagi) 30 min~37 min.

10) at 15~16 sec. and 20~21 sec. The periodgrams of the first coda waves of extremely distant earthquakes such as Mexico (Fig. 11), Peru (Fig. 12) and Chili (Figs. 13, 14) earthquakes also show two high peaks. Of these two peaks, one is always seen at a period that agrees well

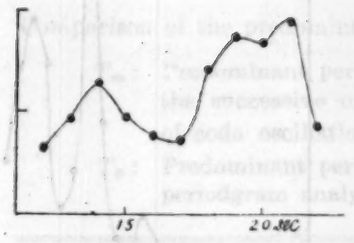

Fig. 6.
No. 36 (Celebes) 42 min~44 min.

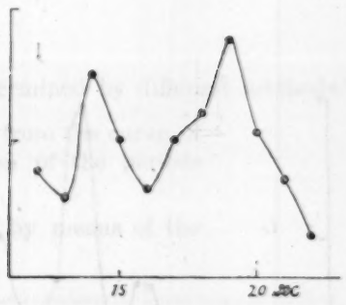

Fig. 7.
No. 36 (Celebes) 52 min~53 min.

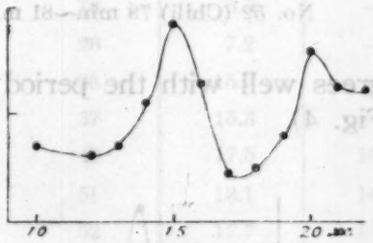

Fig. 8.
No. 37 (New Guinea) 55 min~56 min.

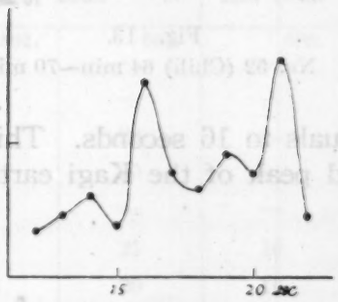

Fig. 9.
No. 37 (New Guinea) 80 min~83 min.

with the predominant period of the same earthquake determined in the preceding chapters, while the other peak is seen at the period T equals to about 20 seconds in all earthquakes regardless of the difference in their epicentral distances. Contrary to this the periodgrams on the second coda waves of extremely distant earthquakes such as Peru and Chili earthquakes (Figs. 15, 16) show a very high single peak at

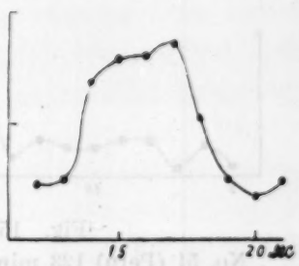

Fig. 10.
No. 37 (New Guinea)
102 min~103 min.

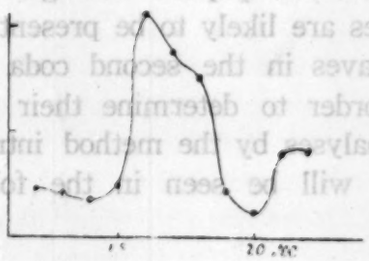

Fig. 11.
No. 49 (Mexico) 80 min~83 min.

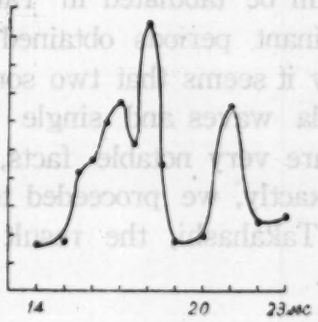

Fig. 12.
No. 51 (Peru) 69 min~75 min.

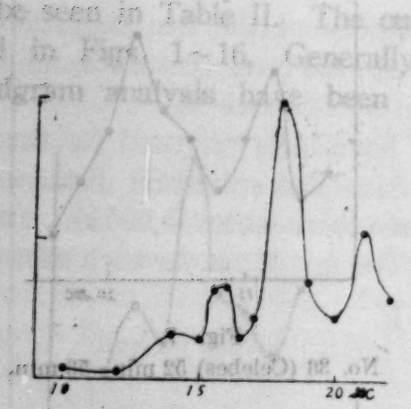

Fig. 13.
No. 52 (Chili) 64 min~70 min.

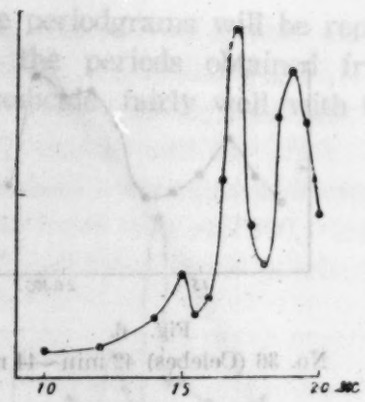

Fig. 14
No. 52 (Chili) 78 min~81 min.

T equals to 16 seconds. This period agrees well with the period of the second peak of the Kagi earthquake. (Fig. 4).

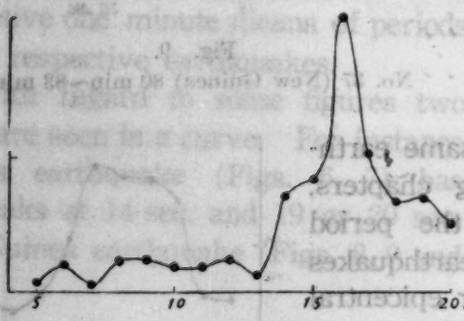

Fig. 15.
No. 51 (Peru) 123 min~130 min.

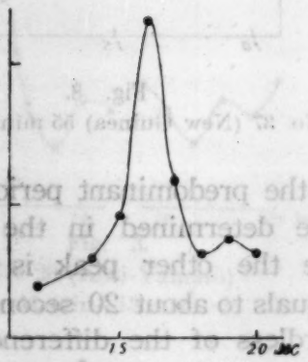

Fig. 16.
No. 52 (Chili) 138 min~141 min.

Predominant periods determined by means of these periodgram analyses will be tabulated in Table III and for the purpose of comparison predominant periods obtained in the previous papers[4] are given also. Anyhow it seems that two sorts of waves are likely to be present in the first coda waves and single sort of waves in the second coda waves. These are very notable facts, and, in order to determine their periods more exactly, we proceeded to make analyses by the method introduced by K. Takahashi, the result of which will be seen in the following chapter.

4) S. OMOTÉ, *loc. sit.*, 1).

Table III.

Comparison of the predominant periods determined by different methods.

T_m: Predominant period determined from the curve of the successive one minute mean of the periods of coda oscillations.

T_p: Predominant period determined by means of the periodgram analysis.

Earthq. No.	T_m		T_p		
	1st coda	2nd coda	1st coda		2nd coda
	sec.	sec.	sec.	sec.	sec.
16	6.5	—	8	—	—
20	7.2	—	7	—	—
36	15.9	—	14	20	—
37	15.3	—	15	20	—
49	17.5	16.9	16	—	—
51	18.1	16.5	18	21	16
52	17.7	16.6	18	20	16

10. Earthquake Damages in Yokohama City Due to the Great Kwanto Earthquake of September 1, 1923.

By Syun'itiro OMOTE,

Earthquake Research Institute.

(Read April 19, 1949. — Received Nov. 30, 1949.)

1. On the extensive damages done by the Great Kwanto Earthquake of 1923, detailed investigations have been made over the wide area of the affected regions and voluminous reports have been published. But, strangely enough, the city of Yokohama remained an exception among these regions, and precise aspects of the earthquake damages within the city are scarcely known. No map of Yokohama City showing the distribution of damaged houses within the city has yet been published.

This is not without reason, for although the destroyed houses in Yokohama were so numerous, the fire that broke out soon after the shock burnt down almost eightly per cent of the whole city, so that sufficient materials could not be collected to make possible the investigation of the distribution of destroyed houses, and accordingly no careful study of the damages in the city has ever been carried out.

2. But recently a new interest is being entertained by seismologists as to whether there is any close relation between earthquake damages and the condition of the ground of the place, and it is being earnestly desired that details should be made clear about the distribution of the damages in Yokohama City at the time of the Kwanto Earthquake.

With a view to providing an answer to these demands the present writer collected as many materials as possible that are likely to throw light on the study of earthquake damages in Yokohama, and attempted from them to draw a map to show how the damages were distributed in the city. As some of these materials were reliable enough while others were not, we examined them minutely and came to the conclusion that the numbers of the totally destroyed wooden houses were the most dependable indices to represent the degree of earthquake damages objectively and accurately.

For convenience sake we divided the city into small portions following the administrative division and we took each "cho" (an area bound-

ed by streets) as the unit area of the division. There existed about 150 cho's at the time of the Kwanto Earthquake, their average area was about $(500\ \mathrm{m})^2$, and the average number of wooden houses in each cho was assumed to be about three hundred. In these respects, cho has been considered the most suitable unit division in calculating the percentage of destroyed houses.

3. We have looked up as many materials as possible and worked out the numbers of totally destroyed wooden houses in each of the unit areas. As the total numbers of the wooden houses in the respective unit areas are to be known from the statistical reports published before the earthquake by the prefectural authorities, the percentage of the totally destroyed houses in each unit area can also be easily calculated. We will call this percentage the "seismic damage rate". It is tabulated in Table I. The figures in brackets in column A are the presumed numbers of the totally destroyed houses where only the ratios of the destroyed houses instead of their real numbers had been given in the literature consulted. Materials used for the preparation of Table I are listed after the table.

Table I.

Seismic damage rate in Yokohama due to the Kwanto Earthquake of 1923.

A; Numbers of totally destroyed houses.
B; Numbers of half destroyed houses.
C; Total numbers of wooden houses.
D; Percentag of totally destroyed houses.
L; Literatures refered to.

Name of unit area	A	B	C	D	L
Isezaki	(69)		106	65	C
Tan-machi	(180)	Ca 20	261	70	C
Sueyoshi 2	(415)		61	90	C
Hisakata	(42)		65	70	C
Naniwa, Umegae	(92)		02	90	C
Sugatami	(66)		83	80	C
Wakatake	(48)		53	90	C
Ashibiki	155		178	88	C
Yoshioka	400		450	89	C
Suruga	(64)		81	80	C
Kumoi	(198)		248	80	C
Horai	(196)		207	95	C
Chojamachi 1-4	(442)		525	85	C
" 6	(45)		50	90	C
" 8	(262)		291	90	C
Fukutomi	(646)		808	80	C
Takasago, Futaba	—		—	75	C

(to be continued)

Table I. (*continued.*)

Name of unit area	A	B	C	D	L
Sakuragi	(123)		130	95	C
Hidemachi 1-3	(84)		120	70	C
South-Ota Azuma-kôchi	2		561	0.4	C
„ Kasumiya, Hara-Kôchi	43	270	789	5.5	C
„ Yaichi-Buraku	(300)		600	50	B
Kumyoji	(60)		180	33	C
Tobe 1	(40)		80	50	G
„ 2	(151)		171	90	C
„ 3	(192)		383	50	C
„ 4	(360)		400	90	C
„ 5	(151)		216	70	C
Takashima 1-10, Ura-Takashima	(420)		478	90	C
South Sengencho	(175)	(400)	700	90	C
„ Shimonoshita Gyoyunagaya	(83)		93	25	C
„ Sanshu-nagaya	—		—	90	C
Okano	(721)		1044	70	G
South Saiwaicho	(1800)		2000	90	C
Hiranuma	(1010)		1122	90	C
Okano, Hiranuma	—		—	90	H
Oimatsu	3		61	1	B
Hanasaki	1		10	10	B
Nishitobe	(495)		9810	50	C
„ Oogida, Uzawa	(109)		1389	8	G
Sannô-yama	70		772	9	C
Tidesman's hous group.	21		25	84	B
Prefectural officer's hous group	(130)		146	90	B
Nishi Tobe-Furuido	20		830	24	C
Kubo	(650)	(650)	1300	50	C
Masago	(140)		201	70	C
Sumiyoshi	(315)		396	80	C
Aioi	(281)		296	95	C
Oota	(175)		250	70	C
Benten	(150)		166	90	C
South-Nakatôri	(115)		128	90	C
North Nakatôri	21		24	87	B
Hommachi	(124)		155	80	C
Motohamachi	(103)		129	80	C
Kaigan-dôri 1	21		27	78	B
Sakai	(48)		53	90	C
Yoshihama	(260)		323	80	C
Matsukage	(352)		705	50	C
Kotobuki	(322)		460	70	C
Oogi	225		145	50	C
Okina	(231)		298	80	C
Furo	(445)		557	80	C
Banda	(124)		155	80	C
Sankichi	(574)		820	70	C
Chitose	(276)		345	80	C
Yamada	—		—	60	C
Fujimi	(222)		370	60	C
Hagoromo	(296)		448	60	G
Yamabuki-front stree t	(122)		153	80	C
„ -back street	(30)		76	40	C
Magane, Eiraku	(398)		419	95	B
Magane	(75)		83	90	E
South-Yoshida 4-7	(4900)		5439	90	C
„ East part	(2080)		2600	80	C
„ West part	(2340)		2600	90	C
„ South part	(126)		139	93	C

(*to be continued.*)

Table I. (*Continued.*)

Name of unit area	A	B	C	D	L
Ryuzu-Hama, Kamie	(133)		404	33	C
Isogo-hama	150	200	500	30	C
Maita; Enoki-Tsubo	(40)		50	80	C
„ other	0		223	0	G
Ooka	(344)		688	50	C
„ Nakano, Kunôshita	2	32	62	6	B
Kitagata; Chiyozaki Izumi	(1442)		2060	70	C
„ Nishinoya level part	180	400	580	30	C
„ „ hill	7	80	204	7	C
„ Kominato	(67)		222	30	C
Amanuma and Suwa	—		—	30	C
Hommoku; level land	—		} 830	80	B
„ hill	—			40	B
„ 1	(291)		970	30	C
„ 2	(975)		1300	75	C
Negishi; Mugita and others	(1560)	(660)	2224	70	C
„ northern part	(1110)	(660)	1850	60	C
„ Southern part	(80)		800	10	C
Nakamura; Western part	(640)		1600	40	C
„ Nakai-Yamaya	(1110)		3700	30	C, B
„ Yamate Nakamura	(73)		1462	5	C
Ishikawa, Nakamachi	(400)	(1190)	1973	20	C
Aoki; Takinoshita, Takara	0		190	0	C
„ Miyanosu, Ono	(81)		163	50	C
„ Hichikencho	153		219	70	C
„ Hichikencho 3610	—		—	95	C
„ „ 2	40		147	17	C
„ Upper Daimachi	1	8	160	0.3	C
„ Lower Daimachi	(19)		192	10	C
„ Tsuruya	6	(274)	280	2	C
„ Motomachi	1		147	0.7	C
„ Kôgaya, Iwasaki	0	(100)	340	0	C
„ Miya, Taki, Yoko	0		317	0	C
„ Uperp Tammachi and other	0	23	780	0	C
„ Lower Tammachi	6		350	2	C
„ Tammachi 1	40		500	8	B
„ Hinodai	17		236	7	C
„ Oota	4	20	210	2	C
„ Karuisawa	Ca 50	Ca 250	570	9	C
Aoki; Matsumoto and other	4	20	290	2	C
„ „ „	3		163	3	C
Takashima 9-10	(75)		107	70	C
Kanagawa; Shimmachi	28		650	4	C
„ Urashima	7	5	339	2	C
„ Myojin Chiwaka	26		74	35	C
„ Inaricho	(144)		160	90	C
„ „	(80)		160	50	G
„ Tate, Saito-bun	0		246	0	C
„ Urashimaoka	41		173	24	C
„ Yanagi	40	50	400	10	C
„ Hakuraku	3		100	3	C
„ Nakagawa	34	60	170	22	C
„ Hiraomae N-E port.	12	100	440	3	C
„ Nishinomachi	1		83	1	C
„ Goten	10		315	3	C
„ Ryôshi, Kotemma	0	30	355	0	C
West Koyasu	50		1300	4	C
East Koyasu	200	150	700	29	C
Hodogaya	1429	1979	4086	30	C
Ohokagawa-mura	383		508	75	E
Byobuga-mura	103		478	22	E

Literatures for Table I.

A: Imperial Earthq. Inv. Comm.: Reports of the Imperial Earthquake Investigation Committee in Japanese Language. No. 100. (1925). (in Japanese)

B: Police Department, Kanagawa Prefecture: Report of the Great Earthquake Disasters in Taisho Era. 1926. (*do.*)

C: Yokohama City: Earthquake Disasters in Yokohama City. Nos. 1–5. (1925) (*do.*)

D: Yokohama City: Report on the Reconstruction Works in Yokohama. (1929) (*do.*)

E: Kanagawa Prefecture: Earthquake Disasters in Kanagawa Prefecture. (1927) (*do.*)

F: Central Meteorological Observatory: Report of the Investigations of the Great Kwanto Earthquakes. (1926) (*do.*)

G: K. Nishizaka: Great Earthquake Disasters and Activities of Police in Kanagawa Prefecture. (1926) (*do.*)

H: T. Koike; A Note of the Reconstructions in Yokohama. 1927 (*do.*)

I: Yokohama Municipal Office; The 18th Statistical Report of Yokohama City. (1921) (*do.*)

J: Kanagawa Prefecture; Statistical Report of Kanagawa Prefecture in 1923. (*do.*)

4. Geographic distribution of damage rates is shown in Fig. 1. In this Figure we notice at once that the area whthin which the damage rate exceeded 90% occupies a no small portion of the city. Now, when we compare this with the case of Tokyo City[1] where nowhere the percentage was as high as 90% in the same earthquake, we are struck by the difference. However, if we take into consideration the distribution of the damage rates in the recent Mikawa[2] or Fukui[3] Earthquake, it will be easily recognized that the difference noticed in these two maps means nothing contradictory, as Yokohama was situated much nearer the epicenter of the Kawanto Earthquake than Tokyo.

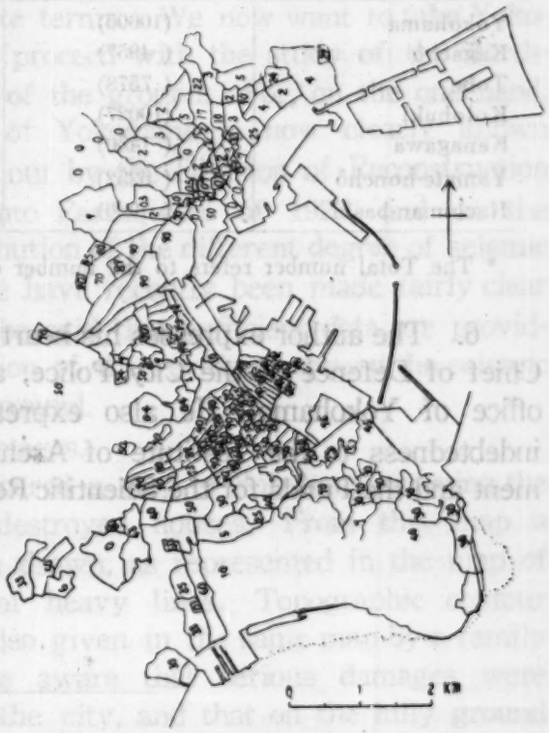

Fig. 1. Distributions of the damage rate in Yokohama.

1) H. Kawasumi, "The Earthquake Damages and the Structure of Ground in Tokyo" Paper read at the meeting of the Earthq. Res. Inst., on Apr. 19, 1949.

2) S. Omote, *Bull. Earthq. Res. Inst.*, **24** (1946), 87.

3) H. Kawasumi, *Advanced Report of the Fukui Earthquake of* 1948, 1.

5. Before concluding we wish to add a few words on the damage rates in the districts under the jurisdiction of the respective police stations. Though they are given in tables in several reports, some figures in such reports are evidently incorrect. Especially those figures arranged in the cloumn headed "destroyed houses" in these reports apparently do not include the houses that first collapsed under the shock and then were burnt down. According to his study the author believes the figures in the Table below show the most reasonable estimates for the destroyed houses.

Table II.

Revised Table for the number of presumed destroyed houses in the district under the jurisdictions of the respective police stations.

Police Station	Totally destroyed houses	Percentage of totally destroyed houses.	Total number*
Yokohama	(10605)	68.8%	15414
Kagachô	(4957)	81.9	6053
Tobe	(7578)	37.1	22222
Kotobuki	(10027)	44.7	22431
Kanagawa	(1450)	11.9	12240
Yamate-honchô	(6252)	42.3	14781
Hachiman-bashi	(926)	30.0	3087

* The Total number refers to the number of all the houses under the jurisdiction.

6. The author expresses his hearty thanks to Mr. Hirotada Sudo, the Chief of Defence of the City Police, and the members of the municipal office of Yokohama. He also expresses his gratefulness for financical indebtedness to the Institute of Architecture of the Construction Department and the Funds for the Scientific Research of the Education Department.

11. *The Relation between the Earthquake Damages and the Structure of Ground in Yokohama.*

By Syun'itiro OMOTE,

Earthquake Research Institute.

(Read April 19, 1949.—Received Nov. 30, 1949.)

1. Introduction.

It has long been known that destruction by earthquakes has a close relation with the geologic structure of the ground of the place. But our knowledge of the relation between the two is still very imperfect for the lack of concrete evidence, and it is now being earnestly hoped that it should be expressed in more definite terms. We now want to take Yokohama as a favourable example and proceed with the study of the earthquake damages and the condition of the ground. For, on the one hand, the subsurface geologic structure of Yokohama is now clearly known thanks to the 297 borings carried out by the Division of Reconstruction Bureau[1] soon after the Great Kwanto Earthquake of 1923, and on the other hand the details of the distribution of the different degree of seismic damages due to the same earthquake have recently been made fairly clear over the whole city, so that it may be said that sufficient data are provided by Yokohama for the investigation of the relation between the seismic damages and the condition of the ground.

2. Topography and earthquake damages.

In the previous paper[2] we prepared a map of Yokohama showing the distribution of the ratio of totally destroyed houses. From this map a sort of iso-seismic lines have been drawn, as represented in the map of Yokohama in Fig. 1 by a family of heavy lines. Topographic contour lines at every twenty meters are also given in the same map by a family of thin lines. We at once become aware that serious damages were restricted to the lower parts of the city, and that on the hilly ground damages were definitely slight. We are, however, able to point out some places which were exceptions to the above rule; we shall revert to the case of these places later on.

1) Reconstruction Bureau, *Geology in Tokyo and Yokohama.* (1929).
2) S. OMOTE, *Bull. Earthq. Res. Inst.*, **27** (1949), 57.

3. The thickness of alluvium and the degree of earthquake damages.

A thick layer of alluvium overburdened by a thin layer of reclaimed soil covers the lower regions of the city of Yokohama. It is generally

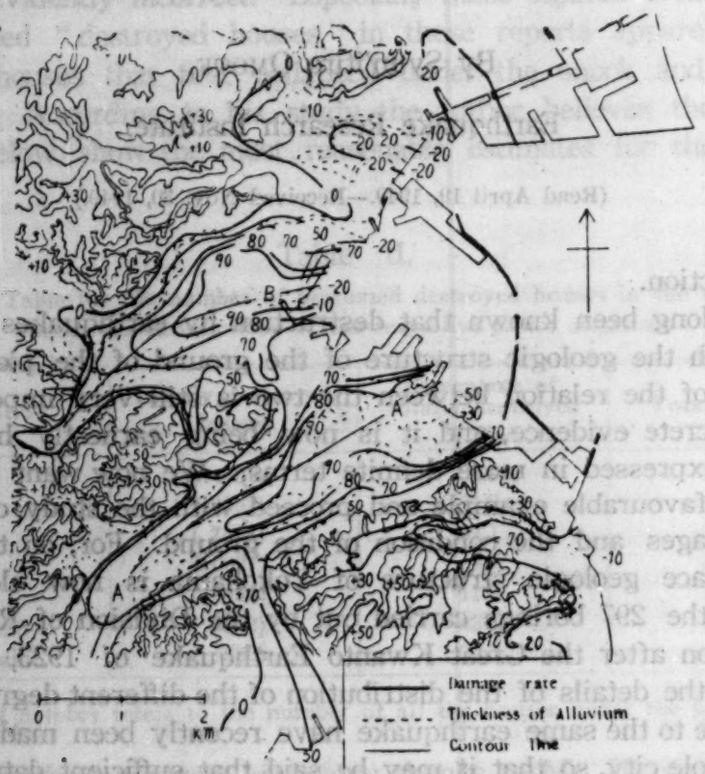

Fig. 1.

held that the degree of damages has the closest relation with the thickness of alluvium, and so here, to begin with, we will examine this relation. According to the geological maps prepared by the Reconstruction Bureau, the alluvium of Yokohama is subdivided into three layers: upper, middle and lowere. The respective contour lines in the geological maps showing the thickness of the three layers are so like each other that it does not appear likely that there should exist any specially close relation between the degree of damages and any one of these layers. These considerations necessitate that the relation between the damage rate and the thickness of the whole of the alluvium instead of the respective layers should be studied. The thickness of the alluvium along the lines A′-A and B′-B in Fig. 1 is shown by white circles in Figs. 2 and 3, and the damage rates in the same areas by black dots in the latter Figures. Comparison

of these Figures will show that the thicker the alluvium is, the larger is the proportion of the destroyed houses. As seen in Fig. 1, the alluvium plain in Yokohama is divided into two parts, namely A-plain and B-plain. With regared to each of the unit areas whose damage rates have been

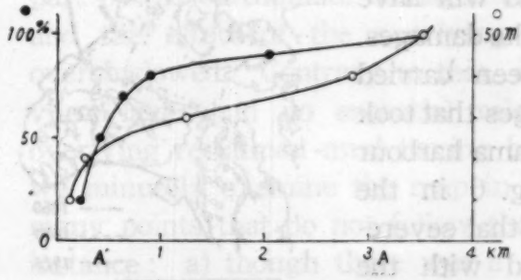

Fig. 2. ●; Damage rate along A′—A line
○; Thickness of alluvium along A′—A line.

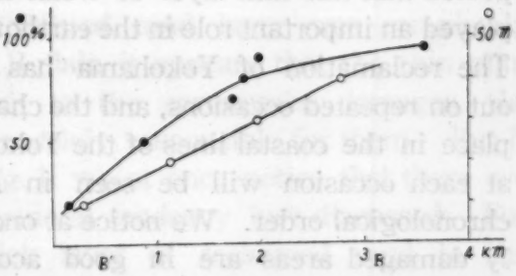

Fig. 3. ●; Damage rate along B′—B line
○; Thickness of alluvium along B′—B line.

calculated in the previous paper, the mean thickness of the alluvium has also been calculated, and the results have been summarized in Figs. 4 and 5 respectively for A and B plains. From these figures we can see that the thickness of the alluvium layer is closely related to the damage rate.

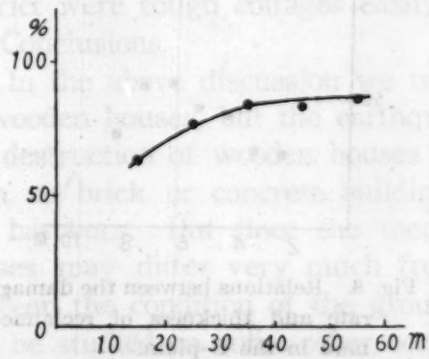

Fig. 4. Relation between thickness of alluvium and damage rate in the A-plain.

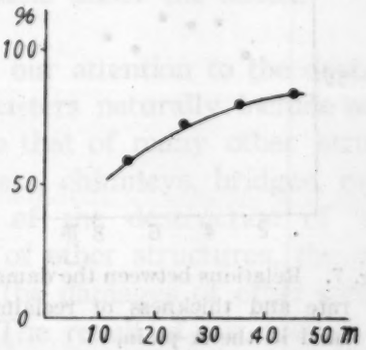

Fig. 5. Relation between thickness of alluvium and damage rate in the B-plain.

We notice in particular that as the thickness of the alluvium exceeds some thirty meters the damage rate suddenly becomes conspicous. It appear probable that the thickness of some thirty meters of the alluvium constitutes a sort of critical value.

4. The thickness of reclaimed superficial soil and earthquake damages.

The uppermost thin layer that covers the alluvium in Yokohama is largely composed of artificially reclaimed mud. As these reclamations belong to quite recent years it will be easily suspected that this thin layer of weak mud will have played an important role in the earthquake damages. The reclamation of Yokohama has been carried out on repeated occasions, and the changes that took place in the coastal lines of the Yokohama harbour at each occasion will be seen in Fig. 6 in the chronological order. We notice at once that severely damaged areas are in good accord with the reclaimed ground. The relation between the thickness of this mud layer and the damage rate due to the earthquake motions will be seen in Fig. 7 (A-plain) and Fig. 8 (B-plain). The relation between the uppermost mud layer and the damage rate is clearly discernible in B-plain, though it is not so marked in A-plain.

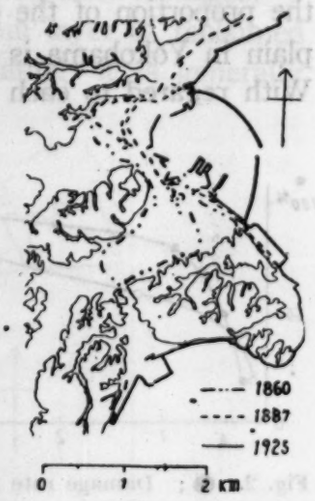

Fig. 6.
Changes of shore lines in Yokohama.

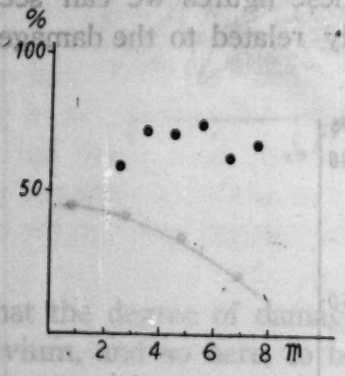

Fig. 7. Relations between the damage rate and thickness of reclaimed mud in the A-plain,

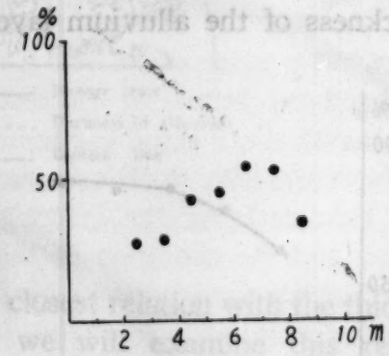

Fig. 8. Relations between the damage rate and thickness of reclaimed mud in the B-plain.

5. Some notes on the above observations.

It must not be overlooked here that in Yokohama it happened that in the area where the alluvium was thick, the reclaimed mud layer was also thick, and consequently it is very difficult to decide at present which layer was chiefly responsible for the earthquake damages. It is our earnest wish that more detailed studies will be made in the near future to give some definite conclusion to this point. Now, if we carefully compare

Fig. 7 with Fig. 8, we learn that black dots in the latter Figure are arranged roughly in a line while those in the former are not. An explanation to this will be as follows: Fig. 7 represents the relation between the thickness of the reclaimed mud and earthquake damage rates in A-plain. The thickness of alluvium is so large in this plain that the greater part of the earthquake damages in this area were due to the alluvium, and the effect of the overlying reclaimed mud layer was completely overshadowed. Contrary to this, in B-plain it appears that the thin alluvium layer had no essential relation to the earthquake damages, the overlying reclaimed mud having been solely responsible for them. But if we minutely examine the map in Fig. 1. we at once notice that there are many points that do not follow the general tendency just discussed. For instance: a) though there was a thick layer of reclaimed mud in the areas near Yokohama station, the damages were not serious there; b) on the contrary, in the central part of Yamashita-cho and the areas immediately to its north, more than 90% of the houses were destroyed though they stood on sand spit overburdened by very thin reclaimed mud; (it must be admitted, however, that most of the houses in Yamashita-cho were not made of wood); c) a part of West-Tobe, where the ground is hilly, suffered very high rate of damage, but this was the result of the landslide that took place there at the shock of the earthquake; d) as to the large damage rate in Yato, the explanation is that the houses in that district were rough cottages easily collapsible under the shock.

6. Conclusions.

In the above discussion we restricted our attention to the destruction of wooden houses, but the earthquake disasters naturally include not only the destruction of wooden houses but also that of many other structures such as brick or concrete buildings, towers, chimneys, bridges, railroads and harbours. But since the mechanism of the destruction of wooden houses may differ very much from that of other structures, the relation between the condition of the ground and the damages of other structures will be studied on some other occasion. The result of our present study will be summarized as follows:

1) The thickness of the uppermost layer of reclaimed soil has a close relation with the earthquake damages.

2) Places where thick alluvium overlies the ground suffer serious damages.

3) As the thickness of alluvium exceeds thirty meters the damage rate also increases conspicously.

4) On the sand spit or compact sand-shores earthquake damages are

often very slight.

5) Exceptions to the above conclusions may be pointed out, but the particular conditions of these places must be carefully investigated.

The author expresses his cordial thanks to Prof. H. Kawasumi for his kind advice to this study. He also wishes to acknowledge his indebtedness to the Scientific Research Fund of the Department of Education and to the Architectural Institute.

12. *A Torsional Pendulum Low-pass Filter Applied to the Study of the Earthquake Waves. (Part 2)*

By Tetuo AKIMA,

Earthquake Research Institute.

(Read June 8, 1948.—Received Sept. 30, 1949.)

§ 4. On some results obtained from the use of the filter to the seismograms of an earthquake :—

After confirming that our apparatus works as a satisfactorily quantitative low-pass filter by the preliminary tests reported in the previous paper, the writer applied the filter for investigating actual seismograms of the earthquake of May 23th, 1938, which took place at the offing of Sioya.

($\lambda=114.45°E$, $\varphi=36.70°N$, Shallow)

The epicenter and the observational positions of the seismograms are shown in Fig. 6. Fig. 7 shows some examples of the original seismograms, and the filtered curves. In this figure, the numbers 1, 2, 3, etc.

Fig. 6. The epicenter × and the observational positions (● and △).

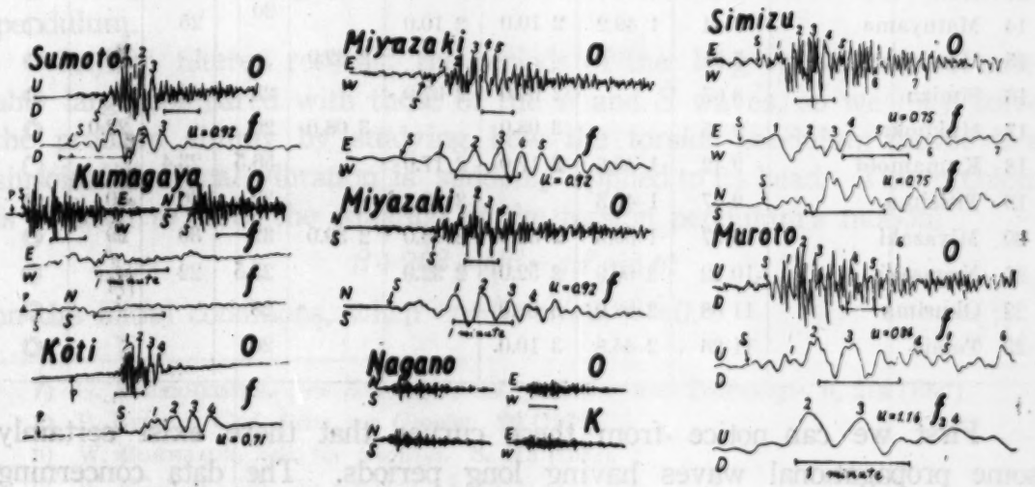

Fig. 7. Some examples of the original seismograms (O) and the filtered long curves (f_1, f_2).

indicate the corresponding waves on the seismograms and on the filtered curves. O's are the seismograms and f_1, f_2 are the curves filtered once and twice respectively. T_0 is the working period of the filter pendulum and u's are the ratio T_0/T, where T's are the periods of the filtered long waves. The last curve in this figure concerning Nagano is not the filtered curves but is the wave forms described by the pen K which is attached to the arm B as was shown in Fig. 2 in the pervious paper. This curve shows how accurately we can follow the seismograms by the hand method reported before.

Table I.

		△ in degrees	p-s	P-L			T			
				E-W	N-S	U-D	E-W	N-S	U-D	
1	Tukubayama	0°18′	0m 12.3s							
2	Kumagaya	1 50	21.7							
3	Yokohama	2 03	24.5		38.5s			31s		O
4	Nagano	2 36	31.2							
5	Kōhu	2 41	33.7							
6	Wazima	3 40	53.2	1m 26.5s	1m 26.5s		14.0s	14.0		O
7	Toyooka	5 30	1 02.2	1 16.5		1m 32.0s	27.0		27.5s	◎
8	Kyōto	5 02	1 13.0	1 40.0			19.0			◎
9	Sumoto	5 55	1 14.5			1 30.0			27.5	◎
10	Sionomisaki	5 47	1 16.0		1 24.0					◎
11	Muroto	6 58	1 18.0			1 52.2		22	25	◎
12	Nemuro	7 10	1 25.9	1 35.0			30			◎
13	Kōti	7 16	1 30.0	2 13.6			23		25	◎
14	Matuyama	7 44	1 49.2	2 10.0	2 10.0		20	25		O
15	Hamada	7 51				2 32.0			26	◎
16	Simizu	8 07		2 04.0	2 07.0		28	22.6		◎
17	Hukuoka	9 35		3 08.0		3 08.0	20		22.0	◎
18	Kumamoto	9 42	1 45.6	2 17.0	2 17.0		56.5	23.4		O
19	Titizima	9 47	1 49.3		2 19.3		32	30	30	◎
20	Miyazaki	9 37	1 59.3	2 34.0	2 44.0	2 39.0	32	30	29	◎
21	Nagasaki	10 22	2 00.9	2 52.0	2 32.9		28.5	22		◎
22	Okusima	11 08	2 08.0	3 08.0			28			◎
23	Tomie	11 26	2 44.8	3 10.0			20			◎

First we can notice from these curves that there exist certainly some propagational waves having long periods. The data concerning these long waves (L) are given in Table 1. Fig. 8 is a travel-time curve for these long waves together with that of the P and S waves. Calcu-

lating the velocity of these waves from this curve, it was found to be approximately 3.8 km/sec.

Besides the dispersion phenomena, many seismologists have observed that the velocities of surface waves are different according to their paths of propagation[7)-12)]. The velocity we have obtained agrees well with that given by *B.* Gutenberg and by C. F. Richter for the Love waves which are propagated under the North American continent (taking the period at 30 sec.). The marks ◎ and ○ in the last column of Table 1 indicate the well-recognizable appearance of the long waves.

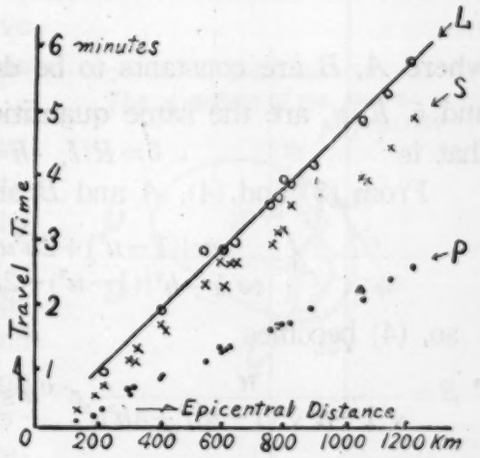

Fig. 8. The travel-time curve of the filtered long waves (L).

There are some seismograms from which the long waves could not be filtered out clearly. Especially on the filtered records for seismograms obtained at Tukubayama, Kumagaya, Nagano and Kōhu, the long waves are not filtered out.

The Kumagaya's is shown in Fig. 7. The positions of these stations are shown in Fig. 6 by △. Concerning the generation of surface waves, this fact is an interesting one and deserves to be studied in future.

There is a point to be considered about the accuracy of the onset of these recorded long waves, that is, about the time lag of the motion of the filter pendulum against the incident torsional vibrations applied to the pendulum.

On our filtered records, the periods of the long waves are remarkably large compared with those of the *P* and *S* waves, so we may solve the problem simply by studying how the torsion pendulum moves if a sinsoidal torsional vibration is suddenly applied to its head. This problem is reduced to solve the equation of the torsion pendulum's motion,

$$\ddot{\beta}+2\varepsilon\dot{\beta}+n^2\beta=an^2\sin pt$$

on the initial conditions, when $t=0$; $\dot{\beta}=0$, $\beta=0$. (3)

7) G. Angenheister, *New Zealand Jornal of Science and Technologie*, **6**, 214 (1921).
8) P. Byerly, *Gerl. Beitr. zur Geophy.* **26** (1930).
9) W. Rohrbach, *Zeit. für Geophys.* **8**, 113 (1932).
10) W. Mühlen, *Zeit. für Geophys.* **8** (1932).
11) D. S. Cardar, *Bull. Seis. Soc. Amer.* **24** (1934).
12) B. Gutenberg, C. F. Richter, *Gerl. Beitr.* **47**,92 (1936) etc.

The general solution of this equation is

$$\beta=e^{-\varepsilon t}(A\sin n\sqrt{1-h^2}t+B\cos n\sqrt{1-h^2}t)+\frac{u^2}{\sqrt{(1-u^2)^2+4h^2u^2}}a\sin(pt-\delta), \quad (4)$$

$$\tan\delta=\frac{2hu}{1-u^2},$$

where A, B are constants to be determined by the initial conditions (3), and ε, h, u, are the same quantities as expressed in the previous paper, that is $\varepsilon=R/I$, $h=\varepsilon/n$, $u=n/p$.

From (3) and (4), A and B are determined as follows.

$$A=\frac{au\{(1-u^2)+2h^2u^2\}}{\sqrt{1-h^2}\{(1-u^2)+2h^2u^2\}}, \quad B=\frac{2hu^2a}{(1-u^2)^2+4h^2u^2},$$

so, (4) becomes

$$\beta=\frac{u}{\sqrt{1-h^2}\sqrt{(1-u^2)^2+4h^2u^2}}e^{-\varepsilon t}a\sin(n\sqrt{1-h^2}t-\Delta)+\frac{u^2}{\sqrt{(1-u^2)^2+4h^2u^2}}a\sin(pt-\delta), \quad (5)$$

where $\tan\Delta=-\dfrac{2hu^2\sqrt{1-h^2}}{(1-u^2)+2h^2u^2}$, $\tan\delta=2hu/(u^2-1)$.

In our case, the value of h is 0.64 ($\because$ $h^2=0.4$).

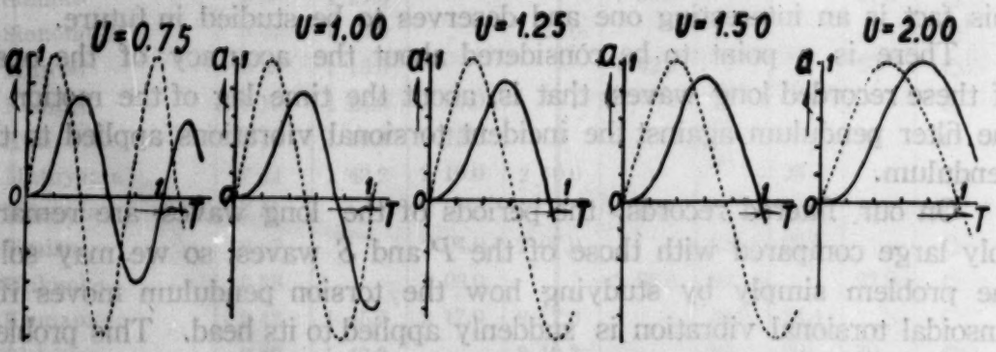

Fig. 9. The initial motion of the pendulum (solid line) caused by a sinsoidal torsional vibration (dotted line) suddenly applied to its head.

Fig. 9 shows the initial motion of the pendulum (solid line) caused by a sinsoidal torsional vibration suddenly applied to its head (dotted line), being calculated from the solution (5) taking $h=0.64$ and $u=0.75$, 1.00, 1.25, 1.50 and 2.00.

In this figure, T, the proper period of the pendulum, and a, the amplitude of the incident waves, are taken respectively as the units of abscissa and ordinate.

Seeing these results, we know that the determination of the onset time of these long waves may have the time error of approximately 5% (when approx. $u<1.50$) and 10% (when approx. $u>1.50$) of T.

In our case, the pendulum was used at the proper period of 20~30 sec, and u was 0.75~1.3, so that the time lags are approximately 1~3 sec. Every point in the travel-time curve of the long waves was taken after these corrections were made.

Judging from the fact that the filtered long waves have all remarkable vertical components, they seem to be of the Rayleigh-type.

In order to examine this point, the writer investigated the vertical ground motion which is parallel to the direction of the wave propagation using the filtered long waves at Miyazaki. (It is regretable that this was the only position at which 3 component seismograms were obtained which were necessary for this purpose.) The result which is shown in Fig. 10 shows a theoretically requested retrograd fashion of the motion of a particle at approximately 50 seconds later from the beginning of the long waves. (The numbers 20~70 on this figure mean the times reckoned from the beginning of the long waves.)

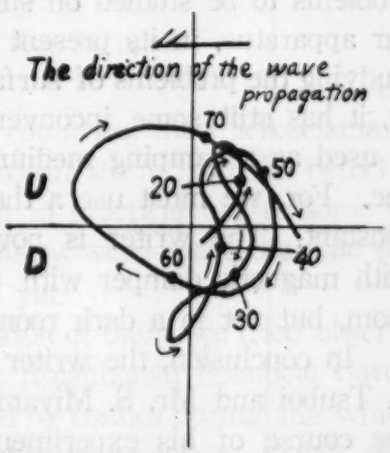

Fig. 10. The vertical ground motion at Miyazaki due to the filtered long waves.

Fig. 11. Some examples of the ground motions in two directions concerning the filtered long waves.

Fig. 11 gives some exmaples of horizontal ground motions concerning the long waves in two directions, (a) parallel and (b) perpendicular to the direction of the wave propagation at Miyazaki, Simizu and Matuyama. In drawing these figures, the writer took the propagational direction to be a straight line drawn from the epicenter to these observational positions, but actually, there may be some deviations. These problems must be studied with much more data in future.

Besides, since all these filtered waves have components perpendicular to the direction of the wave propagation, they seem to be Love waves.

After all, the actual orbit of the ground motion due to the filtered long waves is some complex one, which may be due to the fact that Rayleigh and Love waves are not well separated in these near earthquakes.

§ 5. Conclusion: Though our present study, the filtering of long waves from near earthquakes, is only at first stage, it leaves us many problems to be studied on surface waves in near earthquakes. Although our apparatus, in its present form, has proved to work satisfactorily for studying the problems of surface waves in near earthquakes experimentally, it has still some inconvenient point. Especially, the fact that the oil is used as a damping medium makes this apparatus as an inconvenient one. For, we must use a thermostat to keep the temperature of this oil constant. The writer is now constructing a much more convenient one with magnetic damper with which experiments can be made in lighted room, but not in a dark room.

In conclusion, the writer wishes to express his hearty thanks to Prof. C. Tsuboi and Mr. S. Miyamura who gave the writer many remarks in the course of his experiments, and to Mr. S. Honma, a member of The Central Meterological Observatory, who was kind enough to lend me the seismograms studied.

Most of the expense necessitated for this study was defrayed from the funds for Scientific Research of the Department of Education.

---

12. 捩り振子を應用した低域濾波器による地震波の研究

地震研究所 秋 間 哲 夫

近地地震の記象から表面波をとり出す目的で，捩り振子を應用した低域濾波器を作製し，種々の予備實驗を經た後で，實際にある一つの地震についての各地の記象をこの濾波器にかけて見たところ，表面波とおぼしき 30 秒前後の周期をもつた傳播性の波が，S 波の後に存在することが分つた．走時曲線をつくつて見ると，その速度は約 3.8 km/sec である．三成分そろつた記象がごく僅かだつたので，この波の性格ははつきりきめられないが，ラヴ波的な面も，レーリー波的な面も見られる．又震央距離が約 2° 30′ 以内の地點の記象からは，之等の長周期の波が濾波しえなかつたことも注意されよう．之等の點に關して今後いろいろの地震について調べてゆきたいと思つている．

13. *A Study on the Propagation of Microseismic Waves.*

By Ryôhei IKEGAMI and Fuyuhiko KISHINOUYE,

Earthquake Research Institute.

(Read Apr. 19, 1949.—Received Sept. 15, 1949.)

1. Recently in America and some other countries, the microseisms are regarded as progressive waves caused by ocean storm, and the detect of it by the observations of microseisms is put to practical use to some extent[1]. In Japan many studies on microseisms were made, but the propagation of them have not been ascertained yet.

For the purpose of studying the propagation of them, we tried observations from Nov., 1948 to Feb., 1949 at the Koishikawa Botanical Garden in Tokyo, where no disturbances were caused by traffics during the winter.

The apparatuses used were the portable tromometers which were designed by one of us[2], and we adjusted their period of free vibrations to 10 sec., their magnification to 1920, and the damping to critical. The speed of recording bromide-paper was 4.5 mm/sec.

2. In order to study the phase differences of the waves, when the intervals between the two tromometers are apart far at a distance, we set up one of them at a fixed position and the other at the distance of 1.48, 10 and 50 meters in sequence, and observed the microseisms simultaneously. In the case of 1.48 and 10 m, the records of both tromometers showed the same phases, and we could not distinguish a time lag of the phases of both positions as shown in Fig. 1.

At the distance of 50 m, the arrival times of both phases were slightly different, but those time differences were too short to measure.

From the observations mentioned above, we see that there is difference in the arrival times between two positions as distance increases.

Thereupon, we tried to observe it at the distances of 164 and 266 m again. We could read a difference of the arrival times at both positions on these records. From these records, we obtained about 3.4 km/sec as

---

1) J. E. RAMIREZ, *Bull. Seism. Soc. Amr.*, **30** (1940), 35—84, 139—178.
M. H. GILMORE, *ditto*, 36 (1946), 89—120.
M. H. GILMORE and W. E. HUBERT, *ditto*, 38 (1948), etc.

2) F. KISHINOUYE, *Bull. Earthq. Res. Ins.*, **20** (1942), 215—219.

average velocity of propagation of the microseisms. This value might be near the maximum value of the true velocity, or the true velocity of microseisms might be less than this value.

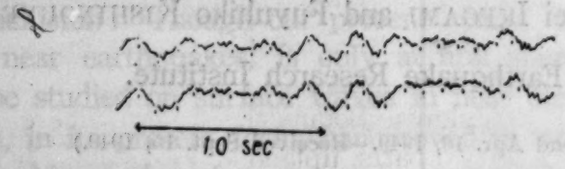

Fig. 1. The records of two tromometers, 148 cm apart.

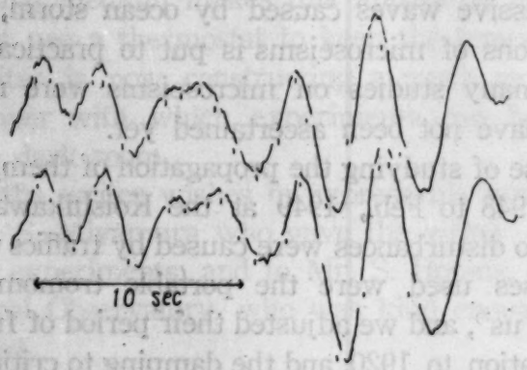

Fig. 2. The upper record shows microseisms at the bottom of the pit. (The depth was 130 cm.)
The lower, at the surface of ground. (The interval was 7 m.)

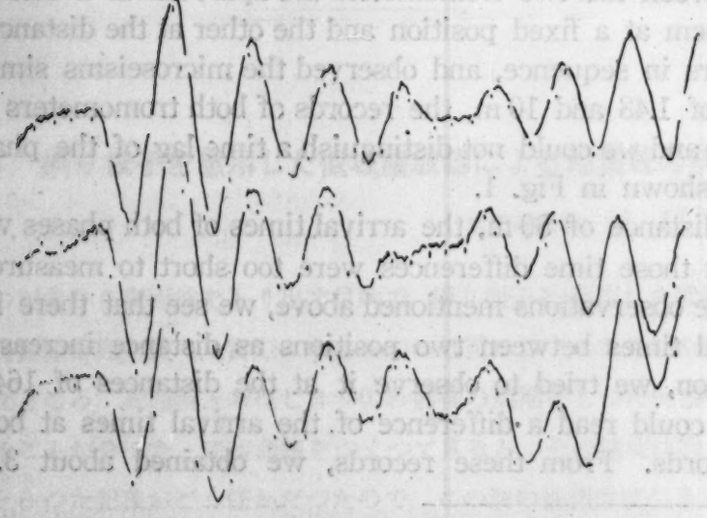

Fig. 3. The records of the tripartite observation.
The upper record shows microseisms at R-station.
The middle, at M-station.
The lower, at S-station.

Moreover, because we were doubtful of the phases at the underground of a certain depth, we set up two tromometers 7 m apart at the ground surface and the bottom of a pit, the depth of which is 1.3 m, and observed the microseisms simultaneously. These records showed also no phase difference at both positions as shown in Fig. 2.

3. The lay of the Koshikawa Botanical Garden, where we tried the observations, is divided into two parts, upland and lowland. It is neccessary to investigate the disparity of the microseismic phases between the two parts of the lay. We observed them at *A* and *M* in Fig. 4. simultaneously.

On these records the microseisms of 4 sec. periods were the same wave-forms at both positions, although there were phase differences in accordance with distances. But the wave-forms of the short periods (0.2–0.3 sec.), which might probably be caused by traffics, showed some differences. That is to say, the amplitude of the short period motion of the lowland was larger than the one of the upland, and also the phase did not exactly correspond to each other.

From these results, it is expected that the propagations of microseismic waves of 4 sec. periods may be ascertained, when the tripartite observation is tried more than 150 m apart.

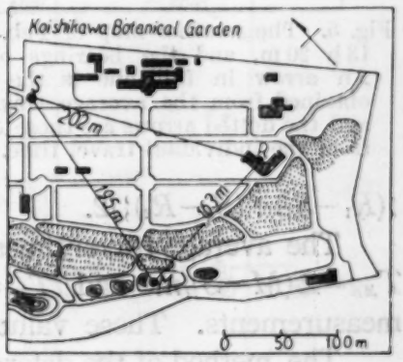

Fig. 4. A part of the Koishikawa Botanical Garden in Tokyo.

4. Three tromometers were stationed at the three positions *R*, *M* and *S* in Fig. 4 in the same directions respectively, and the observations were held on Feb. 9th, 11th and 14th. The weather maps of those days are shown in Figs. 5, 6, 7 and 8. Fig. 3 shows parts of the records of these three tromometers on Feb. 9th.

The first step in the actual calculation of bearing is to measure the differences in times of arrival between the stations R and *M*, *M* and *S*, and *S* and *R*. For example, the linear distances (as shown in Fig. 9) from the time break of certain well-formed microseisms recorded at all the three stations are measured in millimeters to the nearest crests and troughs respectively, and these values are converted into seconds.

The values to the actual travel time between the stations *R* and *M*, *M* and *S*, and *S* and *R* were calculated from the expressions, $R-M=\{(R_1-M_1)+(M_2-R_2)\}/2$, $M-S=\{(M_1-S_1)+(S_2-M_2)\}/2$, and $R-S=$

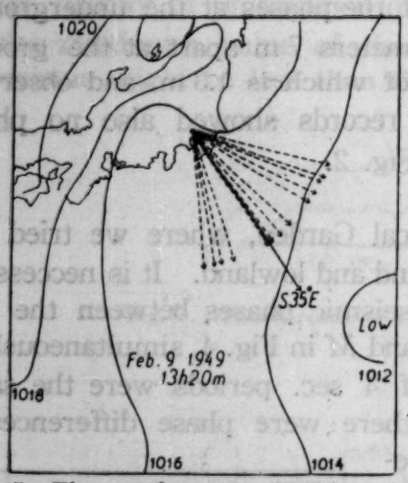

Fig. 5. The weather map of Feb. 9, 1949, 13 h 20 m, and the bearings obtained. An arrow in full line is the bearing obtained from the average travel time, and the dotted arrows are those obtained from the individual travel time.

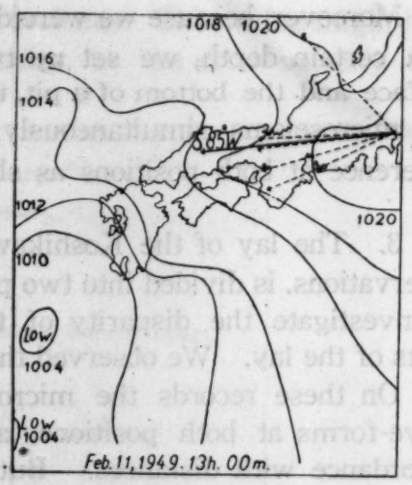

Fig. 6. The weather map of Feb. 11, 1949, 13 h 00 m. and the bearings obtained.

$\{(R_1-S_1)+(S_2-R_2)\}/2$.

The average travel times were obtained as follows, $T_{RM}=\Sigma(R-M)/n$, $T_{MS}=\Sigma(M-S)/n$. and $T_{RS}=\Sigma(R-S)/n$, where n was the numbers of measurements. These values are shown in Table I.

The method of the determination of the arrival direction of microseisms was similar to that derived by Gilmore[3].

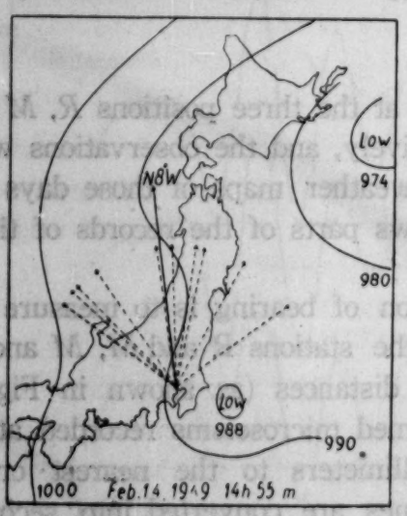

Fig. 7. The weather map of Feb. 14, 1949, 14 h 55 m, and the bearings obtained.

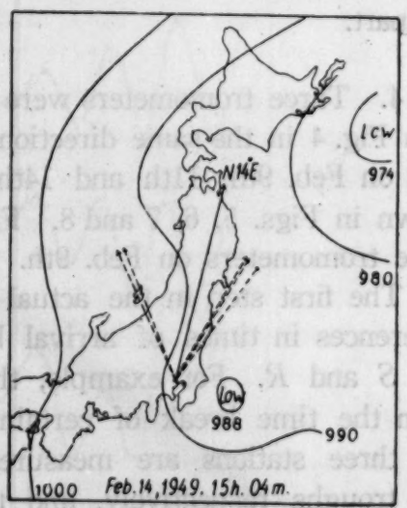

Fig. 8. The weather map of Feb. 14, 1949, 15 h 04 m, and the bearings obtained.

3) M. H. GILMORE: *Bull. Seism. Soc. Amr.*, 36 (1946), 95.

The bearings obtained from the average travel times by that method are shown in Figs. 5, 6, 7 and 8 by arrows in full line respectively. Much interest was aroused by the fact that each bearing was nearly in line with the position of an atmospheric depression at that time.

The microseisms recorded at *R*-Station.

at *M*-Station.

at *S*-Station.

Fig. 9. The method to measure the linear distances from the time break to the nearest crest and trough.

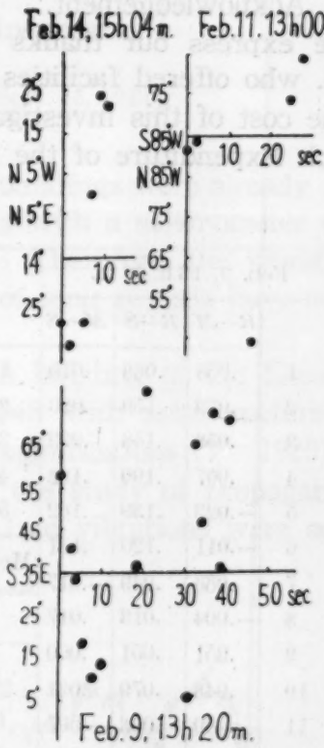

Fig. 10. The relations between the bearings and the measured time of these bearings.

The bearings calculated individually from the actual travel time are shown in those figures by dotted arrows, and they are scattered within the angular deviation of 30–40 degrees. These deviations might be attributed to observation errors, but in this case there might be some causes besides errors as referred to below. The relations between the bearings and the measured times of these bearings are shown in Fig. 10. According to this figure, the deviations of the bearings seem to have some systematical changes. When atomospheric depression extends over a wide area, it is possible to consider that the bearings may be deviated in variant directions. But in such a case it is difficult to expect the systematical changes of the bearings. These systematical changes of the bearings may be able to be elucidated by the consideration that these changes are caused by the resultant waves of the ones propagated from

a depression and the ones caused by the free vibration of that ground. This subject must be established by future investigations.

The average velocity of microseisms obtained was 239±0.02 km/sec.

5. Acknowledgement.

We express our thanks to the staffs of the Koishikawa Botanical Garden. who offered facilities for our observations.

The cost of this investigation has been defrayed from the Scientific Research Expenditure of the Department of Education.

Table I.

Feb. 9, 13 h 20 m.			
	$R-M$	$R-S$	$M-S$
1	.058	.068	.010
2	.079	.159	.080
3	.058	.158	.099
4	.007	.190	.182
5	−.023	.139	.162
6	−.011	.120	.131
7	.066	.049	−.017
8	−.004	.013	.017
9	.051	.051	.000
10	.048	.079	.031
11	.040	.033	−.007
12	.041	.102	.061
13	.054	.047	−.007
Mean	.036	.093	.057

Feb. 11, 13 h 00 m.			
	$M-R$	$S-R$	$M-S$
1	.066	.072	.017
2	.075	.051	.024
3	.020	.050	−.030
4	.069	.035	.034
5	.084	.028	.056
Mean	.063	.047	.020

Feb. 14, 15 h 04 m.			
	$S-M$	$S-R$	$R-M$
1	.080	.033	.047
2	.118	.039	.079
3	.113	.046	.066
4	.046	.039	.007
5	.052	.064	−.012
6	.082	.097	−.015
Mean	.082	.053	.029

Feb. 14, 14 h 55 m.			
	$S-M$	$S-R$	$R-M$
1	.080	.035	.045
2	.102	.080	−.020
3	.065	.087	−.065
4	.012	.075	−.063
5	.036	.067	−.031
6	.071	.033	.019
7	.046	.015	.061
8	.027	.029	.013
9	.047	.059	−.016
10	.077	.075	.002
Mean	.056	.056	.000

14. *On the Vibrations of a Building caused by Microseisms.*

By Ryôhei IKEGAMI,

Earthquake Research Institute.

(Read Feb. 15, 1949.—Received Sept. 15, 1949.)

1. The vibrations of various kinds of buildings were already studied by many investigators[1], but few observations with a seismometer of long period and large magnification were made. Therefore, the vibrations of a building caused by the ground vibrations of long periods have not been investigated yet.

We observed the vibrations of the main building of the Koishikawa Botanical Garden in Tokyo, on Dec. 7th, 1948 with seismometers which have long periods ($T_0=15$ sec.) and large magnifications ($V=1920$). The seismometers were the same ones used for the study of propagations of microseisms at that place, but the periods of free vibrations were adjusted to 15 sec..

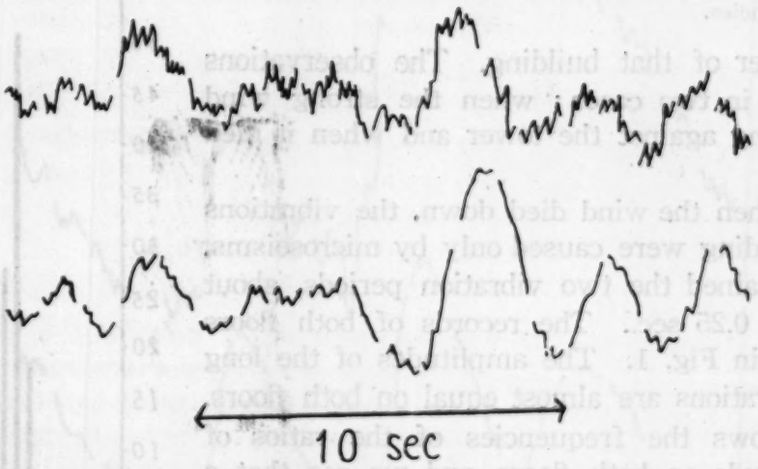

Fig. 1. The vibrations of the 5th floor (upper figure) and the 2nd floor (lower figure) caused by microseisms, when the wind died down. (Actual size.)

1) F. ŌMORI, *Rep. Imp. Earthq. Inv. Comm.*, 97 (1921), 1.
A. IMAMURA and F. KISHINOUYE, *Bull. Earthq. Res. Ins.*, 5 (1928), 143.
S. UCHIDA, T. SAIDA and K. MŪTŌ, *ditto*, 6 (1929), 345.
M. ISHIMOTO and R. TAKAHASI, *ditto*, 7 (1929), 175.
K. FUKUTOMI, *ditto*, 9 (1931), 485. etc.

On that day, the amplitudes of microseisms were comparatively large, and maximum wind velocity was about 9 m/sec on the ground. We set up two seismometers in the same direction on the 2nd and the 5th floors

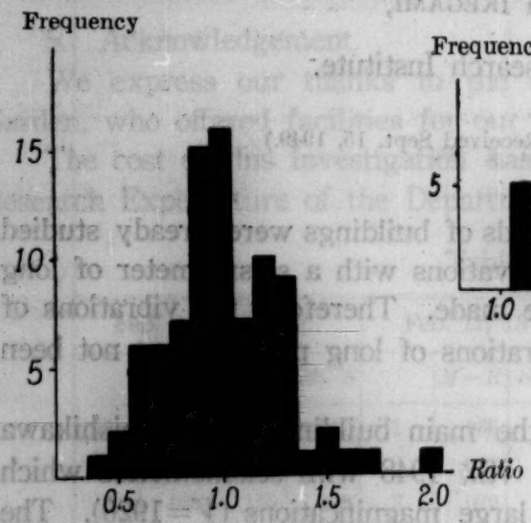

Fig. 2. The relation between the ratios of the amplitudes of about 4 sec. period vibrations on 5th floor to that on the 2nd floor and theis frequencies.

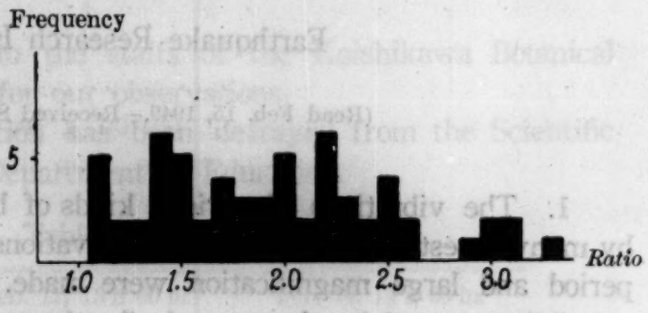

Fig. 3. The relation between the ratios of the amplitude of short period vibrations on the 5th floor to that on the 2nd floor and theis frequencies.

of the tower of that building. The observations were tried in two cases: when the strong wind was blowing against the tower and when it died down.

2. When the wind died down, the vibrations of the building were caused only by microseisms, which contained the two vibration periods, about 4 sec. and 0.25 sec.. The records of both floors are shown in Fig. 1. The amplitudes of the long period vibrations are almost equal on both floors. Fig. 2 shows the frequencies of the ratios of the amplitude on both floors, and we see that a ratio of maximum frequency is about 1.

From this result, it may be concluded that the vibrations of this building are horizontal motions which are parallel to ground motions rather than rocking motions.

But this phenomenon is not always seen in short period motions. Namely, Fig. 3 shows

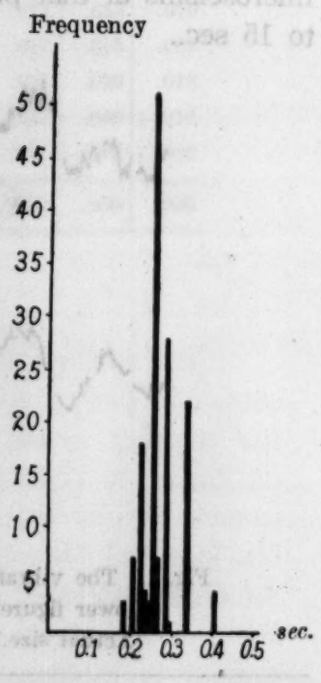

Fig. 4. The relation between the vibration period and the frequencies on the 5th floor.

the frequencies of the amplitude ratios of short period motions on both floors. In Fig. 3. we see that the values of ratios are scattered over within 1.1 and 3.3, but they are never less than 1.0. This result shows that on the 5th floor the motions caused by short period ground motions are larger than the ones on the 2nd floor. The average value of ratios was 1.89.

Judging from these observations, we deduced that this building moves equally to the ground for long period ground motions, but the 5th floor is moved two or three times more than the 2nd floor for short period ground motions.

A maximum frequency of vibration periods on the 5th floor was at 0.25 sec. as shown in Fig. 4. It is considered that this period was perhaps near the period of this building.

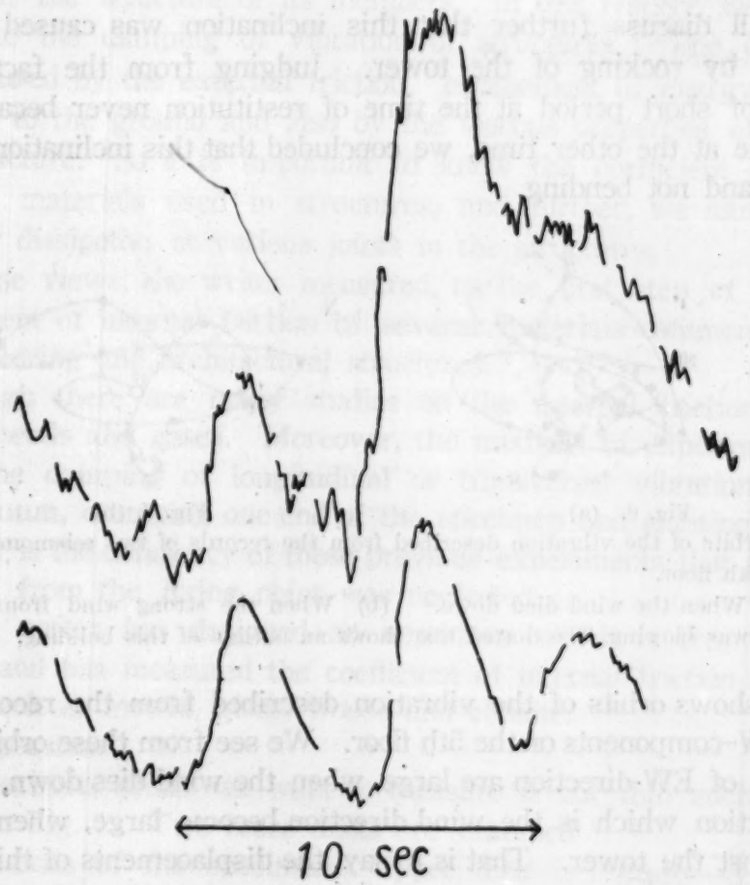

Fig. 5. One example of the records of seismometers set up on the 5th floor (upper figure) and the 2nd floor (lower figure) in the vertical direction to the wind, when the strong wind was blowing against the tower. (Actual size.)

3. When the strong wind from the north (about 9 m/sec on the ground) was blowing against the tower of this building, the vibrations of which presented another conditions.

Fig. 5 shows one example of the records of seismometers set up on both floors in the vertical direction to the wind. In these records we see the large displacements, when the strong wind was blowing against the building.

It is necessary to consider that these displacements are caused either by inclination or by parallel displacement of the whole building. If these displacements are caused by the latter, judging from the directions of displacements of records, this building must be moved to windward. This inference is inconsistent with common sense. If these are caused by the former, these imply inclination to the leeward, and this inference seems to be true.

We will discuss further that this inclination was caused either by bending or by rocking of the tower. Judging from the fact that the amplitude of short period at the time of restitution never became larger than the one at the other time, we concluded that this inclination was due to rocking and not bending.

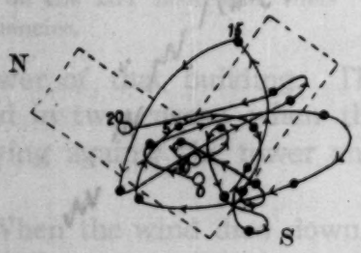

Fig. 6. (a)

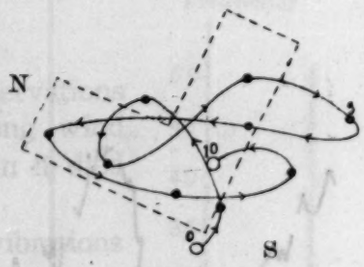

Fig. 6. (b)

The orbits of the vibration described from the records of two seismometers on the 5th floor.

(a) When the wind died down. (b) When the strong wind from the north was blowing. The dotted line shows an outline of this building.

Fig. 6 shows orbits of the vibration described from the records of the NS- and EW-components on the 5th floor. We see from these orbits that the movements of EW-direction are large, when the wind dies down, but those of NS-direction which is the wind direction become large, when the wind blows against the tower. That is to say, the displacements of this building are caused on the 5th floor by the wind as much as by microseisms.

In future we will observe the microseisms inside and outside a building simultaneously and compare both records each other. Then the motions of a building caused by microseisms will be ascertained.

15. *Study on the Coefficient of Internal Friction of Materials used in Civil Engineerings and Architectural Structures. (1st Report)*

By Daisuke SHIMOZURU,

Earthquake Research Institute.

(Read April. 19, 1949.—Received Sept. 20. 1949.)

1. Purpose.

It is well known that for earthquake-proofing the absorption of energy in a vibrating structure is a factor as important as the natural period or stiffness of the structure or its members. In this respect, we must pay attention to the damping of vibration of structures. The damping is usually caused by the external friction, escapement of energy from the foundation to the ground and also by the viscous properties of materials of the structure. So it is important to know the coefficient of internal friction of materials used in structures, and further, we must measure the energy dissipaton at various joints in the structures.

In these views, the writer measured, as the first step of his study, the coefficient of internal friction of several materials commonly used in civil engineering and architectural structures.

Although there are many studies on the internal friction, they are almost of metals and gases. Moreover, the methods of experiment are to measure the damping of longitudinal or transversal vibration of specimen in vacuum, cramping one end of the specimen and exciting the other end. But it is the deficiency of these previous experiments that the energy escapement from the fixing point was neglected.

So the writer has designed an apparatus which is free from such deficiency, and has measured the coefficient of internal friction of several materials such as metals, glass, woods and ebonite.

2. Apparatus.

The specimen which we want to measure is cut into such a shape as shown in Fig. 1. Two brass disks are cramped to the both ends of the specimen. Upper disk is two times thicker than the lower, and from the opposite surfaces of the two disks, two pairs of brass arms, strong enough compared with any specimen, are equipped. Each of the upper arm has an electro-magnet, and

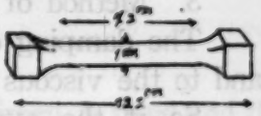

Fig. 1.

at the upper part of each of two lower arms, thin iron plates are soldered facing to the electro-magnets. These conditions are shown in Fig. 2.

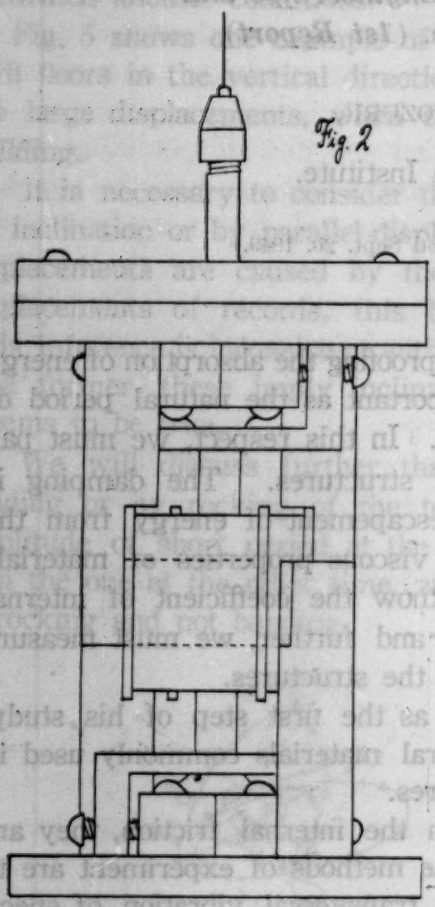

This vibrating system is suspended by a piece of thin piano wire (0.35 mm in dia.) in a bell-jar. The core of magnet and thin iron plates are of pure iron so as not to produce residual magnetism. Lead wires of the magnet coils are fine springs which do not give any tension to the coil. (By these arrangements, the vibrating system is practically isolated.)

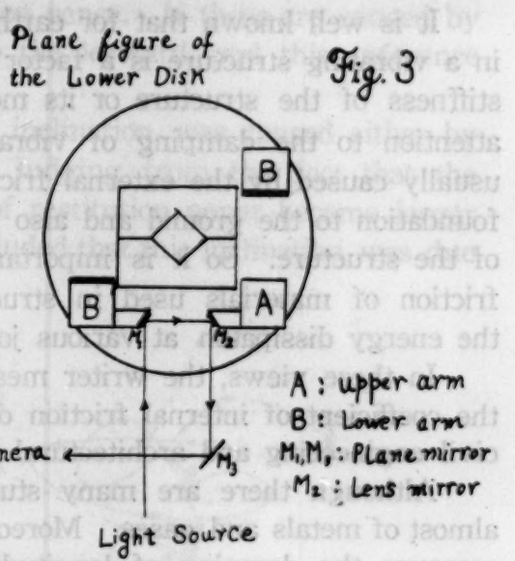

The recording system of damping vibration is as follows. As shown in Fig. 3, the light from a straight line filament lamp is reflected by a plane mirror and a lens mirror, which are soldered to the opposite ends of lower and upper arms, and then reflected once more by a plane mirror at the outside of the bell-jar, making an image of the filamnt on the recording film wound on a revolving drum. Time marks of each second are also recorded on the same film. By means of these mirror system, we can record only the relative torsional deflection of the two disks.

3. Method of Measuring.

The damping of these torsional vibration is due to the friction of air and to the viscous properties of the specimen.

So if the experiment is performed in a vacuum, the damping is wholly due to the latter quantity, and we can obtain the coefficient of internal friction, free from other factors.

By means of a momental excitation due to the electro-magnet, two opposite arms, each of which has an iron plate, are attracted instantly and after that the system begins its natural vibration, the period of which depends on the rigidity of the specimen. The records obtained are such as shown in Fig. 8.

If the dimension of the specimen is large, this apparatus can not be applied and need a larger vessel such as an oil-can. In such a case, high vacuum would be difficult to be obtained. So we must know the relation between the logarithmic decrement δ and the pressure of air p. This relation in the case of ***keyaki*** (zelkova tree) is as Fig. 4. It is exactly linear.

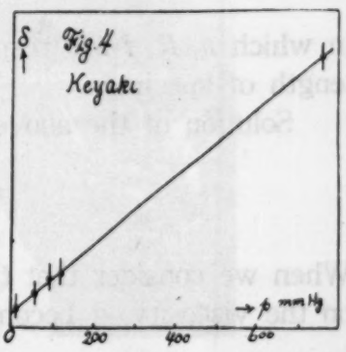

Next it is necessary to know the relation between the period of vibration and the air pressure. The relation was obtained by using specimens (cold drawn steel wires) of different diameters. (Fig. 5.).

The facts which can be inferred from these results are as follows.

1. The shorter the period, the smaller the effects of air upon δ.
2. From 0 mmHg to 20 mmHg, relation between δ and p is almost linear. So we can deduce the value of δ corresponding to zero pressure from several measurements done in the range of 0 mmHg to 20 mmHg.

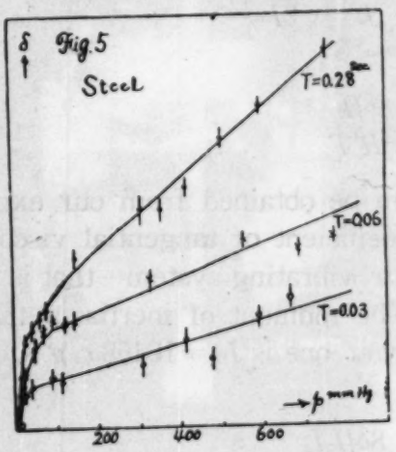

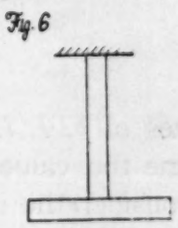

4. Results of Experiment.

As is shown in Fig. 6, if the upper end of specimen is fixed and the other end carries the disk of which the moment of inertia is I, which is large compared with that of the specimen, the internal friction of the

specimen acting as a damping force, the equation of free vibration of this disk is

$$I\frac{d^2\theta}{dt^2}+\alpha\frac{d\theta}{dt}+\beta\theta=0 \quad \cdots\cdots\cdots\cdots\cdots\cdots\cdots\cdots (1)$$

where α is a constant depending on the coefficient of internal friction and energy escapement, and

$$\beta=\frac{\pi nR^4}{2l},$$

in which n, R, l are respectively the torsional rigidity, the radius and the length of specimen.

Solution of the above equation is

$$\theta=\theta_0 e^{-\frac{\alpha t}{2I}}\cos\left(\frac{2\pi t}{T}+\varepsilon\right)$$

When we consider that the 2nd term of equation (1) is dependent only on the viscosity, α becomes as follows:

$$\alpha=\frac{\pi\eta R^4}{2l},$$

where η is the coefficient of tangential viscosity of the specimen.

Since the period of this system is

$$T=2\pi\Big/\sqrt{\frac{\beta}{I}-\left(\frac{\alpha}{2I}\right)^2},$$

we have

$$\eta=\frac{8\delta lI}{\pi R^4 T}$$

As the values of δ, I, l, R, T can be obtained from our experiments, we can determine the value of the coefficient of tangential viscosity η.

Next, consider the case of our vibrating system—that is the specimen carrying the disk at both ends. The moment of inertia of the upper disk is $I_1(=32535\ c.g.s.)$ and of the lower one is $I_2(=16458\ c.g.s.)$ respectively.

Then η becomes as follows:

$$\eta=\frac{8\delta l I_1 I_2}{\pi R^4 T(I_1+I_2)}$$

According to the experiments, the logarithmic decrements of torsional vibration are in these two cases clearly different—the decrement in the former case is larger than the decrement in the latter. The apparent

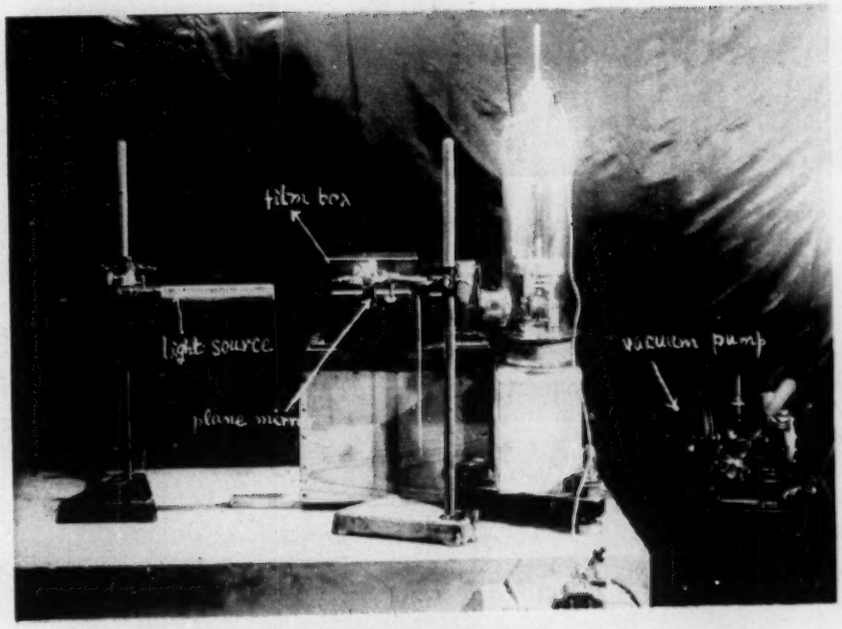
film box
light source
plane mirror
vacuum pump

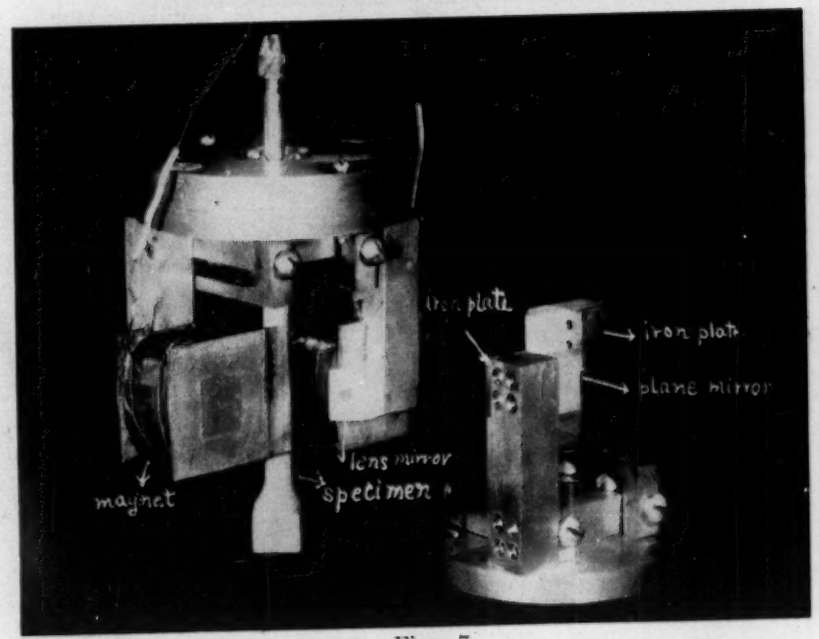
iron plate
iron plate
plane mirror
lens mirror
specimen
magnet

Fig. 7.

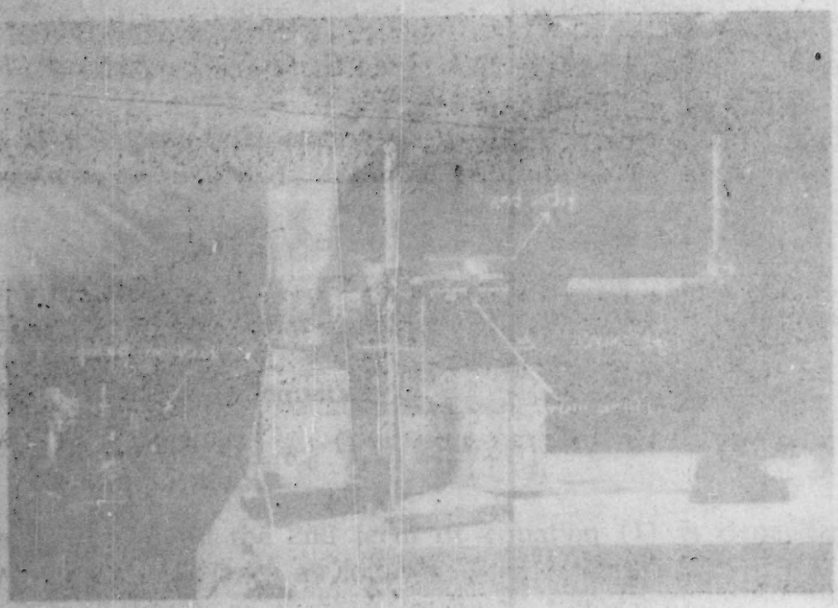

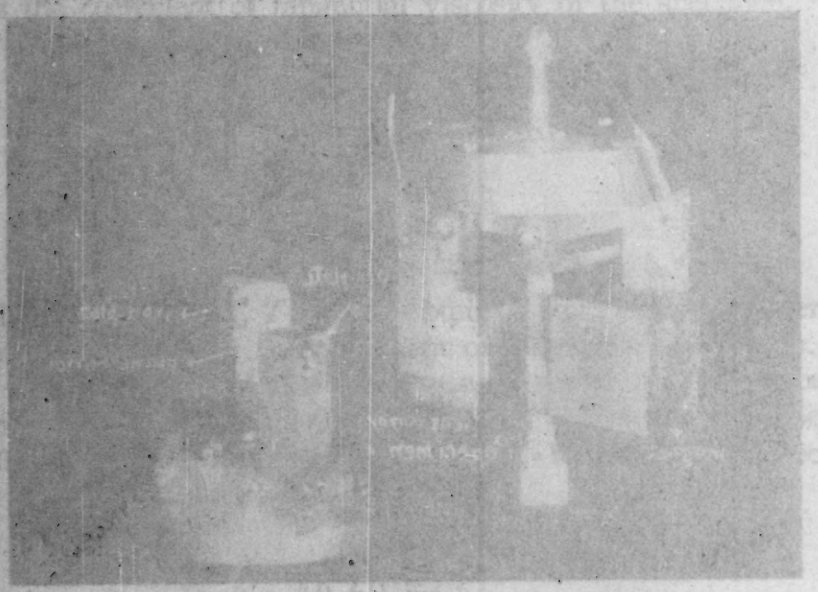

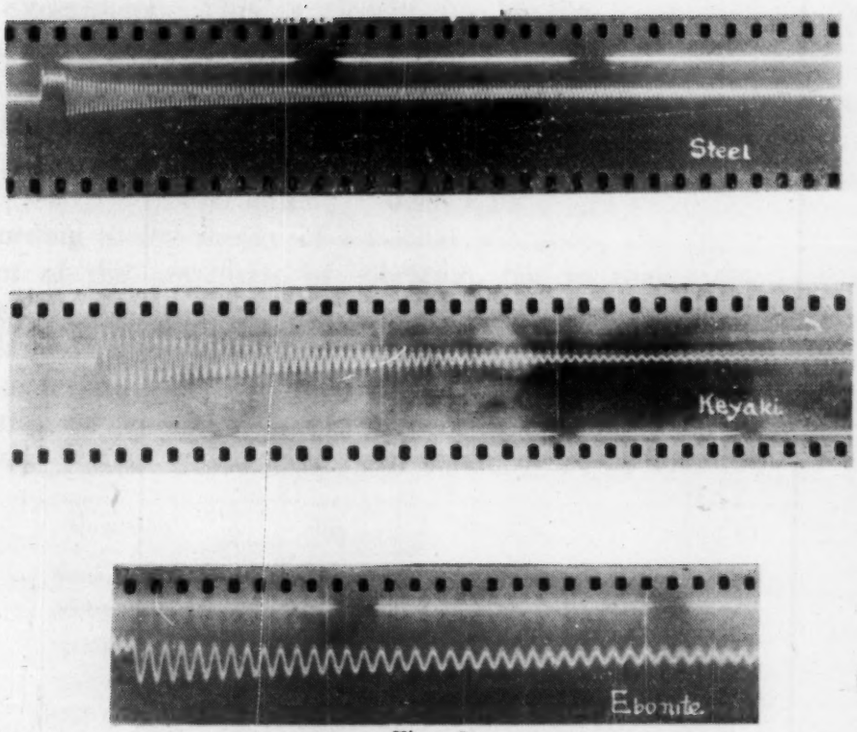

Fig. 8.

internal friction accordingly became much larger in the case of the former experiment. This is clearly due to the energy which escaped from the fixed point in the former case.

The value of coefficient of tangential viscosity of the above two cases was as follows:

The former: 2.396×10^6 (*c. g. s.*)
The latter: 0.937×10^6 („)

According to the theory of torsional vibration, the decrement is independent of the amplitude of vibration, but in reality the logarithmic decrement at the beginning of the vibration decreases linearly with its amplitude and only when the amplitude become small enough, the decrement becomes constant. If the angle of twist of specimen is very small, the logarithmic decrement is independent of its amplitude.

Several results which have been obtained are as follows:

specimen	dia.	temp.	η (*c. g. s.*)
steel	0.15 cm	14°C	0.44×10^6
aluminium	0.18	14	0.43
ebonite	1.00	13.5	0.58
keyaki	1.00	21	0.69
sugi (Cryptomeria)	1.00	21	0.72

Air pressure is in all cases 0 mmHg.

The purpose of this experiment is to find out material which has a large value of η and large rigidity, because for the purpose of earthquake-proofing of structures, the quantity $\eta \times n$ must be large.

In conclusion, the writer wishes to thank Prof. R. Takahasi for his advice and helpful criticism.

16. *Vibration Experiments with the Actual Buildings.*

By Kiyoshi KANAI, Teiji TANAKA and Tomisaburo SUZUKI,

Earthquake Research Institute.

(Read June 21, 1943.—Recieved Nov. 30, 1949.)

1. *Vibration experiments with an actual precast reinforced concrete building.*

The building that the writer conducted experiments was a two-storied building of $3m \times 4m$, the column height of $3.41m$ and $3.26m$, and the weight $7250\,kg$ in the second floor and $7560\,kg$ in the first floor respectively including the live load (1200, $1260\,kg$). The characteristic of the building is that pin joints are fitted to connect the column and beam, and the rigidity of the building is kept with brace-struts. The brace-struts are made of iron and the diameter is $16\,mm$ in the first floor and $13\,mm$ in the second floor respectively.

The experiments static as well as dynamic were conducted alternately. In the present paper are mentioned only dynamic experiments which were conducted by us.

The vibration of the building was caused by a vibrator utilizing the centrifugal force installed in the central part of the roof. Four revolving discs were used and the eccentric mass was $11.43\,kg$. Two sets, each of which consists of two revolving discs, were revolved inversely with a driving electro-motor. Thus the vertical component being cancelled, the vibrational force of the horizontal component only was generated. By changing the eccentric distance from 0 to $11\,cm$ the vibrational force was regulated. The vibration displacements properly magnified was recorded by applying the principle of lever to an arm attached to the pillar. The following four places were selected for the present experiments:—between the ground and the second floor, the second floor, between the second floor and the roof, and the roof.

Keeping the eccentric distance of the vibrator definite and by changing the number of revolution in various ways, the amplitude in each number of revolution was recorded. In such a way the so-called resonance curves were obtained. Such experiments were conducted in succession, and the relation between the vibrational force and the resonance period as well as the resonance amplitude was investigated.

The results obtained are shown in Fig. 1 and Fig. 2. Fig. 1 shows the relation between the vibrational force and the resonance amplitude, and Fig. 2 the relation between the resonance amplitude and the resonance period respectively.

(i) The first experiment (◎); Without the boards.

(ii) The second experiment (○); After hair-cracks were produced in the upper part of column by the static experiment.

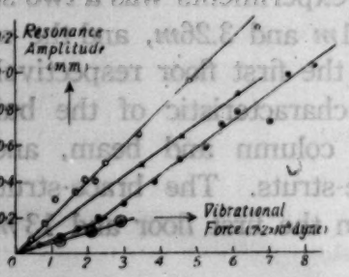

Fig. 1. Relation between the vibrational force and the resonance amplitude.

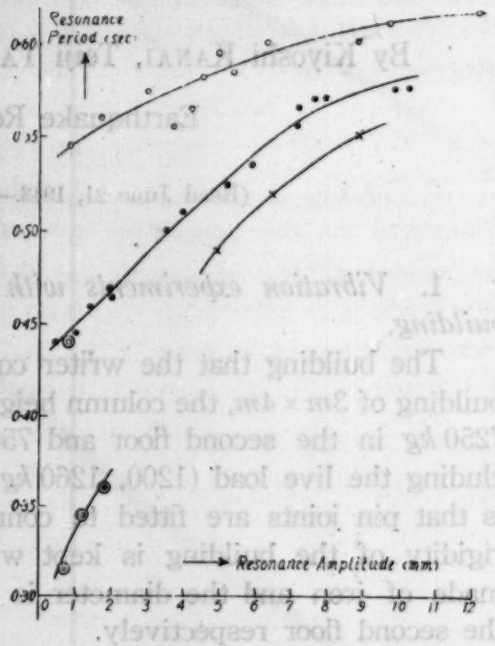

Fig. 2. Relation between the resonance amplitude and the resonance period.

(iii) The third experiment (×); Iron brace-struts covered with concrete.

(iv) The fourth experiment (⊙); With the wall boards.

(v) The fifth experiment (●); After hair cracks were produced by the static experiment in the greater part of morter filled up in the wall board pointing, the capital and the beam.

From Fig. 1 it is known that in the case of (ii), (iii) and (iv) the vibrational force and the resonance amplitude are in the linear relation and apparently the Hook's law holds good of the whole building. In the case of (v) they are arranged on two straight lines, and as long as the vibrational force is small, the same tendency as the case mentioned above is observed, and when the vibrational force reaches to a certain magnitude, the condition changes abruptly. After the condition changed, however, the vibrational force and the resonance amplitude are arranged on a straight line again.

In the case of (ii) the ratio of vibration displacement at the four measuring points takes a almost definite value without any relation with the vibrational force (or the vibration displacement). Namely, even if the

vibrational force increases and the vibration displacement becomes large, the mode of vibration of the whole building remains unchanged. The mode of vibration stated above and resonance period correspond with the results of theoretical study upon vibrations of buildings fitted with pin joints and brace-struts. At least in the case of (ii) no change accompanying the increase of the amplitude was found in the elastic constant and the constructive conditions (mainly the connecting conditions of beams, pillars and brace-struts). Nevertheless, it is shown in Fig. 2 that the resonance period becomes larger as the resonance amplitude increases.

It is known from ⊙ and × of Fig. 2 that when the damping of the iron brace-struts covered with concrete increases, the resonance period becomes shorter and resonance amplitude becomes very small at the same time. This nature has already been clarified by theoretical study.[1)]

It is known from Fig. 1 and Fig. 2 that the wall boards strengthen the rigidity of the building as long as no crack is produced in the wall boards, while the wall boards increase the mass more than the rigidity of the building, when crack is produced in the pointings.

2. *Vibration experiments with an actual wooden school building.*

The vibration of a wooden school building built according to the Japanese Government standard was measured by us. The school building is a tile-roofed, two-storied building. The column height is 3.5 *m*, the width is 6 *m* in the class room and 2 *m* in the corridor respectively, and the length is 10 *m*. In both sides of the building there are partitions, and the part between the partitions is assigned to a classroom. Many brace-struts are fitted. The brace-struts of vertical members are 135×135 *mm*, and those of horizontal members 105×105 *mm* respectively. To connect the vertical members with horizontal ones many partial braces and metal fittings are fitted. Therefore, the school building is a much more rigid construction than those in the past.

The vibration of the building was caused by a vibrator utilizing the centrifugal forces, which was set in the middle part of the second floor, and the vibration was measured with a portable seismograph installed on the beam and on the second floor. The seismograph, the period of which was 4 *sec*, was kept in the critical damping condition, and the geometrical magnitude was arranged so as to be 5.8 times on the beam and 9.6 times on the second floor.

Changing the number of revolution in various ways, the relation between the number of revolution and vibration amplitude was examined.

1) K. KANAI, *Bull. Earthq. Res. Inst.*, **17** (1939), 695—712.

From the resonance curve the relations between the vibrational forces and resonance amplitude as well as resonance period were read. The results are shown in Table I and Table II.

Table I. Relation between the vibrational forces and resonance amplitude as well as resonance period in the beam direction.

Vibrational force (10^6 dyne)	Resonance period (sec)	Resonance amplitude (mm)		
		On the beam	On the second floor	On the beam / On the second floor
7.4	0.348	0.16	0.10	1.6
27.4	0.362	0.48	0.31	1.6
62.3	0.380	1.00	0.63	1.6
92.4	0.395	1.48	0.93	1.6
113.3	0.418	1.88	0.47	1.3

Table II. Relation between the vibrational forces and resonance amplitude as well as resonance period in the girder direction.

Vibrational force (10^6 dyne)	Resonance period (sec)	Resonance amplitude (mm)		
		On the beam	On the second floor	On the beam / On the second floor
9.7	0.305	0.26	0.24	1.1
35.4	0.319	0.48	0.45	1.1
80.2	0.335	—	0.85	—
129.0	0.334	1.25	1.10	1.1
135.0	0.383	1.43	1.10	1·3

In Table I, the amplitude is almost in proportion to the vibrational force. This shows that the elastic constant does not undergo change by the amplitude of vibration (or the vibrational force). The ratio of displacement 1.6 on the beam and on the second floor of the beam direction corresponds to the case of rigid connections at the floors and the base, and shows that the boundary conditions of the construction does not change by the amplitude of vibration, while the period of rasonance becomes larger as the vibrational force (or the amplitude of resonance) increases.

In the girder direction, from the relation between the vibrational force and the resonance amplitude, the slight vibrational force suffices when the amplitude is small. And in this case the displacement on the beam does

not differ much from that on the second floor. These phenomena may probably due to the stiffness of building and the vibrational force consumed to some extent to the bearing power of the ground. Accordingly, in this case the vibration of the building may probably be the resultant vibration of the usual elastic vibration and the rocking vibration with the base as the axis.

The phenomenon that the proper period becomes longer as the vibration amplitude of the building increases is very important regarding the destruction of buildings due to earthquake shocks. If a part of building is destroyed at the time of earthquake, the proper period becomes longer as a matter of course. By the present investigation it has been explained that the proper period may change even if the condition of structure remains unchanged.

In conclusion, we wish to express our thanks to the Ministry of Education, for financial aid (Funds for Scientific Research) granted us for a series of investigations, of which this study is a part.

17. *Relation between the Earthquake Damage of Non-wooden Buildings and the Nature of the Ground.*

By Kiyoshi KANAI,

Earthquake Research Institute.

(Read July 19, 1949.—Recieved Nov. 30, 1949.)

Most of building in Japan being constructed out of wood, many data as to the earthquake damage of wooden buildings were obtained in all destructive earthquakes since 1868, and investigations based upon the data have been done from various points of view.

On the contrary, as non-wooden buildings were relatively small in number and were only in restricted localities, damaged non-wooden buildings were relatively small in number. Accordingly, owing to the shortage of data many aspects are left for investigators to study statistically. There are few data upon the damage of non-wooden buildings that are serviciable to statistical study exept that of the Kwantô earthquake of 1923.

In the present paper the relation between the damage of buildings and the nature of the ground is described based upon the data[1] regarding the damage of ferro-concrete and brick buildings in the former Tokyo city at the time of the great earthquake mentioned above.

At first the former Tokyo city was classified into the following three sections: (I) Honjo and Fukagawa where the alluvium is very thick, (II) the southern part of Kôjimachi, Shiba, Kyôbashi, Nihonbashi, Kanda, Shitaya and Asakusa where the alluvium is relatively thin, (III) the north-western part of Kôjimachi, Azabu, Yotsuya, Ushigome, the greater part of Koishikawa Akasaka and Hongô where the ground consists of the diluvium or the tertiary. Next, the percentage between the total number of damaged ferro-concrete buildings and the total number of investigated buildings is called the damage ratio. And the relation between the damage ratio and the nature of the ground is shown in Table I.

The above figures show that the harder the ground, the severer the damage of ferro-concrete buildings.

Next, the writer examined the relation between the nature of the

1) *The Report of the Imperial Earthquake Investigation Committee*, No. 100, C b, p.p. 211-332, *ditto*, No. 100, C a, p.p. 55-178.

ground and the number of story as well as the story that was most severely destroyed. The result is shown in Table II.

Table I. Relation between the nature of the ground and the damage ratio of ferro-concrete buildings.

	Soft Ground			Firm Ground		
	Number of Damage Buildings (A)	Number of Safe Buildings (B)	Damage Ratio $\frac{(A)\times 100}{(A)+(B)}$	Number of Damage Buildings (A)	Number of Safe Buildings (B)	Damage Ratio $\frac{(A)\times 100}{(A)+(B)}$
Fukagawa (District)	7	43	11	—	—	
Honjo	2	29		—	—	
Kyôbashi	13	52	25	7	10	34
Nihonbashi	28	64		—	—	
Kanda	10	35		6	23	
Shitaya	—	10		5	2	
Asakusa	6	27		—	—	44
Shiba	8	13		3	4	
Kôjimachi	15	39		11	13	
Hongô	—	3		2	16	
Koishikawa	2	10		9	10	
Ushigome	—	—		8	3	
Yotsuya	—	—		7	5	
Akasaka	—	2		4	6	
Azabu	—	—		2	2	
Total	91	327		64	94	41

Table II. Relation between the nature of the ground and the number of story as well as the story that was most severely destroyed.

Ground	The number of story / The story that was most severely destroyed	II	III	IV	V	VI	VII	VIII
Soft (Mainly the Down-town)	1	1	10	3	1	1	—	—
	2	2	7	5	4	1	3	—
	3	—	2	1	—	—	3	3
Firm (Up-town)	1	5	19	5	1	—	1	—
	2	1	—	1	—	—	—	—
	3	—	—	—	1	—	—	—

The figures in Table II are to be read as below; the number of three-storied building the first floor of which was most severely destroyd is 10 in the soft ground and 19 in the firm ground respectively, and so on. It is shown in the above table that the first floor was most severely destroyed in the firm ground, while in the soft ground the first floor was most severely destroyed when the number of story was small and the second as well as the third floors were most severely destroyed when the number of story was large.

The facts shown in Table I and Table II correspond with the results of theoretical study[2] based upon the idea that at the time of earthquake the vibration energy of buildings dissipates to the ground again as the elastic wave that starts from the foundation. According to the results obtained by theoretical study, the smaller the rigidity of buildings compared with the rigidity (or elasticity) of the ground is, the more is the dissipation of vibration energy and accordingly the smaller the vibration amplitude of buildings. The nature corresponds with the damage shown in Table I. And, according to the results of theoretical study, as the dissipation of vibration energy increases, the higher part undergoes the maximum stress (or the maximum bending moment). The fact shown in Table II are fairly explained by this nature.

Table III shows the relation between the nature of the ground and the damage ratio of brick buildings in the former Tokyo city at the time of the great Kwantô earthquake of 1923.

Table III. Relation between the nature of the ground and the damage ratio of brick buildings.

The Number of story	Soft Ground			Firm Ground		
	Number of Damage Buildings (A)	Number of Safe Buildings (B)	Damage Ratio $\frac{(A)\times 100}{(A)+(B)}$	Number of Damage Buildings (A)	Number of Safe Buildings (B)	Damage Ratio $\frac{(A)\times 100}{(A)+(B)}$
1	85	106	45	30	13	70
2	131	183	42	96	31	76
3	24	53	31	17	5	77
Tatal	240	342	41	143	49	74

The above table shows that brick buildings in the soft ground were destroyed much more than those in the firm ground without any relation

2) K. Sezawa and K. Kanai, *Bull. Earthq. Res. Inst.*, **14** (1936), 164, 377, 514. K. Kanai, *Bull. Earthq. Res. Inst.*, **17** (1939), 37.

to number of story.

By the above investigation it has been clasified that the softer the ground, the less the damage of ferro-concrete and brick buildings in the former Tokyo city at the time of the great Kwantô earthquake of 1923. The results obtained can be explained by the results of theoretical study upon the dissipation of vibration energy of buildings to the ground.

It has been said that the damage was always large in the soft ground at the time of destructive earthquakes that occurred in Japan. It seems to be quite contradictory to the results obtained at the present investigation. The author explains the apparent contradiction as follows. Most of buildings shown in the statistics of earthquake damage are Japanese wooden houses, and in those houses the pillars and beams are connected with tenons. Those buildings are liable to be destroyed by the secondary action such as the unequal sinking of the foundation at the time of earthquake.[3] Accordingly, if the relation between the nature of the ground and the damage to buildings is clarified with respect to wooden buildings which are constructed by adopting honestly earthquake-proof technique, the results obtained may be much different from the statistics based upon non-earthquake-proof wooden houses.

In conclusion, I with to express my thanks to the Ministry of Education, for financial aid (Funds for Scientific Research) granted me for a series of investigations, of which this study is a part.

3) K. Kanai, *Bull. Earthq. Res. Inst.*, **25** (1947), 61.

18. *Field Determination of the Elastic Property of Soil Layers (1).*

By Nobuji NASU,

Earthquake Research Institute.

(Read May 17, 1949.—Received Sept. 20, 1949.)

Through the measurement of the artificical earthquakes such as caused by blast, vibrating machine and falling body, we can determine the velocities of elastic waves which are propagated in the superficial soil layer, and from these velocities the elastic constants of the material constituting the ground can be deduced. For the longitudinal wave, the velocity may be expressed as

$$V_1=\sqrt{\frac{E}{\rho}\left(\frac{1-\sigma}{1-\sigma-2\sigma^2}\right)}, \quad \cdots\cdots(1)$$

and for the transverse wave,

$$V_2=\sqrt{\frac{n}{\rho}}=\sqrt{\frac{E}{\rho}\frac{1}{2(1+\sigma)}}, \quad \cdots\cdots(2)$$

where E denotes the Young's modulus, n the shear modulus, ρ the density and σ the Poisson's ratio of the wave-transmitting medium. The velocity, however, is not always constant, but it varies with depth, especially, there is a remarkable change near the surface of the ground. Consequently, the travel-time curve of the wave becomes concave downwards when the distance $\triangle$ is taken on the abscissa, such as, for example, the curve which may be expressed as

$$\Delta=at+bt^2, \quad \cdots\cdots(3)$$

wherh t is the travel-time of the wave.

For various superficial layers, the time-distance curves and the subsurface distributions of velocity have been already given in my previous paper[1]. In general, the actual velocities at the ground surface are far smaller than those reported by many authors heretofore for various kinds of soil, because these reported values should hold at a certain depth from the surface where the soils are more or less compacted or hardened under the weight of the overlying parts of the deposits.

1) N. NASU, *Bull. Earthq. Res. Inst.*, 18 (1940), 289.

The elastic properties of the soil layers may be determined statically by another method, i, e., the load test. However, the result of this test is available only for the materials lying near the ground surface, unless the loading plate of a large area is used, because the distribution of the load intensity (load per unit area) in the interior of the earth shows a rapid decrease with increasing distance from the loading plate. Under these circumstances, we often failed in understanding the results of this kind of test when they were compared with those obtained from the velocities of elastic waves. To make this point clearer, a comparison will be made in the following between the results obtained by the two different methods above mentioned.

Let us take up two examples; one was carried out by the Railway Technical Research Institute in 1940, and the other recently by the writer. The both tests were made on the loam in the up-town of Tokyo. By the weight of the water filled in the tanks the ground was loaded and the amount of settlement was measured by the dial gauges.

The deduction of E was made as follows[2]:

As a first approximation, let E be constant. Then, the settlement of the loading plate s may be expressed as

$$s=\frac{1}{E}\int_0^\infty \sigma_z dz, \qquad \cdots\cdots(4)$$

where σ_z denotes the load intensity at depth z and its distribution in the interior of the soil is assumed to be in the form

$$\sigma_z=p(1-\cos^3\alpha), \qquad \cdots\cdots(5)$$

where p is the load intensity applied on the loading plate, and $\cot\alpha=z/r_0$, r_0 is the radius of the circular loading plate.

After integration, we have

$$s=\frac{2r_0p}{E} \qquad \cdots\cdots(6)$$

From the observed values of p and s, E may be calculated. It should be remembered, however, that a certain amount of error is inavoidable in the value of E deduced in this way, because the assumptions above given may not always be qualified for fixing the elastic condition of the subsurface layers.

(a) The first load test was made at Toyamagahara in the N. W. part of the old city of Tokyo. The area of the loading plate was 2,000 cm^2

2) For example, see A. RAMSPECK, *VDI-Zeitschrift*, 83 (April, 1939), Nr. 17.

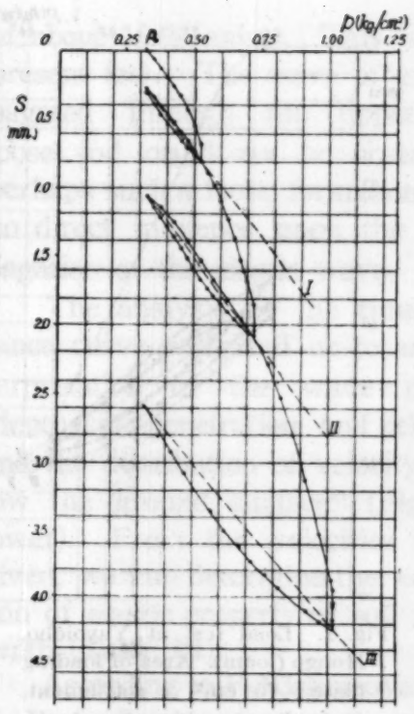

Fig. 1. Load test at Toyamagahara (loam). Area of loading plate= 2,000 cm², s settlement, p= load per unit area of the plate, p_0 that due to the dead weight of the testing apparatus=0.325kg./cm².

and the load intensity was raised to more than 1 kg./cm². in the maximum. Under such a load, the deformation of the ground already exceeded the elastic limit. Indeed, the permanent settlement could be seen, though slightly, when the intensity became larger than 0.5 kg./cm². By gradually increasing and decreasing the load, the hysteresis phenomenon was observed (Fig 1). The speed of loading, the ultimate load intensity (the dead load of testing apparatus is inclusive) and the values of E calculated for the three loops of the curves in this figure are show in Table I.

In the third loop, an increase of E of about 7 % could be seen. The test however, was made on the ground surface somewhat drug down or hardened at the time of installation of the testing apparatus. Hence, the value of E determined by this test may be expected to be rather larger than that at the natural ground surface.

(b) The second load test was made in a new site of the Tokyo University at Yayoicho, Hongo Ward. In this test, a loading plate of 754 cm². in area was used and the load intensity was limited to be 0.37 kg./cm². in the maximum, this enabled the deformation of the ground to be approximately within the elastic limit. To obtain the value of E just at the ground surface, the testing apparatus was set directly on the ground without removing the loose surface. In Fig. 2, we see that during the first course of loading, the

Table I. Load test on loam at Toyamagahara.

Loading (Loop)	Ultimat load intensity (kg./cm².)	Speed of loading (kg./cm.² per minute)	E Calcuated (kg./cm².)
I	0.525	0.001175	196.6
II	0.725	0.00125	189.0
III	1.075	0.00122	211.7

plate sunk rapidly with increasing load, but the rate of settlement suddenly decreased and only a slight difference of the rate could be seen in the successive courses. It will be unreasonable to consider the first rapid settlement to be an elastic deformation. Surely, it is due to the compaction of the loose soil. The conditions of loading and the calculated values of E are shown in Table II.

Table II. Load test on loam at Yayoicho.

Loading (loop)	Ultimate load intensity (kg./cm².)	Speed of loading (kg./cm². per minuts)	E calculated (kg./cm².)
I	0.370	0.0097	153.8
II	0.370	0.0097	160.0
III	0.370	0.0096	163.1

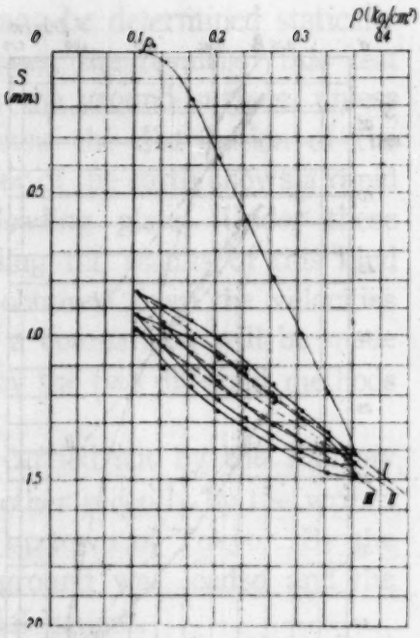

Fig. 2. Load test at Yayoicho, Hongo (loam). Area of loading plate = 754 cm², s settlement, p = load per unit area of the plate, p_0 that due to the dead weight of the testing apparatus = 0.106 kg./cm².

Now, the result of the determination of the velocities of elastic waves is as follows:

The time-distance curves of elastic waves which were obtained in the place where the second load test was made may be expressed as

$$\Delta = 125.30t + 7215.05t^2, \quad \text{(for longitudinal wave)}, \quad \cdots\cdots (7)$$

$$\Delta = 55.02t + 850.00t^2, \quad \text{(for transverse wave)}, \quad \cdots\cdots (8)$$

where Δ denotes the distance (i. e., the distance of seismograph from falling body) and t the travel-time of the wave (Fig. 3, upper). These expressions may hold for a distance less than 10 metres. The velocities of two types of waves at the ground surface are given by the coefficients of the first terms lying on the right-hand side of the above expressions. From these velocities, we have

$$E = 129.4 \text{ kg./cm.}^2,$$

$$n = 46.9 \text{ kg./cm.}^2,$$

$$\sigma = 0.380.$$

The density, ρ, of the loam in this case is taken as 1.52; the mean obtained from five specimens. The order of E here obtained is in good accordance with that obtained in the second load test, though a difference

of about 18% exists. This will be inevitable within the accuracy of the present test. The wave of extremely low velocity which should be propagated through the uppermost loose soil could not be observed, perhaps such a loose formation has no direct influence upon the propagation of the elastic wave.

The analysis of the time-distance curve will lead us to an interpretation of the wave paths (depths of penetration and others) and the distribution of velocity below the ground surface[3] (Fig. 3, lower). From the velocities thus given, we can determine the variation of elastic property of soil with depth (Table III).

According to F. Kishinouye and K. Iwama[4], the mean velocity of longitudinal wave was 300 m./sec. and that of transverse wave was 115 m./sec. in the loam (deposited in the site of the Tokyo University), when they were measured within a

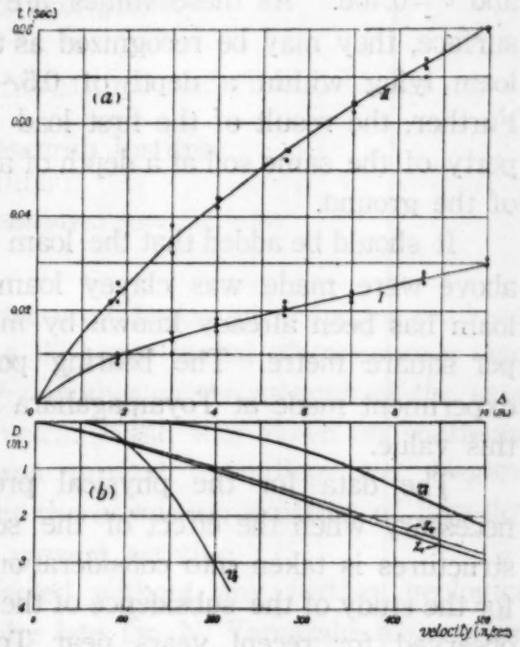

Fig. 3. (a) Time-distance curves. I, longitudinal wave, II transverse wave.) (b) Depth of penetration for given value of Δ (z_1 for longitudinal wave, z_2 for transverse wave) and the variation of velocity with depth D.

Table III. Velocities of waves and elastic constants.
(loam in the up-town of Tokyo.)

Depth (m.)	V_1 (m./sec.)	V_2 (m./sec.)	E (kg./cm.^{2})	n (kg./cm.^{2})	σ
0	125	55	129.4	46.9	0.380
0.1	176	71	219.0	78.2	0.403
0.3	233	91	362.2	128.4	0.410
0.5	274	104	478.7	167.8	0.415
1.0	353	129	750.3	258.1	0.421
1.5	414	151	1012.9	353.6	0.423
2.0	470	170	1287.5	448.2	0.424
2.5	526	187	1560.4	542.4	0.427
3.0	559	201	1762.3	626.6	0.427

3) See 1)

4) F. Kishinouye and K. Iwama, *Bull. Earthq. Res. Inst.*, **22**, (1944), 170.

distance of less than 10 metres. If so, the elastic constants which are deduced from these velocities become as $E=576$ kg./cm.^{2}, $n=206$ kg./cm.^{2} and $\sigma=0.406$. As these values are far larger than those at the ground surface, they may be recognized as the mean values which prevail in the loam lying within a depth of 0.5~1.0 m. measured from the surface. Further, the result of the first load test will account for the elastic property of the same soil at a depth of about 10 cm. below the natural surface of the ground.

It should be added that the loam on which the experiments mentioned above were made was clayey loam and the bearing power of such a loam has been already known by many experiements to be about 5 tons per square metre. The bearing power which was deducible from the experiment made at Toyamagahara also showed a good agreement with this value.

The data for the physical properties of various soil layers are necessary when the effect of the soil layers upon the vibration of the structures is taken into consideration. Further, the data are also helpful for the study of the subsidence of the lowland which has been continuously observed for recent years near Tokyo and Osaka. The study is being continued with the Fund for Science Research of the Ministry of Education for the year 1949.

19. *A Brief Note on the Recent Explosive Activity of Volcano Yakeyama.*

By Takeshi ICHIMURA, Ryōhei MORIMOTO and Hiromichi TSUYA,

Earthquake Research Institute.

(Read Oct. 18, 1949.—Received Sept. 30, 1949.)

Volcano Yakeyama, Niigata Prefecture[1], broke out in sudden explosion on the fifth of February, 1949, after a 95 years period of quiescence since 1854. The explosion was followed by another on the seventh of the same month. In the first explosion, the volcanic ash was blown off southeastwards and fell on the snow-covered ground extending over Nagano, Gunma and Tochigi Prefectures, but there was no eruption of lava-flow throughout the entire period of the present activity.

Yakeyama has long been neglected without any further geological investigation except that carried out by late Dr. N. Yamazaki many years ago[2]. Even after the recent explosions, it had not been intended to be examined before Tsuya and Ichimura had an opportunity in this summer to study the activity in co-operation with Dr. Minakami and his associates. In the beginning of August, they spent several days on the volcano and observed geologically the scene of the present activity. The rock-specimens collected by them were petrologically examined by Morimoto, although their chemical characters have not yet been determined. The present paper is a summarized note of the result of these field and laboratory works.

Yakeyama is an isolated volcano in a highly mountainous area, rising up to 2400.3 m above the sea (Pl. Figs. 1—2). It adjoins Hiuchiyama (2462 m) on the east and Hirukurayama (1840.9 m) on the northwest, while it lowers abruptly northwards to a gently sloping ridge between the rivers Yake-kawa and Ogura-gawa. Although the volcano is in a young stage of the erosion cycle, it is more or less asymmetrical in shape. Thus, looking from the northern foot, its left-hand (eastern) side is convex upward in profile, suggesting the original slope of a lava-dome,

1) The volcano is accessible from Kajiyashiki, a small town along the Hokuriku Railway Line, passing through the villages Otozaka and Yunokochi and the Sasakura hot-spring resort. Its summit is about 16 km distant from Yunokochi.

2) N. YAMAZAKI, *Rep. Earthq. Inv. Comm.*, 8 (1895) 55-60.

Fig. 1. Geologic map of Volcano Yakeyama.

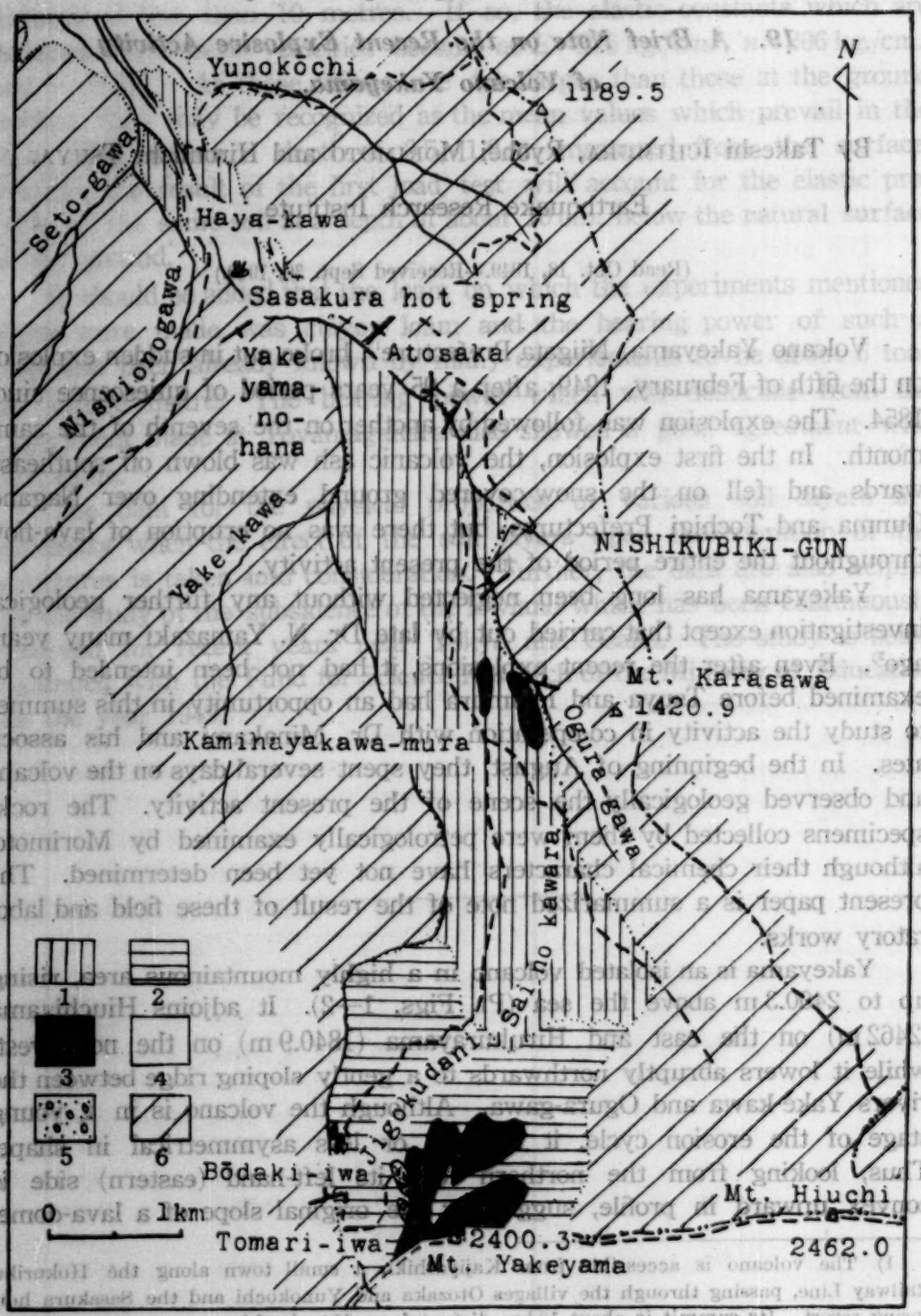

1. Mud flow. 2. Talus deposits. 3. Lava. 4. Recent fluviatile deposits.
5. Agglomeratic lava. 6. Tertiary.

whereas the other side is concave upward, being mostly covered with talus conoid studded with lava crags.

The volcano (Fig. 1) is underlaid by Tertiary sediments composed of dark-gray or black shale and gray or dark-gray sandstone. These sediments are well bedded and highly cliffed along the Yake-kawa and Oguragawa, where there are likely to be two different formations unconformable to one another, dipping 20°—70° northeast or northwestwards. They may be assigned to the Miocene and Pliocene, although their definite

Table I.

Phenocrysts	1	2
Plagioclase	An 65—60, An 55, An 70—47, An 60—54, Commonly An 60—55.	An 78—73.
Augite	β_D=1.700, 2 V=49°	2 V=55°, 57°.
Hypersthene	(−) 2 V=55°, 56°, 58°, 56°—58°, (core) (margin) γ_D=1.712, ρ>v about X	(−) 2 V 56°, 57°. ρ>v about X.
Oxyhornblende	(−) 2 V=74°, 76° α_D=1.666 β_D=1.705 c∧Z ≒ 3°, γ_D=1.730 X=Light orange yellow Y=Orange Z=Dark reddish brown X<Y<Z ρ<v about X.	—
Olivine	−	(−) 2 V=86°
Magnetite	+	+
Groundmass	Andesine Augite Hypersthene Magnetite Glass Tridymite (±)	Labradorite (An 65±) Augite Hypersthene Magnetite Glass

1) Hornblende-olivine-bearing two-pyroxene-andesite.
2) Basaltic inclusions in the andesite.

horizons have not yet been determined by ossils. Some of these Tertiary formations exposed here are intruded by liparite, propylite and allied volcanics. Hiuchiyama, Hirukurayama, Eboshiyama, etc. are the mountains made up of the similar Tertiary sediments and locally covered by andesitic agglomerates. Recent fluviatile deposits form the alluvial flat in the down stream of the Haya-kawa, whereas a volcanic mud-flow accumulates in terraces in the valleys extending from the northern foot of Yakeyama down to the middle of the Haya-kawa.

Yakeyama is a massive volcano, where the lava, partially agglomeratic, is represented exclusively by olivine-hornblende-bearing two-pyroxene-andesite. The andesite here is mostly a compact and porphyritic rock with a dark gray color, although it often has a reddish color due to reheating. It is characterized by the presence of phenocrystic olivine, hornblende, augite, hypersthene and labradorite in the groundmass composed of augite, hypersthene, andesine, tridymite, magnetite and glass. The mineral components, as determined by Morimoto are shown in Table I.

Moreover, the lava includes frequently a number of small fragments of a basaltic rock and white-colored liparite. They must have come

Fig. 2. Doleritic inclusion in the andesite. Crossed nicols.

Fig. 3. Olivine coated with the groundmass similar to that of doleritic inclusions. Phenocryst below is oxyhornblende. Crossed nicols.

from the base rocks through which the lava erupted to the surface. The basaltic inclusions contain phenocrysts of bytownite, olivine, augite,

hypersthene, and microphenocrysts of augite and magnetite in the intergranular groundmass composed of labradorite, augite, hypersthene, magnetite and glass.

Olivine crystals, which occur as phenocrystic grains associated with pyroxene in the andesite lava, are always coated with the groundmass similar to that of the basaltic inclusions. Accordingly, it is inferred that the olivine crystals in the lava are xenocrysts derived from a basaltic (or doleritic) rock similar to the basaltic inclusions. Some of the pyroxene and calcic plagioclase that occur as porphyritic minerals in the lava have also microscopic characters suggestive of xenocrystic origin.

The mud-flow, which extends about 16 km from the volcano down to Otozaka along the valleys of the Yake-kawa, Ogura-gawa and Haya-kawa, with the width of 250–1500 m and the thickness up to 200 m, is one of the remarkable products of the volcano. It forms the bush-covered flat land (Fig. 4) of Saino-kawara, about 1450 m in height above the sea and 1500 m in width, on the northern foot of the volcano, and is traceable up to the middle of its northern flank. The mud-flow is a chaotic mass consisting of andesite-blocks, angular to sub-angular, and light-gray sandy material, together with fragments of various rocks (lamprophyre, silicified sandstone, shale, etc.) which must have come from the base of the volcano. The andesite-blocks, which are most abundant and attain

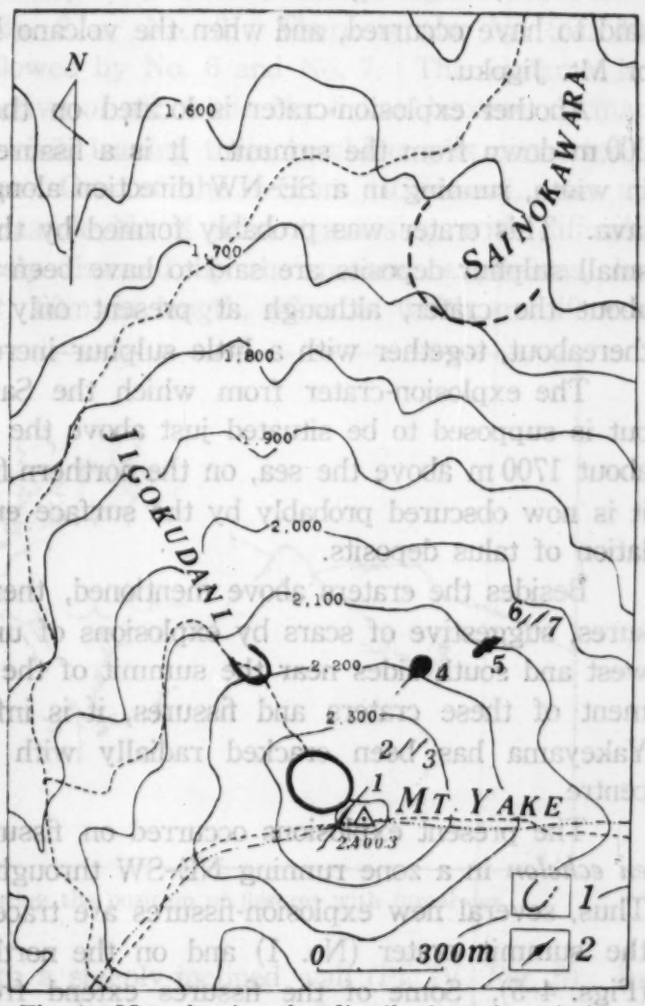

Fig. 4. Map showing the distribution of explosion craters and fissures
1...Explosion crater, 2...Fissures with fumaroles.

sometimes up to 2 m in diameter, are petrographically uniform, being quite similar to the lava (olivine-hornblende-bearing two-pyroxene-andesite) that forms the main part of the volcano.

The volcano has, at least, three explosion-craters. One of these is found on the summit, where it forms a bowl, about 150 m (E–W) and 60 m (N–S) in diameter, surrounded by walls, partly vertical and 30–70 m in height. Its bottom is buried with ashes and lava-blocks crumbled down from the surrounding walls. This crater was probably formed in 1361 when, according to a local tradition, an eruption of the volcano is said to have occurred, and when the volcano had been called Mt. Chausu or Mt. Jigoku.

Another explosion-crater is located on the northwestern flank, about 200 m down from the summit. It is a fissure-like opening, 10 m or more in width, running in a SE–NW direction along a cliff of the agglomeratic lava. This crater was probably formed by the explosion of 1852. Some small sulphur deposits are said to have been worked before on the ground about the crater, although at present only a feeble fumarole is found thereabout, together with a little sulphur incrustation on the rock.

The explosion-crater from which the Sainokawara mud-flow poured out is supposed to be situated just above the upper end of Saino-kawara, about 1700 m above the sea, on the northern flank of the volcano, although it is now obscured probably by the surface erosion and the thick accumulation of talus deposits.

Besides the craters above mentioned, there are several lines of fissures, suggestive of scars by explosions of unknown ages, on the southwest and south sides near the summit of the volcano. From the arrangement of these craters and fissures, it is inferred that the lava-dome of Yakeyama has been cracked radially with the summit crater as the centre.

The present explosions occurred on fissures arranged in parallel or *en echelon* in a zone running NE–SW through the summit of the volcano. Thus, several new explosion-fissures are traceable on the eastern wall of the summit crater (No. 1) and on the northeastern flank (No. 2–No. 7) (Figs. 4–5). Some of the fissures extend from the summit to several scores of meters down the southern flank. When the writers visited the scene, there were a number of fumaroles on the fissures, issuing whitish vapour-clouds from fissures or crater-like openings, with rumbling and hissing noises. On the summit were found eight fumaroles (Pl. IV, Figs. 3–4), of which the most active one was situated on the highest part of the eastern wall of the summit crater (Pl. IV, Fig. 4). The ground about

the fumaroles has been covered with incrustations of sublimates, the most predominant of which are sulphur and halotrichite [$FeAl_2(SO_4)_4 \cdot 24H_2O$][3]. The fumaroles showed a temperature ranging from 90.2° to 94,5°C. at their mouth, their exhalations being composed mainly of superheated steam with a small amount of H_2S and SO_2.

The fumaroles on the northeastern flank are located on the slope between 1950 m and 2300 m in height above the sea (Figs. 4–5; Pl. IV Fig. 2). Of these, No. 2 and No. 3 are at the highest level, about 70–80 m below the summit, whereas No. 4 is found by descending the slope, about 100 m northwards from No. 2 or No. 3. There is also No. 5 in the vicinity of No. 4, being followed by No. 6 and No. 7. The fumarole No. 4 is the largest and most active of all, while No. 5 has become dormant at the time of the writer's visit, leaving three bowl-like pits connected in a line on one of the fissures. One of the writers (Ichimura), who approached the rim of the fumarole No. 4 after traversing with difficulty the dangerous area intensely fissured by the present explosions, has found there a bowl-like pit, 60m in length, 40 m in width and 40 m or

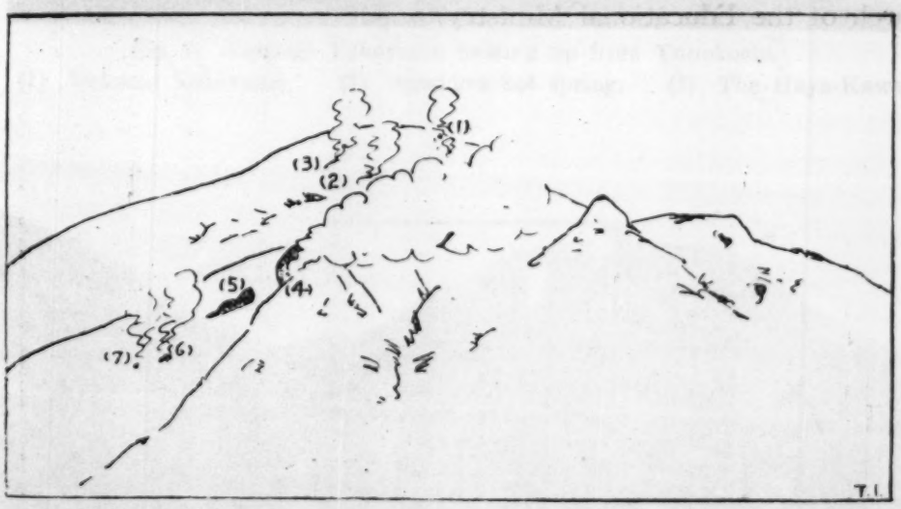

Fig. 5. A sketch showing the position of fissures with fumaroles.

more in depth, bordered with a steeply inclined wall (Pl. IV, Fig. 5). Its southern end passes into irregular crevasses, 4–6m in width, opened on the cliff of old lava (Pl. IV, Fig. 6), where sulphur is deposited beautifully as well as abundantly from the exhalations containing SO_2 and H_2S. The ground about the pit is thinly covered with halotrichite and traversed by small cracks here and there.

3) The writers owe Prof. T. Shirai for the chemical identification of the mineral.

As is shown by the fumarole No. 4, the explosion-pits have a tendency to from a bowl or funnel-shaped opening on the unconsolidated ash or talus-covered ground, but they become narrower and pass into crevasses in the hard and massive lava, representing the fissures that cut the volcano in the NE–SW direction through the summit. Though enlarged and came clearly into sight by the present explosions, these fissures seem to have been formed, together with other radial fissures on the volcano, either by the contraction due to cooling of the lava-dome or by the expansion due to upthrusting of the dome.

The present activity of Yakeyama is a type of the simple steam explosions that occur near the earth's surface without incorporation of the incandescent material. Thus the solid ejecta newly accumulated several scores of centimeters deep on the ground about the explosion-pits are exclusively fragments, ranging in size from blocks to ash, of the pre-existing lava of the volcano, neither new lava nor juvenile pyroclastic material having been ejected by the present explosions.

Expense of this research was defrayed from the fund for Scientific Research of the Educational Ministry.

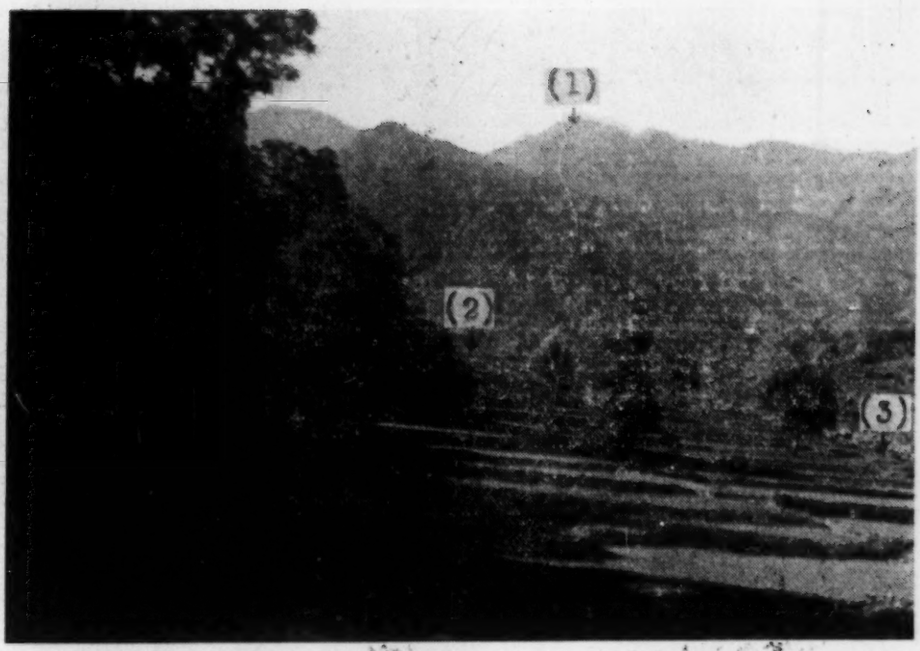

Fig. 1. Volcano Yakeyama looking up from Yunokochi.
(1) Volcano Yakeyama, (2) Sasakura hot spring. (3) The Haya-Kawa.

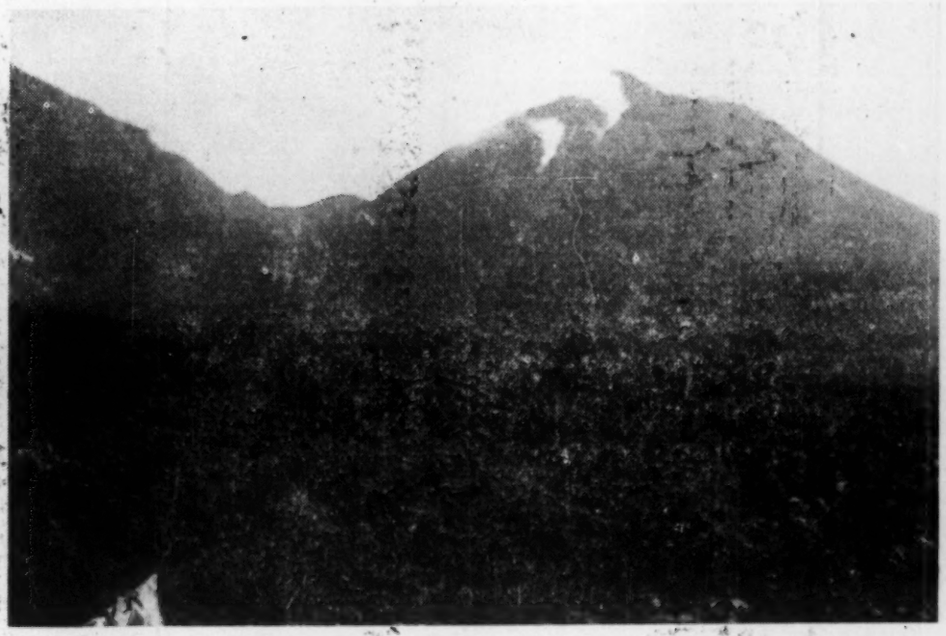

Fig. 2. Volcano Yakeyama viewed from near Sainokawara.

（震研彙報 第二十七號 圖版 市村・森本・津屋）

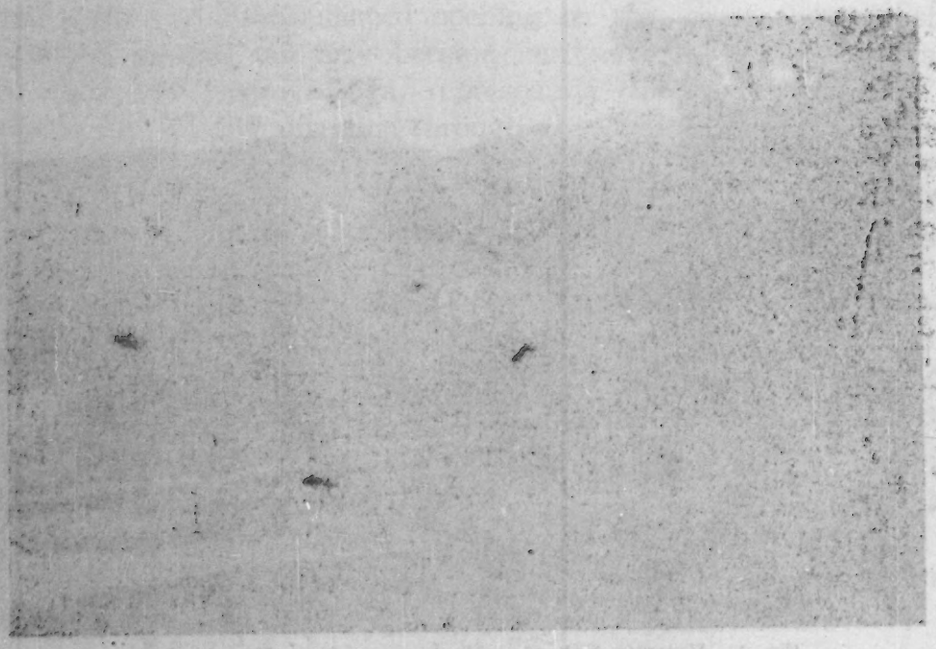

Fig. 3. Fumaroles on the summit (I).

Fig. 4. Fumaroles on the summit (II)

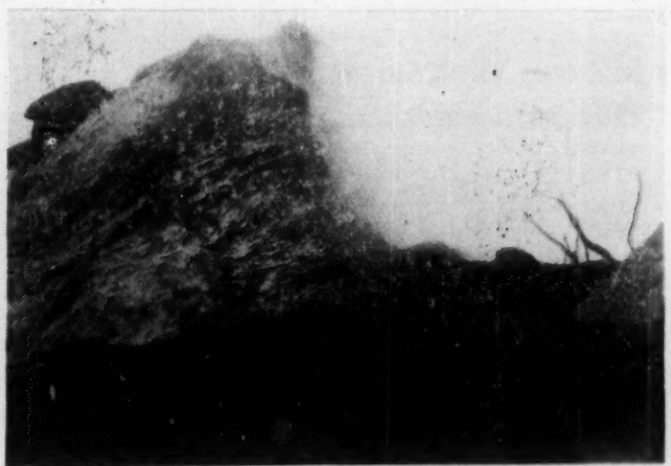

Fig, 5. The most active fumarole on the northeastern flank. The white substance on the surface is halotrichite.

Fig. 6. The largest crevasse cutting through the andesite lava exposed on the northeastern flank. It is connected with a bowl-like pit northwards.

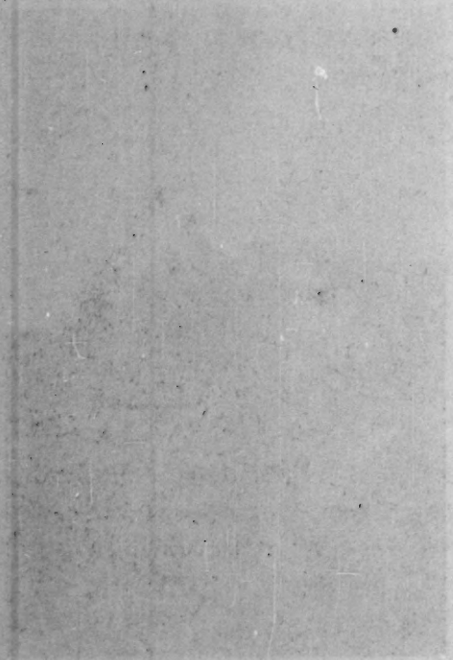

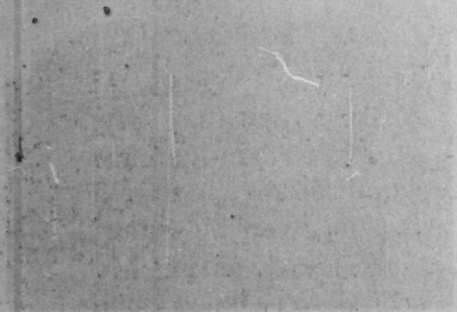

20. *Hydrated Aluminium-Sulphate Minerals from New Fumaroles on Volcano Yakeyama, Niigata Prefecture.*

By Hiromichi TSUYA, Takeshi ICHIMURA
and Toshiaki SHIRAI,

Earthquake Research Institute.

(Read Nov. 15, 1949.—Received Sept. 20, 1949.)

By the explosive activity of Volcano Yakeyama in February, 1949, a number of fumaroles were formed on the new explosion-fissures which, passing through the top of the volcano, run in the NE.-SW. direction. In August, 1949, when two of the writers (Tsuya and Ichimura) visited the volcano, rocks around most of the fumaroles had been covered thickly with sublimates consisting principally of white fibrous minerals, besides sulphur. Ichimura collected two samples of the minerals—one (sample 1) from a fumarole on the summit (Fig. 1, a) and the other (sample 2) from a fumarole on the northeast flank of the volcano (Fig. 1, b), and Shirai analyzed them chemically with results as shown in Table I.

Table I. Composition of hydrated aluminium-sulphate minerals from Yakeyama.

	Al_2O_3	SO_3	H_2O	FeO	Other components
Sample 1	10.5	32.1	52.1	4.5	CaO 0.2, As_2O_3 0.3, Cl trace.
Sample 2	13.5	33.0	50.2	2.5	Cl trace.

The minerals occur in a white mass of delicate acicular crystals, as shown in Figs. 2, 3. They taste inky astringent. Heating them strongly, they lose water, leaving a light-brownish powdery material. The chemical composition shows the minerals to be of halotrichite group (hydrated aluminium-sulphates). General formula for the group is given by Dana[1] as $MAl_2(SO_4)_3$ 22 (or 24) H_2O, where M is a bivalent metal such as Fe, Mg or Mn. But many examples of chemical analyses of fibrous halotrichite minerals shown in the Dana's book have not any definite composition as expressed by this formula. The chemical analyses of the minerals in

1) DANA, E. S., "Dana's System of Mineralogy," 1892-1915, 929.

question also do not agree exactly with the formula, being intermedite between the ideal composition of halotrichite $FeAl_2(SO_4)_4\,24(H_2O)$—Al_2O_3= 11.0, SO_3=34.5, FeO=7.8 and H_2O=46.7—and that of alunogen $Al_2(SO)_3\,18H_2O$—Al_2O_3=15.3, SO_3=36.0 and H_2O=46.7. Judging from their mode of occurrence and physical properties, however, it may be safe to identify them with halotrichite.

Fig. 1. a. Fumaroles on the eastern wall of the summit-crater of the Volcano Yakeyama.

Fig. 1, b. A fumarole viewed from a short distance, on the northeastern flank of Volcano Yakeyama.

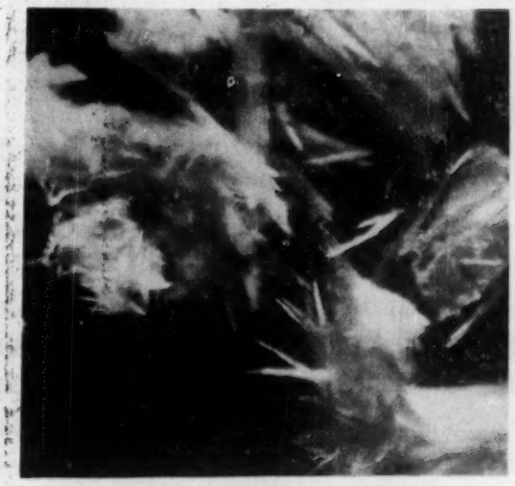

Fig. 2. Halotrichite from a fumarole on Volcano Yakeyama (Sample 1.). ×220.

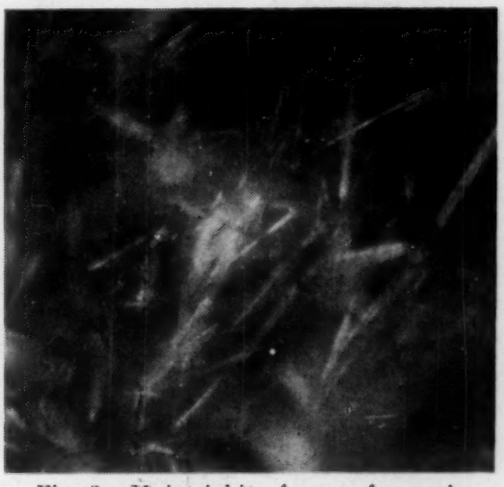

Fig. 3. Halotrichite from a fumarole on Volcano Yakeyama (Sample 2.). ×220.

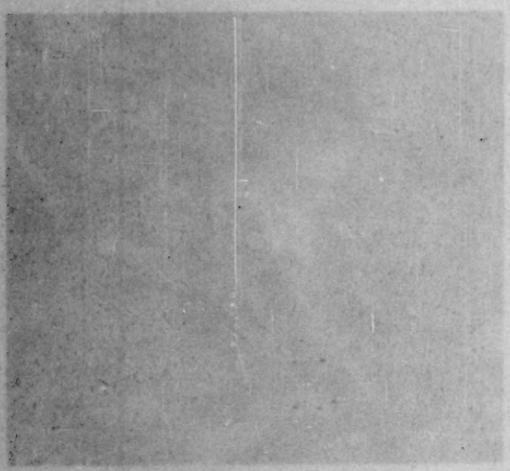

21. *Minor Activity of Volcano Yake-yama in 1949.*

By Shūzō SAKUMA and Takeshi MINAKAMI,

Earthquake Research Institute.

(Read Dec. 20, 1949.—Received Nov. 30, 1949.)

In the morning of February 5, 1949, Yake-yama which is situated nearly at the boundary of Niigata and Nagano prefectures, resumed its activity with detonations like those of avalanche or thunder and lasted about 20 minutes. Soon after that, ash began to fall over the villages on the eastern skirt of Volcano Myōkō, although neither the mountain body of Yake-yama nor smoke column of explosion could be seen at that time because of the thick snowy cloud. Slight precipitation of ash was also noticed at the northern Kwanto Plain. Since then, the volcano continued to emit thick smokes of water-vapour mixed with slight SO_2, H_2S and ash from newly opened fissures.

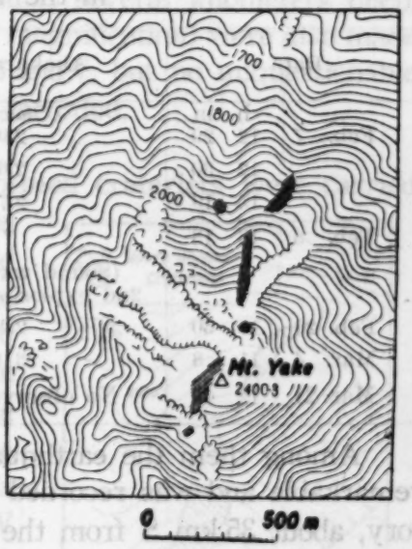

Fig. 1. Topographical map near the summit of Mt. Yake. hatched area; positions of newly formed craterlets, fissures and fumaroles.

Seismometric Observation.

The second took place on 13 h 38 m, February 8, with detonation, which was heard even at Takada. After the second explosion, the volcanic activity decayed by degree. But it manifested ebb and flow sometimes. For instance, detonations like a rushing train and sudden increase water-vapour, with no ash precipitation, were observed on February 15 and September 13. Volcanic ash, detritus and fragments of old lava fell and deposited on the snow of the eastern side of the volcano.

It is well known that not only volcanic tremors but earthquakes of ordinary type also take place before and during the eruptions of andesite volcanoes in which fresh lavas are extruded.

It is, however, an important problem whether earthquakes occur or not in such a minor activity as the present case. For, those volcanic activities

not accompanied by ejection of incandescent lava fragments as the present activity of Yake-yama are often classified into the fumarolic activity of large scale and sometimes ascribed to an extremely shallow origin. However, if earthquakes take place at the depth of several kilometres of the volcano, the volcanic activity may probably be not of extremely shallow origin, but may be caused by deeply seated magma.

Since February 6, the following day of the first explosion, a horizontal seismograph of the improved Ishimoto's type ($T_0=1.0$ sec., magnification $\times$ 200) was set at Akakura, 13 km ESE from the volcano. Since February 11, another seismograph of the same type was operated at Yunokōti, about 9 km NWN. Observations was continued till March 6 at the former temporary station and till June 10 at the latter.

On the basis of those seismometric observation, it was brought out clearly that several non-perceptible earthquakes took place in this period in the vicinity of Yake-yama as given in Table I.

Table I. P-S duration of earthquakes which occurred in the vicinity of Yake-yama.

Date	Akakura	Yunokōti	Nagano
h m	sec.	sec.	sec.
Feb. 7 12 29	2.9		
12 30	2.6		5.0
13 19	2.7	No observation	
Feb. 8 13 13	? (Sound wave of 2nd explosion ?)		
Feb. 20 15 30	2.4	?	
Mar. 4 11 8	3.0	2.1	
Mar 21 12 43	No observation	2.0	

Among them the earthquake at 12 h 30 m, February 7, was the most remarkable and was recorded also at the Nagano Meteorological Observatory, about 35 km S from the volcano. P and S phases of seismic waves of this earthquake could be quite easily distinguished on the seismogram obtained at Akakura, where the P-S duration was 2.6 sec. At Nagano, however, the form of the earthquake-motions was so much complicated that even the P-S duration was estimated with difficulty at 5 seconds.

Judging from our knowledge of the shapes of shallow earthquakes originated from volcanoes as reported in the same Bulletin[1] regarding various earthquakes of the Usu volcano, we can infer that the present

1) T. Minakami, *Bull. Earthq. Res. Inst.*, 27 (1949), 123, 129.

earthquake must have been originated at the depth of not less than a few kilometers, not extremely shallow. Accordingly, it will be reasonable to consider that the activity of Yake-yama also had its source of effusive energy at the depth of a few kilometres at least.

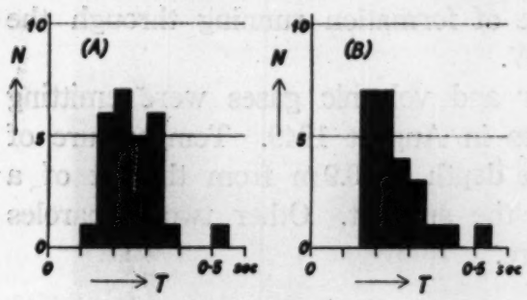

Fig. 2. Frequency distribution of periods of earthquake-motions observed at Akakura.

In order to show a character of two earthquakes recorded at Akakura, we made period analyses of their earthquake-motions and as will be seen on the diagram of Fig. 2, the shorter periods than 0.3 second are markedly predominant for both earthquakes, being 0.25 and 0.26 second in the mean periods respectively. The characteristics just mentioned are similar to the earthquakes of tectonic and volcanic origin, of which hypocentres are found several kilometers deep.

More minute observations (4,000 times in magnification) were also made at Akakura during two nights on February 6 and 7, but no unquestionable micro-earthquake and volcanic tremor were recorded.

Topographical Survey.

Detailed investigations of the newly formed craterlets were carried out in August of the same year. Positions of craterlets and fissures were determined with a transit by triangulations from three base-points whose positions were also fixed with regard to the triangulation points of the Land Survey Department. As shown on the map of Fig. 3, fissures and craterlets were aligned on the several lines running towards N 10°–30° W and as a whole in a single N 20° W zone which is about 150 m wide, 1 km long horizontally, cutting across the eastern wall of the top crater. The lowest fumarole newly in action was about 1880 m high above the sea-level on the northern side of the volcano. Largest craterlet was 50 m in diameter, and some craterlets opened into the others and become cocoon-shaped.

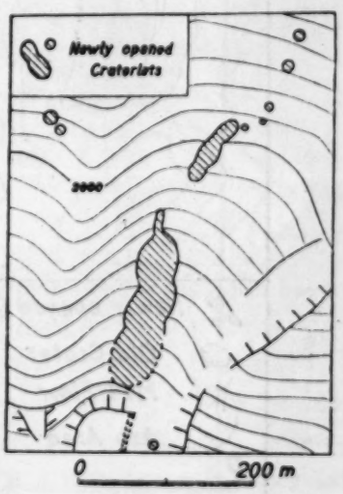

Fig. 3. Newly opened craterlets on the northern side of the volcano.

According to the present investigation, it was made clear that the newly opened fissure passed through the central part of the old summit

crater, in which a craterlet of conical shape, about 30 m in diameter, was newly formed in the present explosion, though it had been already in dormant state at the time of our investigation.

In short, we can conclude that the present explosive activity of minor scale took place along the weak line of formation running through the top in the direction of nearly N 20° W.

On the other hand, water-vapour and volcanic gases were emitting from some of craterlets and fissures in August 1949. Temperature of gases was measured at 92.5° C in the depth of 0.9 m from the jet of a newly formed small fumarole near the summit. Other two fumaroles near by showed the same temperature.

Mud Flow.

Ash and detritus which were ejected in the series of the present explosions and deposited on the snow of the eastern side of the volcano, flowed down mixed with abundant water in spring when the snow began to melt by degree. Namely, the water of the riverlet Ogura (Hiuti) which

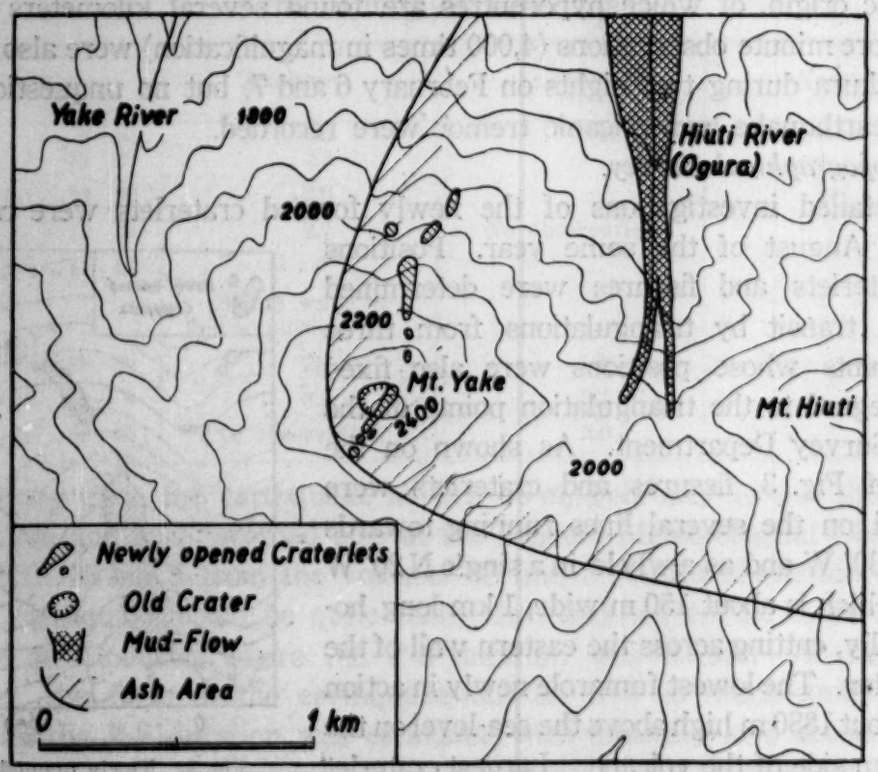

Fig. 4. Devasted area caused by the mud-flow on July 30 and the craterlets newly formed.

runs between Mt. Hiuti and this volcano, became muddy of greyish black colour and piled muddy ash upon the rice-fields under irrigation. After

Fig. 5. Mt. Yake viewed from the northern side.

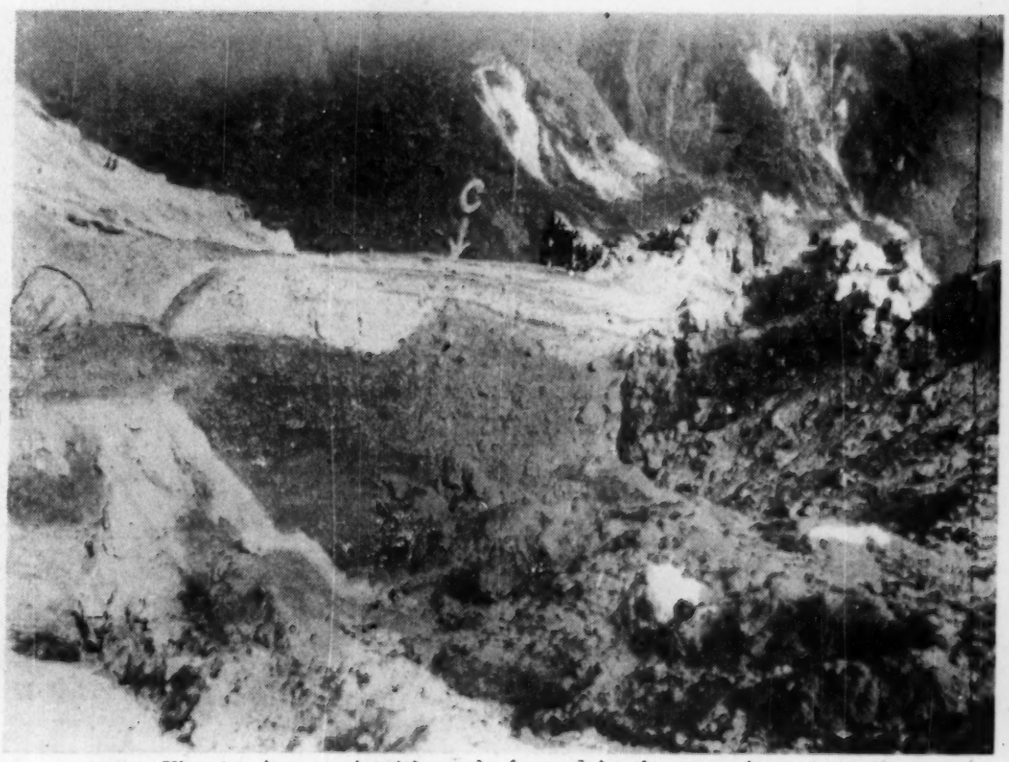

Fig. 6. A craterlet (c) newly formed in the summit crater.

（震研彙報　第二十七號　圖版　佐久間・水上）

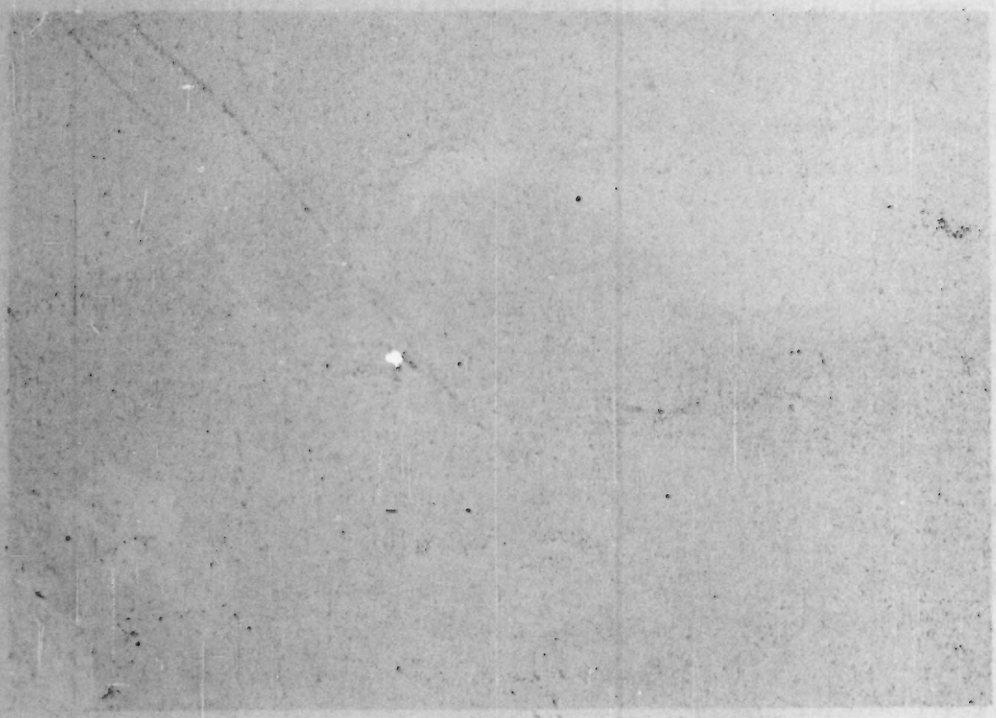

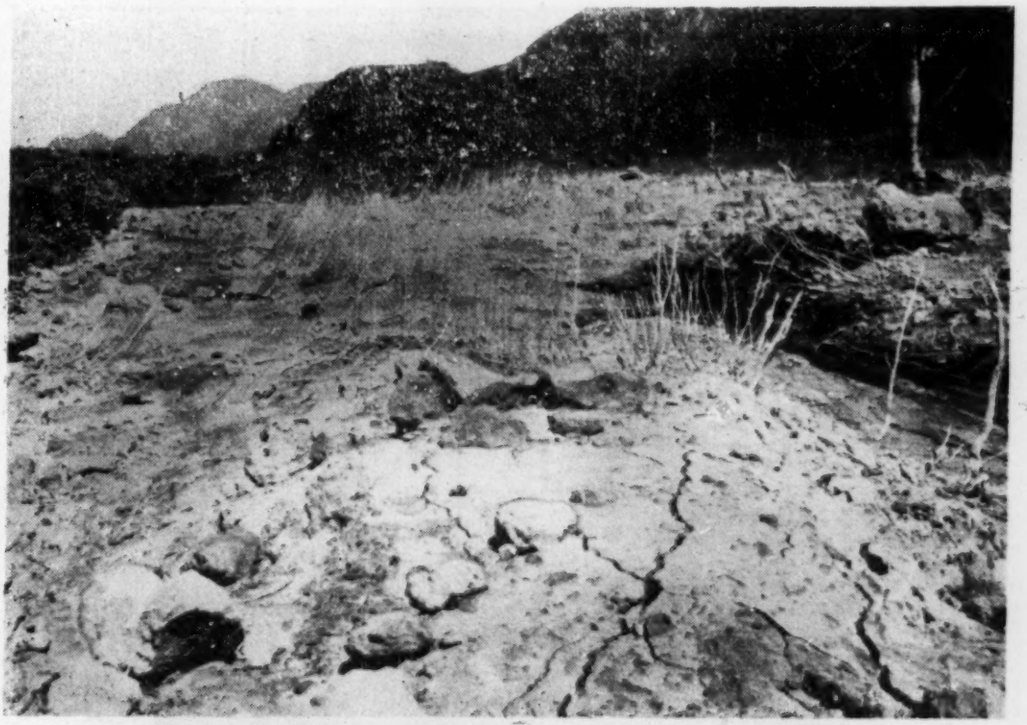

Fig. 7. Devastated area caused by the mud-flow on July 30, 1949.

Fig. 8. Mud and water dammed up by collapse of riverside cliffs.

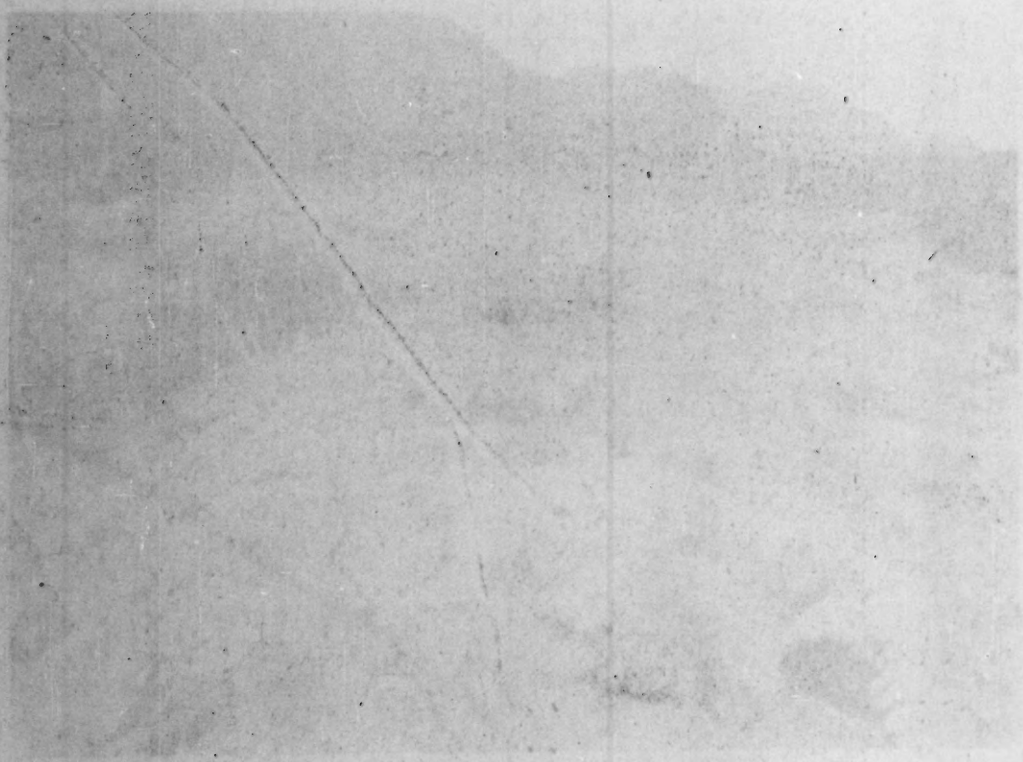

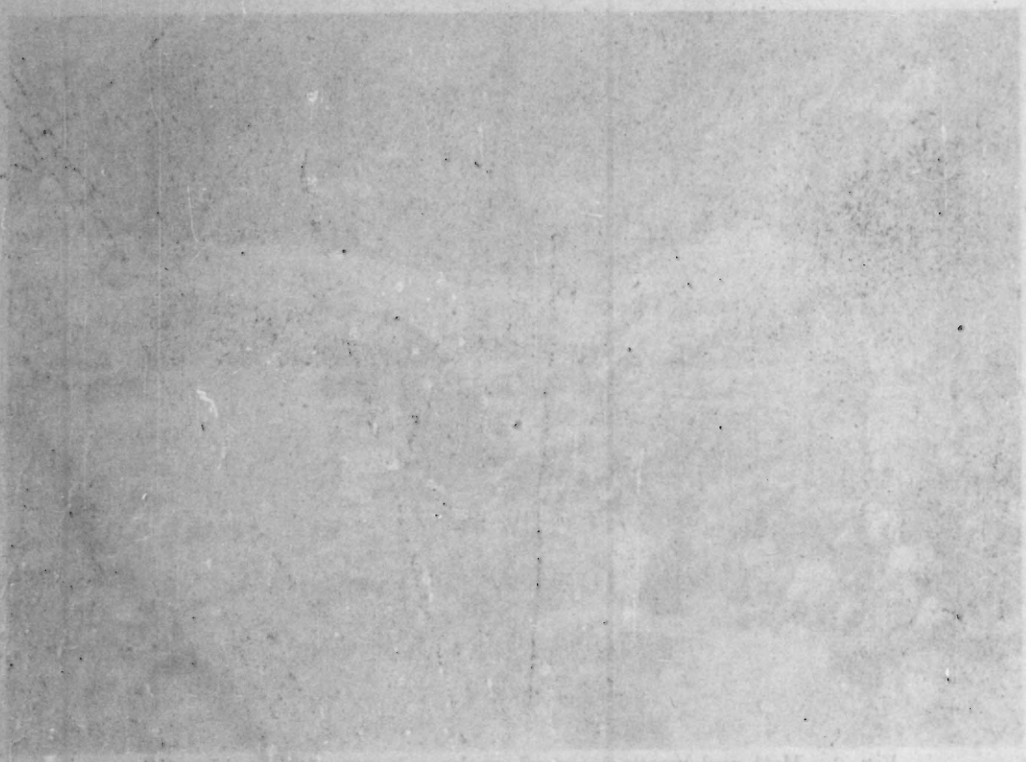

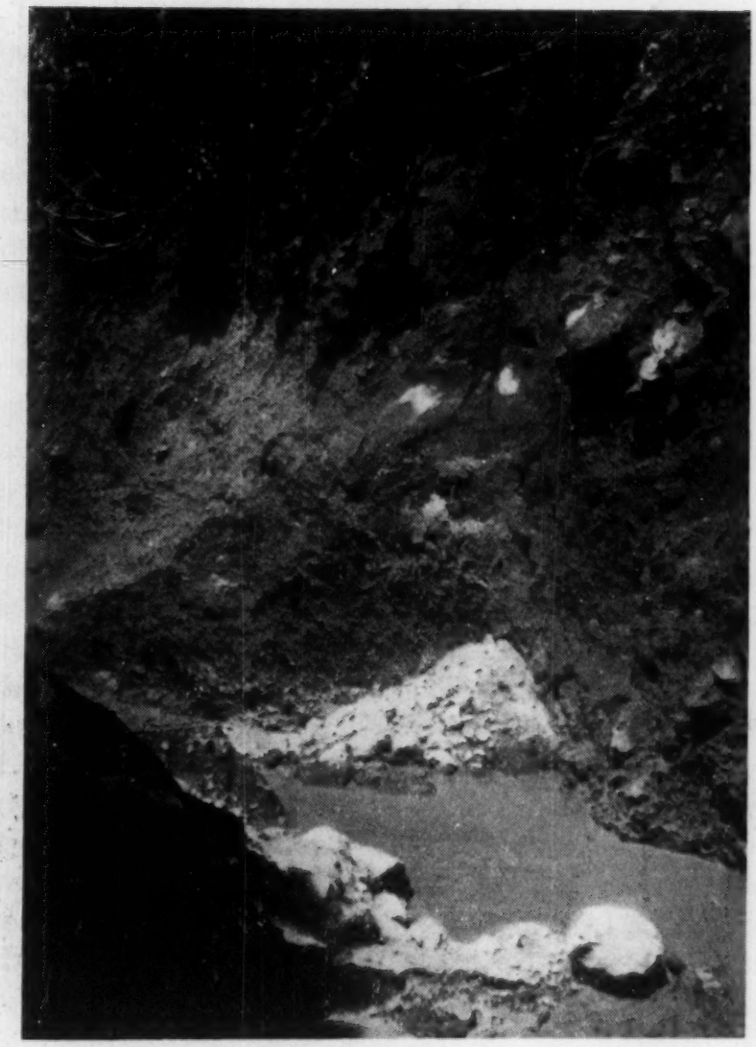

（震研彙第　第二十七號　圖版　佐久間・水上）

Fig. 9. Mud and water dammed up by collapse of riverside cliffs.

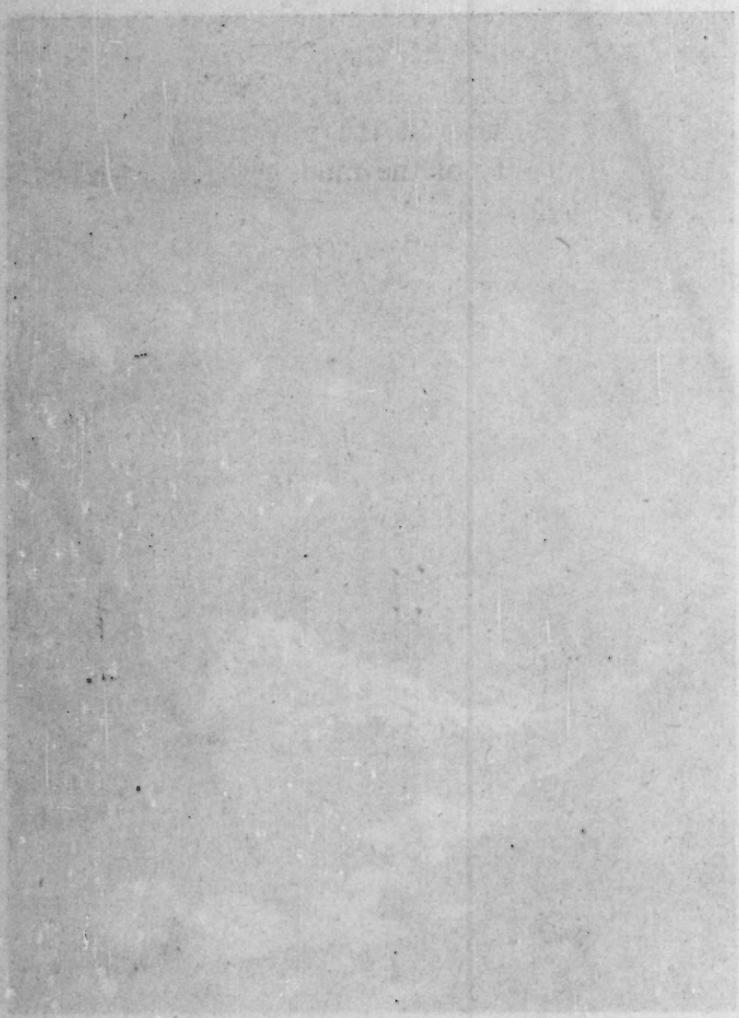

heavy rainfalls on the upperreaches on 30th July 1949, extremely thick mud-flow rushed down the Ogura (Hiuti) river, buried some of the rice-fields and destroyed wooden bridges. (Fig. 4). Especially at a narrow valley of U-shape and of 8 m wide, about 4 km south of Yunokōti, trace of mud-flow was about 10 m higher than the usual water-level. Moreover, difference of height of mud trace in the both sides at a curved channel attained to 3.5 m. On the basis of the investigation just mentioned, the flowing velocity and viscosity of the mud-flow were roughly estimated at 8 m per sec. and 2×10^4 c. g. s..

Though, of course, the mud-flow consisted not only of newly ejected ash and detritus but also of fragments of old formations on the riverside, it may be properly called a kind of minor mud-flow of volcanic origin or secondary volcanic origin. When the writers ascended the upperreaches of the mud-flow on August 5, ash and fragmental detritus still remained on the snow, and as will be seen in Figs. 8 and 9 mud together with water was dammed up by collapses of riverside-cliffs at several spots. Judging from the result of field investigation, it may be evident that the mud-flow on July 30 might have been caused by sudden collapse of such dammed muddy water as described above.

The detailed study of this volcano and its present activity is under way on the basis of the seismometric observations and the present field investigation. The writers report here only an outline of the present activity of Volcano Yake-yama.

Finally, it may be added that the writers made the present research in cooperation with Dr. T. Ichimura, Dr. H. Tsuya and Dr. R. Morimoto[2] and most of the expense necessitated for the field investigations was defrayed from the funds for Scientific Research of the Department of Education, which were given to Dr. H. Tsuya and one of the writers.

---

2) T. Ichimura, R. Morimoto & H. Tsuya, *Bull. Earthq. Res. Inst.*, **27** (1949), 107.

22. *Recent Activities of Volcano Usu (III). Earthquakes at the Stage of Paroxysmal Eruption.*

By Takeshi MINAKAMI,

Earthquake Research Institute.

(Read Dec. 20, 1949.—Received Nov. 30, 1949.)

As already reported in the previous paper[1], the recent eruption of the Usu volcano began with marked earthquakes on December 28, 1943, and from that time on, the seismic activity lasted incessantly throughout the three stages of the recent volcanic activity, namely, pre-volcanic stage, stage of the paroxysmal eruption, and that of birth and development of the lava dome, though it often manifested some ebb and flow in frequency of earthquakes and their intensity.

For the purpose of precise investigations of earthquakes, seismographs of high sensibility were set at Tōya Hot Spring at the northwestern foot, Sōbetu at the north-eastern foot, the village Usu at the southern foot, Kami-Osaru at the south-eastern and Hukaba on the rising area at the eastern foot of the volcano. Seismometric observations were continuously carried out during the period from June to September, 1949, and particularly the observations at Tōya Hot Spring were continued for about a year from March 1944 to March 1945. Seismographs used in the present investigation, had been operated at the volcanic activities of Miyake-sima in 1940 and Sakura-zima in 1946, Asama since 1937, and for the observations of after-shocks of strong earthquakes. The instrumental constants of seismographs are 1.0 second in their period, and 350 or 200 in the geometrical magnification.

However, after several days of observations, the seismograph set at Hukaba was replaced by an acceleration seismograph, seeing that earthquake-motions were too strong for the use of the former instrument.

On the basis of these seismometric observations, the distribution of seismicity on and around the volcano is illustrated in Fig. 1 by the daily frequencies of shocks recorded at the above mentioned five stations. The seismic activity shown in Fig. 1 includes the period from the end of June to August in 1944, when the paroxysmal eruptions were most fierce in the recent activity of Usu.

1) T. MINAKAMI, *Bull. Earthq. Res. Inst.* 25 (1947), 65, 71.

Although the acceleration seismograph records only such strong earthquakes as can be felt, the frequency at Hukaba was more than ten times of those of the other locations. According to investigations of perceptible area, most of earthquakes recorded at Hukaba were felt only at a limited area in the vicinity of that station, being less than 1 km in its diameter.

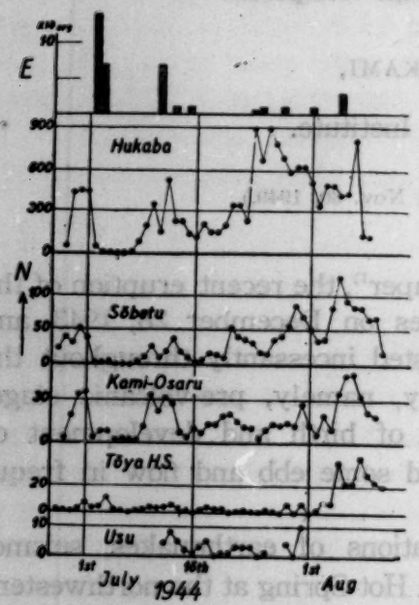

Fig. 1. Daily frequencies of earthquakes recorded at the five stations around Mt. Usu during the stage of paroxysmal eruption.
N; Daily frequencies.
E; Energies of main explosion (Unit; 10^{19} ergs.)

Table I. Depth of hypocentres and distance coefficients.

Date		Time h	m	Z km.	K km/sec
July	13	0		2.7	5.2
	13	4	28	3.6	4.8
	14	1	11	3.4	4.4
	„	3	50	4.1	4.8
	18	10	26	3.1	3.3
	„	14	06	1.0	2.5
	„	14	06	3.8	5.0
	24	21	17	3.5	5.2
	26	0	11	1.7	3.3
	„	2	50	4.1	4.0
	31	22	50	2.3	5.0
	„	22	50	3.0	3.6

Since the durations of preliminary tremors observed at Hukaba ranged mostly between 0.0 second and 0.4 second, or 0.3 second in the mean value, the hypocentres of these earthquakes are estimated at depth between the earth's surface and 1 km, if the distance coefficient is assumed to be 2.0 (Fig. 2). However, this assumption may be reasonable in view of the distance coefficient of deeper earthquakes originated from the southern side of this volcano, as will be seen in Table I. According to the seismometric study of the Oosima volcano made by R. Takahasi and T. Nagata[2], the dis-

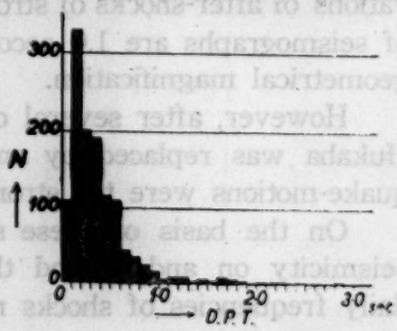

Fig. 2. Frequency distribution of duration of preliminary tremors observed at Hukaba.

2) R. TAKAHASI and T. NAGATA, *Zisin*, 11, No. 4 (1939), 161.

tance coefficient was found to be 2.2 and 2.4 for the earthquakes originated from the earth's surface and 0.5 km deep.

From these investigations, it is evident that a greater part of numerous earthquakes observed at Hukaba, occurred on and directly below the rising area including the village Hukaba, accompanied by the marked topographical deformations, tilting of the earth's surface, and cracks of various scales.

Of these earthquakes originated from the Hukaba area, only the few earthquakes of strong intensity were recorded by the seismographs of higher sensibility at the other stations.

Bisides the earthquakes which occurred near Hukaba, other earthquakes were recorded by all the seismographs located around this volcano, though their frequency was not so notable as that of the Hukaba earthquakes.

With respect to the earthquakes recorded at the four stations, positions of their hypocentres and the distance coefficients of the respective earthquakes were studied on the basis of preliminary tremors, and the distribution of hypocentres was illustrated in the previous report[3].

A glance at the seismograms of two kinds of earthquakes (Fig. 6 and Fig. 7) of which one took place at the depth between two and five km of the southern side of the mountain, and the other was originated from the Hukaba area near the earth's surface, will show the conspicuous differences in their characters of earthquake-motions, that is, amplitudes and periods of the seismic waves. For convenience of description, the former and latter earthquakes will be called A and B types of earthquakes respectively.

In order to throw a light on the nature of the A and B types of earthquakes, period analyses of earthquake-motions were carried out for those of the two types recorded at the four or five stations.

As an example, the frequency distribution of periods of an A type earthquake-motions recorded at Kami-Osaru, Sōbetu, Tōya H. S. and the village Usu are represented in

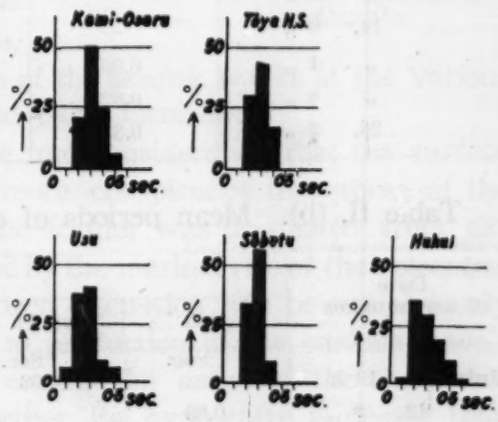

Fig. 3. Frequency distribution of periods of the A type earthquake-motions, and that of an after-shock observed at Hukui.

3) T. Minakami, *loc. cit.*

Fig. 3, together with that of an after-shock of tectonic origin, while those of a B type earthquake recorded at the four stations just mentioned and the Hukaba station are shown in Fig. 4. In addition to that, the mean periods of earthquake-motions were obtained for seven A type earthquakes and six B type ones both recorded at the four or five stations respectively, of which the results are represented in Table II. As being shown clearly in these diagrams and the table, the mean periods of earthquake-motions of the A type except that of Hukaba are always shorter than those of the B type, being almost 0.3 second for the former, and from 0.2 to 0.7 second for the latter. Judging from the result of the period analyses and the form of the seismo-

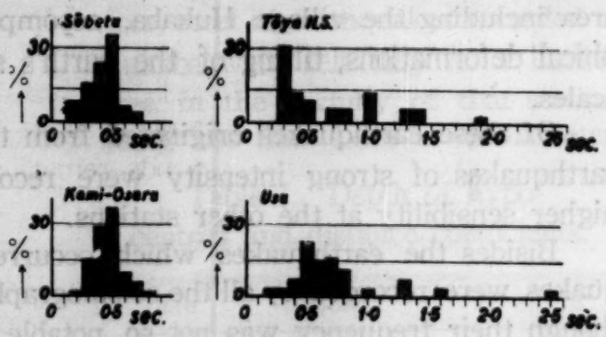

Fig. 4. Frequency distribution of periods of the B type earthquake-motions.

Table II, (a). Mean periods of earthquake-motions of the A type.

Date of earthquakes.	Mean periods			
	Usu	Tōya H. S.	Sōbetu	Kami-Osaru
	Sec.	Sec.	Sec.	Sec.
July 13, 0 h	0.24	0.22	0.22	0.26
„ 4 „	0.27	0.29	0.27	0.30
„ 22 „	—	0.19	0.19	0.19
14, 0 „	—	0.25	—	0.22
„ 1 „	0.36	0.35	0.26	—
„ 8 „	0.32	0.33	0.30	0.31
26, 3 „	0.33	0.33	0.23	0.28

Table II, (b). Mean periods of earthquake-motions of the B type.

Date of earthquakes	Mean periods				
	Usu	Tōya H. S.	Sōbetu	Kami-Osaru	Hukaba
	Sec.	Sec.	Sec.	Sec.	Sec.
July 9, 19 h	—	0.68	0.33	0.49	0.28
12, 9 „	0.69	—	—	0.51	0.24
„ 17 „	0.69	0.65	0.32	0.50	0.20
13, 0 „	—	0.63	0.37	0.50	0.20
20, 19 „	0.70	—	—	0.49	0.18
22, 1 „	0.76	0.69	0.40	0.46	0.21

grams, we can not find any different character in earthquake-motions between the A type earthquake and the so-called tectonic one.

In contrast to that, that of the B type shows distinguished characters as if it were a distant earthquake of tectonic origin, and as will be seen in Fig. 7, the amplitudes of the B type earthquake decrease more rapidly with the epicentral distance than those of the other type.

It may be noted that, though the mean period of earthquake-motions of the A type is almost constant in spite of the various epicentral distances, that of the B type depends remarkably on the epicentral distance, as seen in the diagram of Fig. 5 clearly.

It is, however, believed that the notable characters mentioned with respect to the B type earthquakes show nothing but the fact that the depths of their hypocentres were extremely shallow and, as a result, the seismic waves were considerably disturbed and dissipated by the complex formations near the earth's surface. In addition to that, the shorter the period of the seismic wave is, the more seriously the dissipation affects on it. Therefore, the characteristics of the B type earthquake-motions are mainly caused by the comlex structures of the volcano, in other words, by remarkable dissipations in loose materials such as pumice, ash and other fragmental ejecta, and frequent reflexions and refractions of the seismic waves at the various boundaries between volcanic ejecta and older formations.

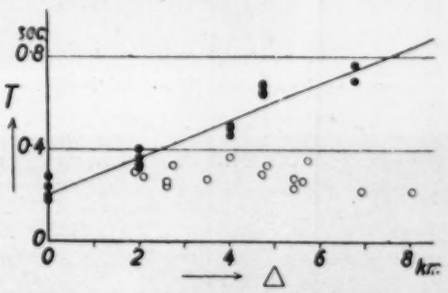

Fig. 5. Relationship between mean period of earthquake-motions and epicentral distances.
black circle; that of the B type earthquake.
open circle; that of the A type earthquake.

On the other hand, we must take into consideration that the surface waves of the B type earthquake are more conspicuous than those of the A type one, owing to the fact that the former was originated from extremely shallow hypocentre accompanied by the marked rise of the epicentral area. But, doubtless the above mentioned discussion will be not seriously affected by the problem with respect to production of the surface wave.

From the fact that whether the earthquake assumes the characters of A type or B type depends on whether its hypocentre is deeper than nearly 1 km or not, we conclude that there may exist a discontinuous boundary in the formations of this volcano at the depth between 1.3 and 0.5 km below the earth's surface.

We must briefly touch upon the time relationship between frequency

of earthquake and the paroxysmal eruptions, which both occurred during the period from June to August 1944. For this purpose, every marked explosion was expressed by its kinetic energy at the moment of outburst, and the seismic activity during the period was indicated by daily frequencies of earthquakes observed at the five stations. The diagram of Fig. 1 shows distinctly that the predominant earthquakes lasted several days prior to every marked eruption, which is as if the former half of a finite amount of energy took the form of seismic activity and the latter half of it the form of paroxysmal eruption, from two to five days after the outburst, the seismic activity grew remarkably weak.

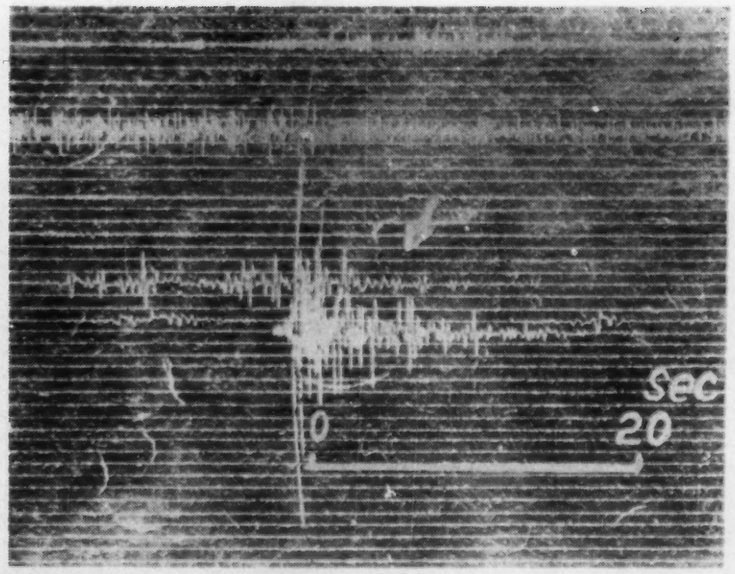

(a)

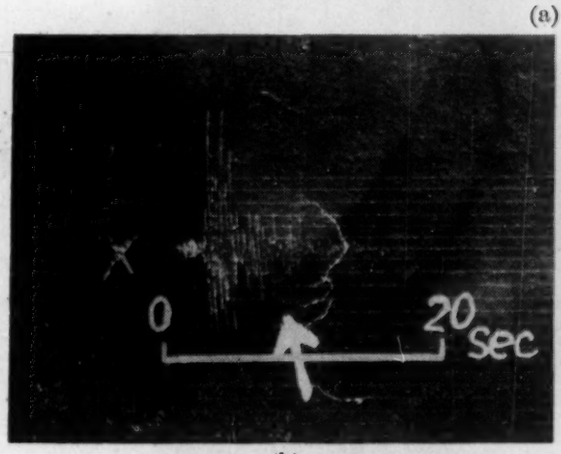

(b)

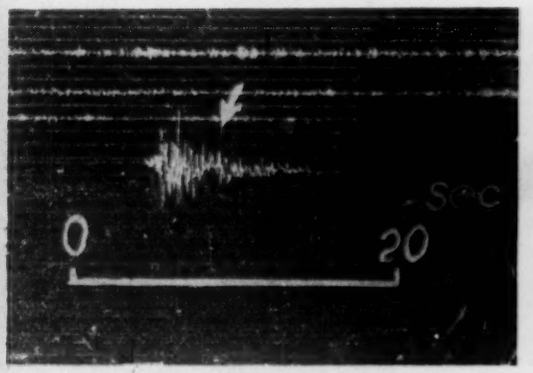

(c)

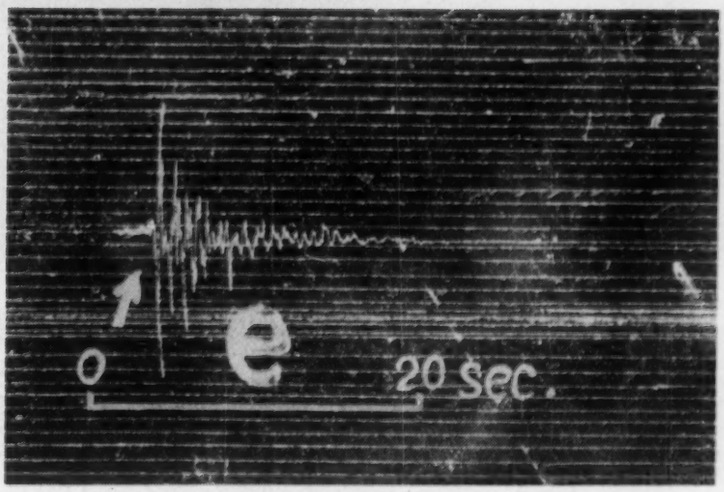

(d)

Fig. 6. Seismorams of the A type earthquake.

(a) Recorded at Kami-Osaru ($\Delta = 1.9$ km) (Seismograph magn. = 350).
(b) " " Village Usu ($\Delta = 3.5$ km) (" = 350).
(c) " " Toya H. S. ($\Delta = 4.7$ km) (" = 200).
(d) An after-shock recorded at Hukui. (" = 350).

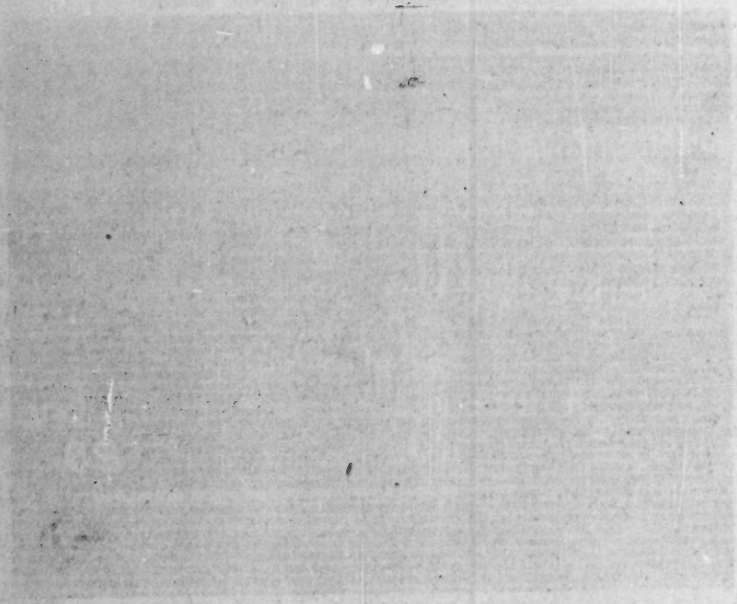

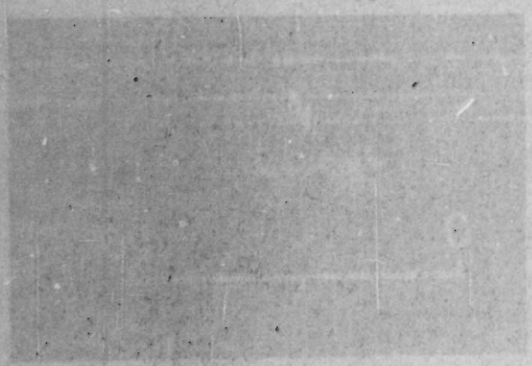

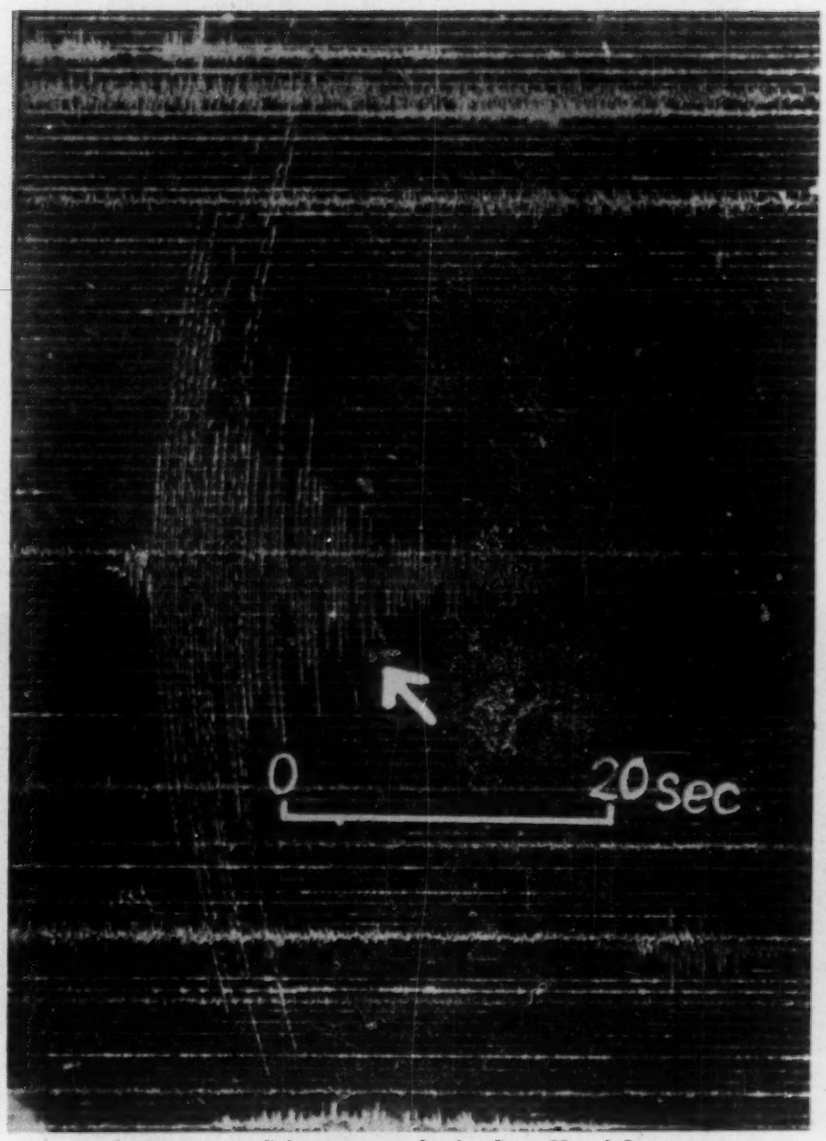

Fig. 7. (a) Seismogram obtained at Kami-Osaru
($\Delta = 4.0$ km, Seismograph magn. $\times 350$).

Fig. 7. (a), (b), (c), (d).
Seismograms of the B type earthquake on July 22, 1944.

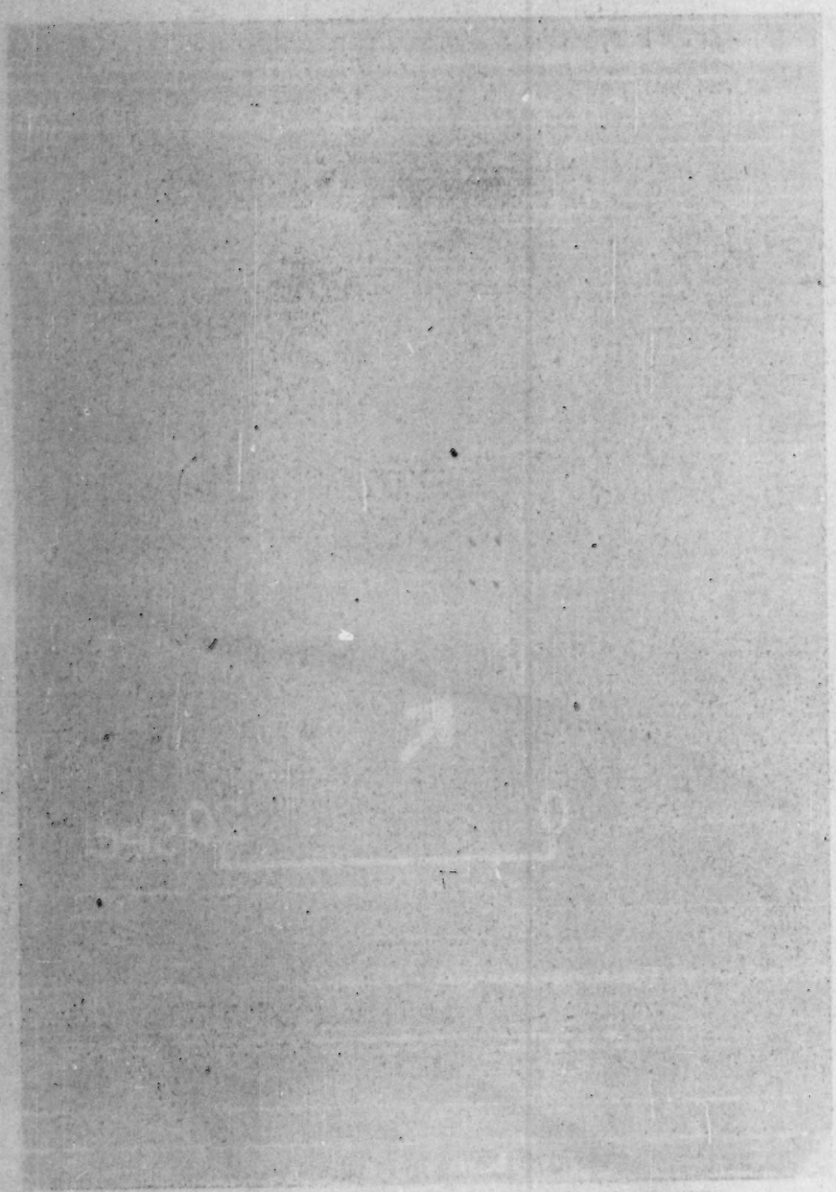

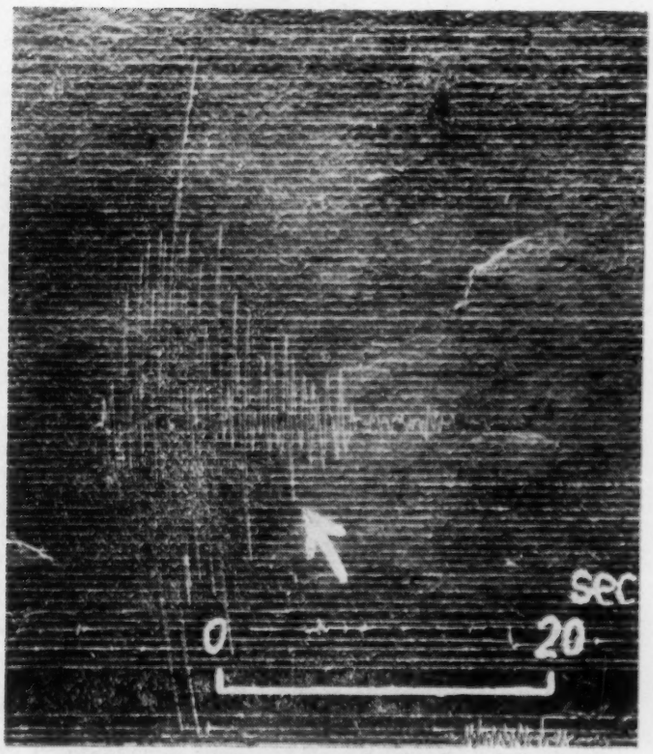

Fig. 7. (b) Seismogram obtained at Sobetu
(Δ=2.0 km, Seismograph magn.×200).

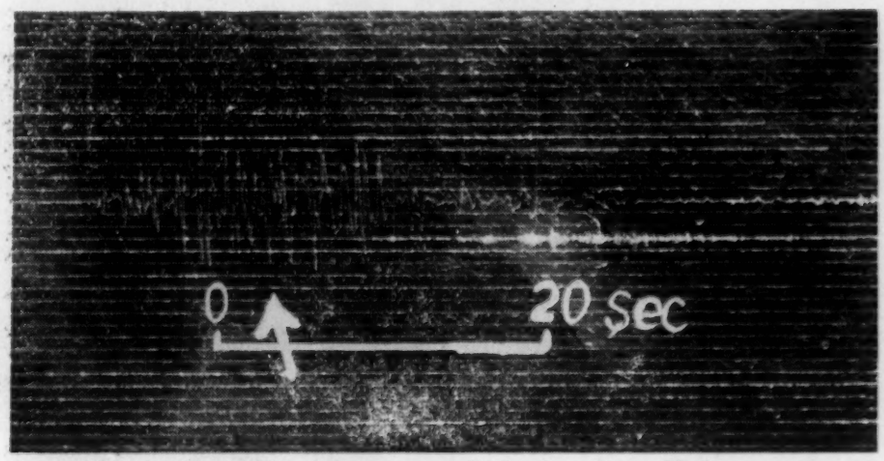

Fig. 7. (c) Seismogram obtained at Toya H. S.
(Δ=4.7 km, Seismograph magn.×350).

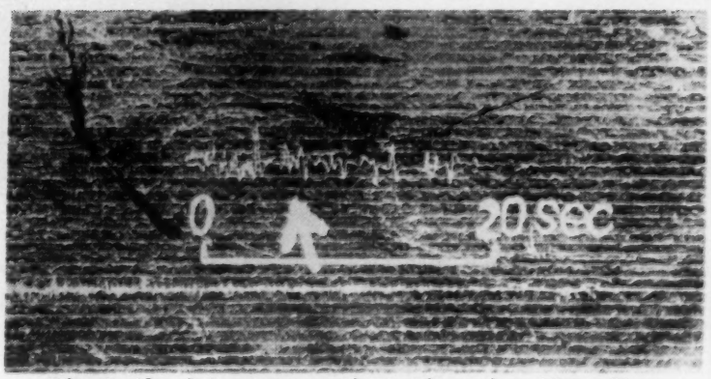

Fig. 7. (d) Seismograms obtained at the village Usu
(Δ=6.7 km, Seismograph magn.×200).

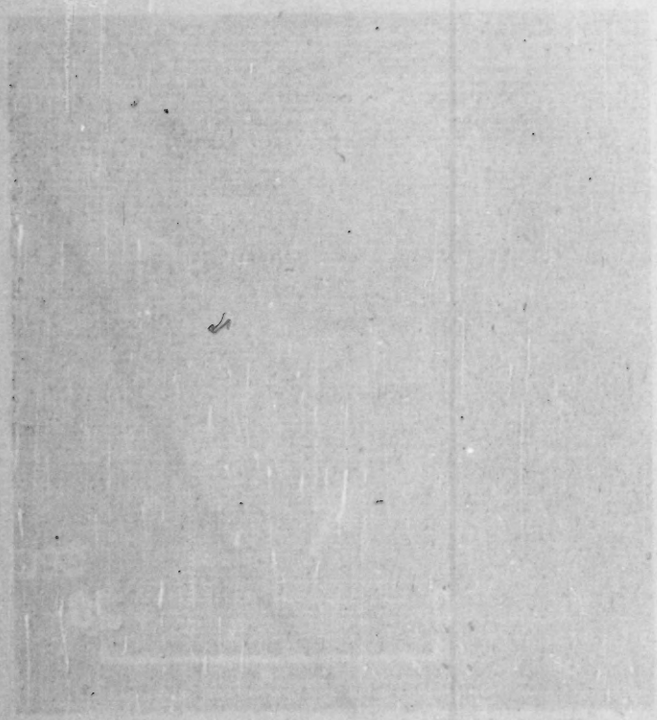

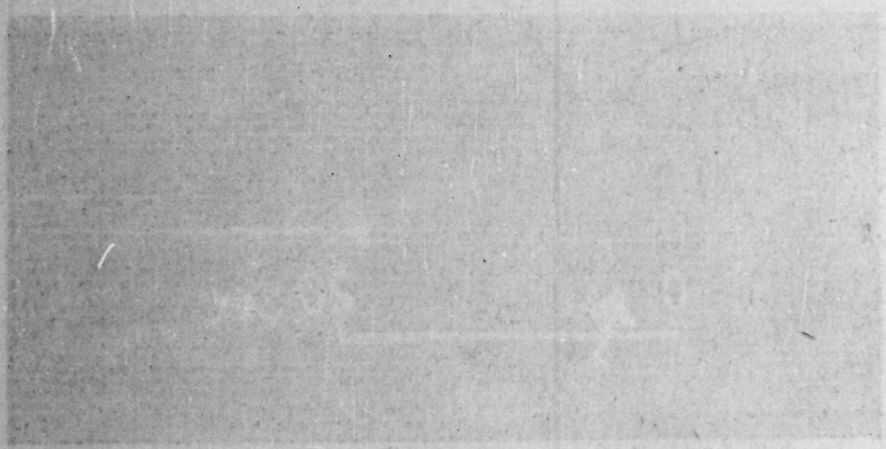

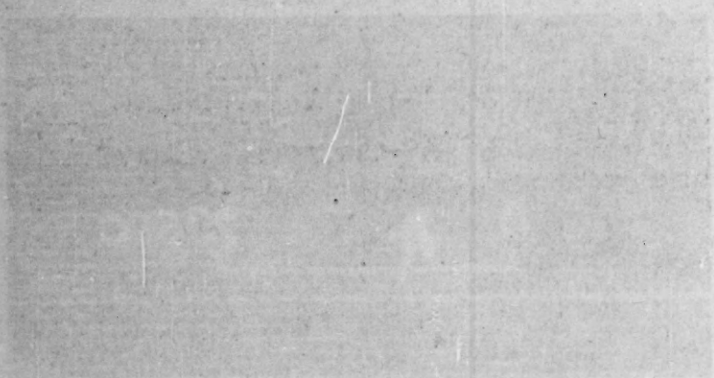

23. *Recent Activities of Volcano Usu (IV). Earthquakes Followed by the Birth and Development of the Lava Dome.*

By Takeshi MINAKAMI,

Earthquake Research Institute.

(Read Dec. 20, 1949.—Received Nov. 30, 1949.)

Paroxysmal eruption came to an end almost at the later part of October, 1944, when numerous earthquakes of another new type were recorded by the seismograph and lasted till the formation of the dome was completed. The developments of seismic activity are shown in Tables I, II by means of the daily frequency of earthquakes which were recorded by seismograph at Tōya Hot Spring covering the whole period of the paroxysmal eruptions, and birth and development of the lava dome.

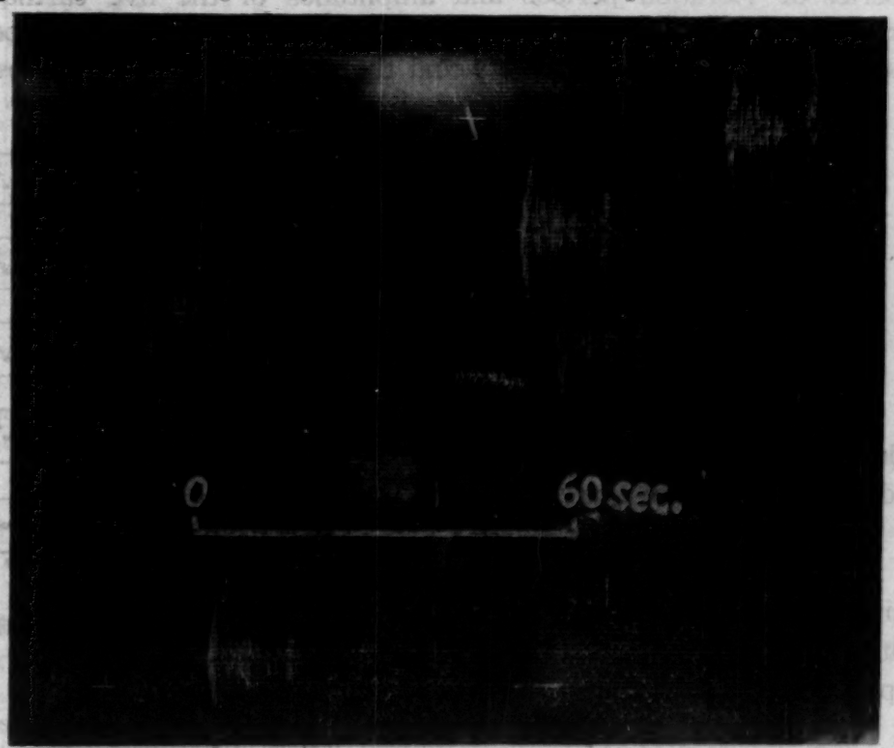

Fig. 1. Seismograms of the *C* type earthquakes.

But the earthquakes, which occurred in the various stages of the recent eruption, were entirely different in their forms of earthquake-motions.

According to the seismograms obtained at Tōya H. S., the earthquakes during this period have noticeable features in the form of earthquake motions, being very much different from those of the former two types, described in the previous paper. For convenience' sake, this type of earthquakes will be here called the *C* type. The *C* type is manifestly characterized not only by the stage of extrusion of lava, but also by the particular features, of which the forms and phases of the seismic waves and their magnitude are considerably similar to each other as is shown in Fig. 1.

In order to make clear the similarity of the *C* type earthquakes, the following investigations were made on the basis of the seismograms. The seismic waves of a seismogram of the *C* type were numbered one by one from its head to tail, as is seen in Fig. 2, and then the numbered waves were measured with respect to their periods, T_1, T_2, T_3, ...T_n together with their amplitudes, A_1, A_2, A_3, ...A_n. The procedures were carried out in regard to five seismograms (I, II, III, IV, V), which were chosen at random in many numbers of seismograms.

Series of vibration periods and amplitudes of the five earthquakes obtained in this manner, are illustrated in Fig. 3 and Fig. 4, taking periods (T_n) and amplitudes (A_n) in ordinate and the number of waves in abscissa.

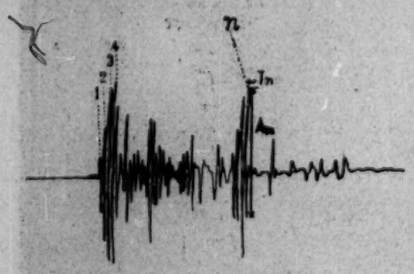

Fig. 2. A seismogram of the *C* type earthquakes.

In addition to these diagrams, series of periods and amplitudes, are compared with respect to periods, T_n and T_n', and amplitudes A_n and A_n', respectively. (Fig. 5).

It is, in fact, wonderful that the *C* type earthquakes resemble with another in full detail as if they were copies of the same earthquake.

It will be reasonable to consider that the marvellous similarity of earth-

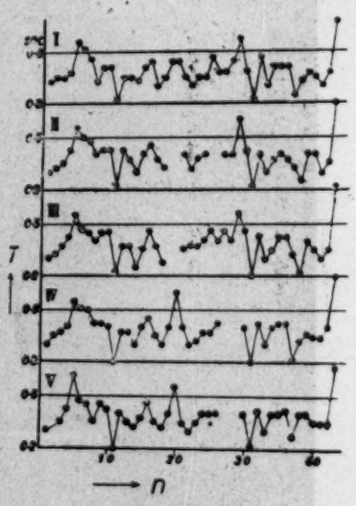

Fig. 3. Similarity of earthquake-motions of the *C* type earthquakes.
n; seismic wave numbered from the head of seismogram.
T; period of the corresponding waves.

quake-motions is caused by repetition of the same mechanism of production of the seismic waves at the same location of hypocentre and by the mode of propagation passing through the identical path from the origin to the station.

Judging from the general rule in natural phenomena that a complex phenomenon is hardly repeated in a perfectly similar manner, we may believe, as T. Matuzawa[1] remarked with respect to the similarity of earthquakes of the same origin, that the dynamical mechanism producing the seismic waves of the *C* type at the hypocentre must be so simple as to be easily repeated.

However, the seismograms of the *C* type earthquakes recorded at Tōya H. S., 5 km distant from their epicentre show rather complex in com-

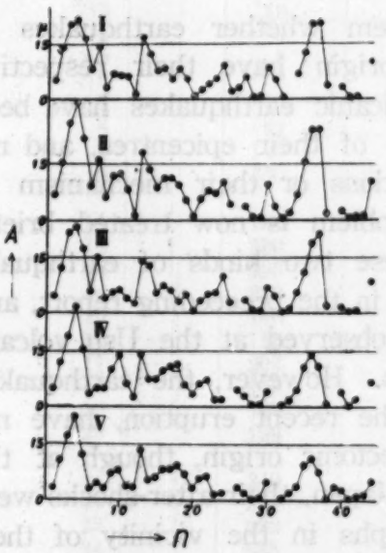

Fig. 4. Similarity of earthquake motions of the *C* type earthquakes.
n; seismic waves numbered from the head of seismogram.
A; amplitude of the corresponding waves.

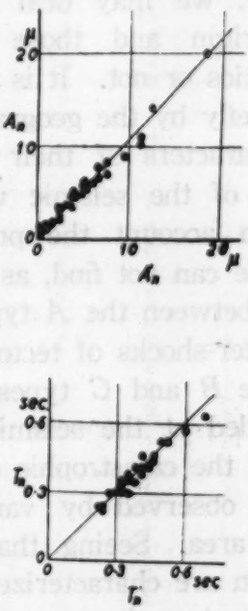

Fig. 5. Comparison of periods (*Tn*, *Tn'*) and amplitudes (*An*, *An'*) of corresponding waves of two *C* type earthquakes.

parison with the *A* type ones. As already mentioned, the complexity of this kind depends on the more complicated formations of the upper part of the volcano than those of the deeper formations.

On the other hand, the hypocentres of the *B* type earthquakes which occurred during the stage of the paroxysmal eruption were estimated within the semi-spherical domain of 1 km in diameter, including the earth'

1) T. Matuzawa, *Zisin* (*Earthquake*), (1932).

surface of the rising area. According to examinations of the *B* type seismograms, their earthquake-motions are similar to some extent, though not so evident, to those of the *C* type. Moreover, the *C* type earthquakes have intermediate characters between the *A* and *B* types earthquakes in the mean periods of earthquake-motions as well as in the forms of the seismic waves.

From these various facts described in the preceeding and present reports, we can draw the following conclusion——the *C* type earthquakes probably occurred within a more limited domain than that of the *B* type, at the depth of nearly 0.5–1.0 km below the newly forming dome. Accordingly, it seems that the *C* type earthquakes have close relation to the enormous forces which acted on the subterranean base of the dome, namely a lower end of the conduit.

Finally, we may deal with the problem whether earthquakes of tectonic origin and those of volcanic origin have their respective characteristics or not. It is evident that volcanic earthquakes have been defined chiefly by the geographical positions of their epicentres, and not by the characters of their earthquake-motions or their mechanism of production of the seismic waves. The problem is now treated briefly taking into account the properties of these two kinds of earthquake motions, we can not find, as seen in Fig. 6 in the preceeding report, any difference between the *A* type earthquakes observed at the Usu volcano and the after-shocks of tectonic earthquakes. However, the earthquakes such as the *B* and *C* types observed at the recent eruption, have not been recorded at the seismic activity of tectonic origin, though at the occasion of the catastrophic earthquakes in Japan, their after-shocks were frequently observed by various seismographs in the vicinity of their epicentral area. Seeing that the *A* and *B* types earthquakes at the present Usu are characterized chiefly by the extremely shallow depth of their hypocentres, it seems that the tectonic earthquakes do not take place at such shallow depth as in the case of the recent activity of Usu. On the other hand, it must be added that earthquakes resembling the *B* type of the Usu volcano have been observed occasionally prior to and in the course of the eruptions of Asama, Kusatu-sirane and other volcanoes in Japan.

Moreover, the daily frequencies of earthquakes which were recorded at the five stations in the course of the recent eruption, were represented in Tables I and II.

The writer wishes to express his thanks to Mr. T. Utibori and to Miss T. Takahashi for their valuable assistances in seismometric observations at the Usu volcano and in the laboratory works.

Most of the expense necessitated for this research was defrayed from the funds for Scientific Research of the Department of Education.

Table I. The daily frequency of the earthquakes observed by the seismographs at the five stations during June 27—August 11, 1944.

Date		Hukaba	Sōbetu	Kami-Osaru	Tōya H. S.	Usu
June	27	—	22		2	
	28	50	38	3	1	
	29	430	31	19	1	
	30	450	51	33	3	
July	1	445	38	35	7	
	2	48	2	3	3	
	3	10	3	8	4	
	4	5	5	8	11	
	5	0	0	2	2	
	6	0	0	3	1	
	7	10	0	2	0	
	8	82	3	2	1	
	9	190	10	11	2	
	10	350	26	33	4	
	11	166	10	22	3	—
	12	530	19	31	4	4
	13	225	37	27	5	8
	14	228	18	7	3	5
	15	140	10	4	2	2
	16	118	4	10	0	1
	17	203	7	7	2	3
	18	149	16	13	4	5
	19	149	14	13	3	0
	20	198	10	19	3	1
	21	340	52	20	0	1
	22	340	40	15	1	3
	23	233	36	11	2	3
	24	885	32	10	1	3
	25	675	17	3	1	0
	26	893	15	9	2	1
	27	785	36	13	1	0
	28	690	41	12	0	0
	29	587	55	14	6	4
	30	630	85	12	0	0
	31	630	69	27	6	10
August	1	520	52	12	0	
	2	340	35	6	2	
	3	495	37	19	7	
	4	420	82	10	7	
	5	430	27	35	37	
	6	800	92	48	22	
	7	135	84	49	22	
	8	125	82	33	40	
	9		66	22	28	
	10		68	19	23	
	11		17		20	

Table II. The daily frequency of the earthquakes observed by the seismograph at Tōya Hot Spring during August 1, 1944—March 12, 1945.

Date	August	September	October	November	December	January	February	March
1	0	8	11	16	50	35	26	21
2	2	4	5	15	55	39	27	23
3	7	4	30	9	47	34	24	31
4	7	5	18	2	51	33	28	21
5	37	3	25	—	54	30	25	25
6	22	10	25	10	57	34	29	22
7	22	13	28	11	30	28	20	18
8	40	12	4	8	7	10	25	23
9	28	9	0	5	48	—	19	17
10	23	6	12	4	43	18	8	22
11	20	4	27	3	51	34	30	21
12	31	2	31	9	50	30	17	18
13	18	7	29	14	57	44	23	
14	9	7	35	27	45	40	20	
15	13	10	37	20	53	47	31	
16	9	13	46	21	47	37	24	
17	3	10	42	6	48	38	15	
18	10	8	48	—	51	27	27	
19	6	4	56	16	39	15	27	
20	2	4	45	18	47	33	27	
21	11	8	42	26	43	37	31	
22	15	5	37	22	46	30	28	
23	11	7	31	20	52	37	31	
24	12	5	26	24	53	36	25	
25	9	14	13	23	40	35	24	
26	10	13	19	23	38	33	27	
27	2	22	16	11	40	35	27	
28	11	12	—	24	43	31	23	
29	8	15	24	33	40	37		
30	8	11	20	36	45	33		
31	4		22		45	29		

24. *Gases and Deposits from Fumaroles on the New Dome "Showa-Shinzan", Volcano Usu, Hokkaido, Japan.*

By Hiromichi TSUYA and Toshiaki SHIRAI,

Earthquake Research Institute.

(Read Nov. 15, 1949.—Received Sept. 20, 1949.)

After a period of quiescence of thirty-three years since 1910, Volcano Usu, Hokkaido. Japan, became active with forerunning local earthquakes at the end of December, 1943, and in the following two years gave birth to a new composite dome "Showa-Shinzan", about 405 m in height above the sea, on the northeastern flank near its base. The new dome is double in structure as well as in form, consisting of two parts—the first dome ("roof-mountain"), about 200 m in relative height and 1000 m in diameter, accompanied with terrace-like fore-hills and formed virtually by upheaval of the old ground, and the second superincumbent dome, about 150 m in height above the top of the first dome and 300 m in diameter at its base, formed by protrusion of a column of juvenile viscous lava (acidic hypersthene-andesite).

Since its birth in November, 1944, the second dome has been active in belching up a large quantity of vapors from a number of fumaroles on the fissures, with which it is cut in various directions throughout its height. According to their physical and chemical properties, these fumaroles are to be classified into two different types, high-temperature and low-temperature fumaroles. The high-temperature fumaroles, which are very hot and dry, are found for the most part on the fissures in the newly protruded lava exposed on the south and southwest sides of the second dome (Fig. 1), while a few are found on the opposite sides, where they occur in grottos, boring deep in the ash and debris-covered ground and glowing inside. The low-temperature fumaroles, which are wet and 100° or lower in temperature, are developed not only on all sides of the second dome but also on the ground surrounding it (Fig. 2).

The high-temperature fumaroles are mostly inaccessible on account of their heat and dense stimulative gases, but some of them, together with the low-temperature fumaroles, are accessible for the observation of the exhalations. The present report summarizes the results of chemical study

of gases and deposits collected by the writers in 1948 from some of the fumaroles.

High-temperature fumaroles. In 1948, when the writers visited the volcano, one of the high-temperature fumaroles, about 20 cm in diameter at the orifice, was glowing inside with a red-hot rock (700°C ca.) exposed on the floor at a depth of about 20 cm. Gases, about 650°C at the orifice and 100°C in the air 40 cm above it, were being exhaled with hissing noises and with such a high pressure as to blow off a pebble thrown into them. At the orifice, the escaping gases were hardly visible owing to the high temperature. Thus, although superheated steam occupied the main part of the gases, it was disappearing into the air without condensing to visible fume.

The gases from the high-temperature fumaroles consist of hydrogen and some other acidic gases such as hydrogen fluoride, hydrogen chloride and boric acid, besides water vapor and inert gas, as shown in Table I.

Table I. Composition of gases from the high-temperature fumaroles.

	(Vol. %)
Water vapor	96.9
Acidic gases, HCl, HF, H_3BO_3	2.1
Hydrogen sulphide, H_2S	0.7
Hydrogen, H_2	0.3
Inert gas.	0.1

(T. Shirai, analyst)

Close to their orifice, the high-temperature fumaroles were virtually devoid of sublimates, although their wall-rocks were found to have been subjected more or less to some thermal and chemical changes. Thus, for example, the rocks around the orifice of most of the high-temperature fumaroles were found to have become black as if they had been smoked. Our experiment has shown that the black color was due to ferric oxide (Fe_2O_3) contained in the rocks and heated by the gases to a temperature above several hundred degrees. Ferric oxide has a character to turn black at such a high temperature. Moreover, at several places where the high-temperature fumaroles were exhaling gases from openings in a sandy

Table II. Fe^{++}/Fe ratio of the sand on the ground about one of the high-temperature fumaroles.

	Total Fe content (Wt. %)	Fe^{++} (Wt. %)	$(Fe^{++}/Fe)\times 100$
Sand, very close to the fumarole	5.3	1.0	19
Sand, 1 m apart from the fumarole	5.3	0.7	13

in a sandy ground, the sand near the openings was found to have been subjected to a reducing process, probably by the hydrogen gas, as shown by Fe^{++}/Fe ratio of the sand (Table II).

At places where hot gases from the high-temperature fumaroles appeared to have once passed through, were found masses of very fine, deep-red powdered material consisting for the most part of SiO_2, together with 8% Fe_2O_3. Microscopic examination has shown that the silica occurs in grains coated with finer particles of rouge (ferric oxide).

Low-temperature fumaroles. At the writer's visit, the low-temperature fumaroles were exhaling dense white vapor-clouds from small clefts and openings in the ground on and about the second dome. Inside the fumaroles, temperatures varying from 120° to 230°C were measured at a depth of about 1 cm, although at the orifice of the fumaroles, the escaping vapors showed 100°C, the boiling temperature of water at that place. The vapors consist mainly of steam, besides a little acidic gases (HCl, H_2S) and some contaminating air, as shown in Table III.

Table III. Composition of gases from the low-temperature fumaroles.

	(Vol. %)
Water vapor	98.5
Acidic gases	0.1
Air	1.4

(T. Shirai, analyst)

The low-temperature fumaroles are rich in variegated masses of sublimates and other deposits accumulated by the action of their exhalations. Sulphur, boric acid, free silica, and salts such as hydrated aluminium-sulphates and calcium-sulphate are the predominant ones among them.

Sulphur occupies the main part of the sublimates, occurring as acicular crystals on the walls of the fumaroles and also in a massive layer, a few millimeters in thickness, on the ground thereabout. The sulphur layer is often dotted with many scaly lumps, a few centimeters in diameter, of white salts having a chemical composition as shown in Table IV. From the composition, it is inferred that the salts are a mixture of gypsum ($CaSO_4 2H_2O$) and alunogen ($Al_2(SO_4)_3 18H_2O$).

At the bottom of the sulphur layer lies in places a layer of white powdery material cemented with sulphur particles. The material is pure but more or less hydrated silica, as shown by the chemical analysis: 91% SiO_2, 9% H_2O. This silica, together with the rouge-coated silica around the high-temprature fumaroles, must have been produced by some action of the exhaling gases. So far as the writers know, such a mode

of occurrence of free silica like this is very remarkable, and has not been reported by anyone up to this time. Although the process of formation of the silica is not demonstrative, it seems to have been connected with the presence of hydrogen fluoride in the fumarole gases.

The sulphur deposit near the orifice of some of the low-temprature fumaroles is covered densely with fine silky crystal flakes. Both microscopic examination aud chemical test have shown them to be sassolite, native boric acid H_3BO_3 (Fig. 3).

Moreover, the wall of some of the low-temperature fumaroles is covered with lumps, white, pale yellow or brilliant green, of a fibrous mineral, as if it were a moss-grown rock. Chemical analysis has shown the mineral to be one of the halotrichite group (iron alum), having a composition as shown in Table V. The chemical composition corresponds approximately to the formula $Al_2(SO_4)_3 20H_2O$, if the small quantity of iron component is neglected. This is close in composition to alunogen, $Al_2(SO_4)_3 18H_2O$.

Table IV. Chemical composition of a scaly mass of white salts around the low-temperature fumaroles.

	(Wt. %)
CaO	15.8
Al_2O_3	7.2
SO_3	40.2
H_2O	37.0

(T. Shirai, analyst)

Table V. Chemical composition of a fibrous mineral collected from the wall of a low-temperature fumarole.

	(Wt. %)
Al_2O_3	13.3
FeO	0.9
Fe_2O_3	0.7
SO_3	34.5
H_2O	50.6

(T. Shirai, analyst)

Résumé. The fumaroles on the new dome "Showa-Shinzan", Volcano Usu, are divided into two types—the high-temperature fumaroles exhaling gases directly from the red-hot lava, and the low-temperature fumaroles exhaling white vapors through a deposit of volcanic ash and other detritus.

The principal emanation from the fumaroles of both types is steam,

Fig. 1. High-temperature fumaroles exhaling superheated and invisible gases from fissures in the new lave exposed on the southwest side of the dome "Showa-Shinzan." Most of the fissures were glowing inside. (May, 1943)

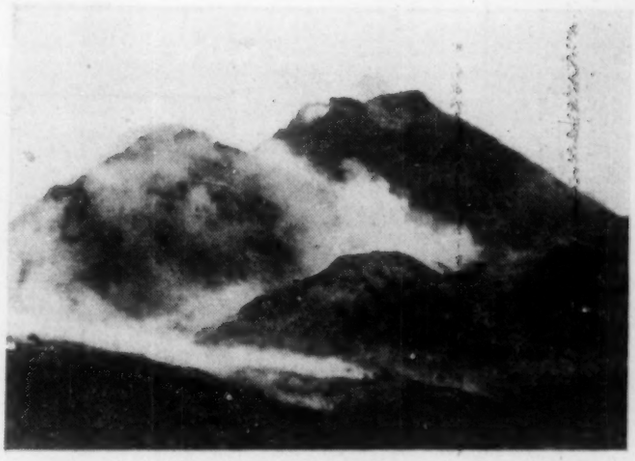

Fig. 2. Low-temperature fumaroles exhaling white vapor-clouds, on the southwest side of the dome "Showa-Shinzan." whose top is seen in the centre of the figure.

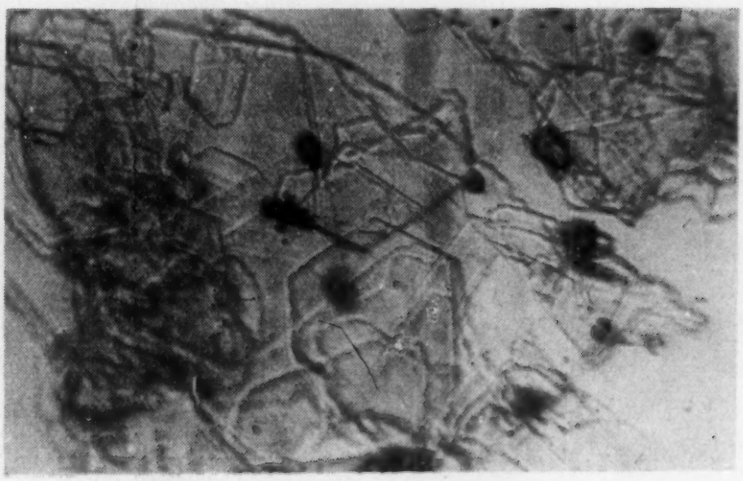

Fig. 3. Sassolite crystals from the sublimates around the low-temperature fumaroles on the dome "Showa-Shinzan." ×200. Black spots in the figure are particles of sulphur.

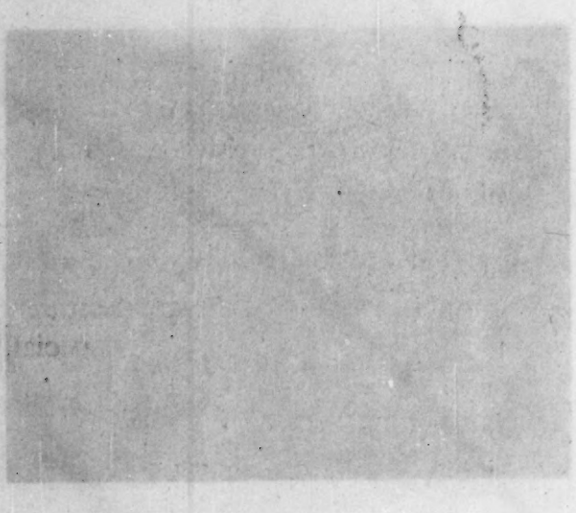

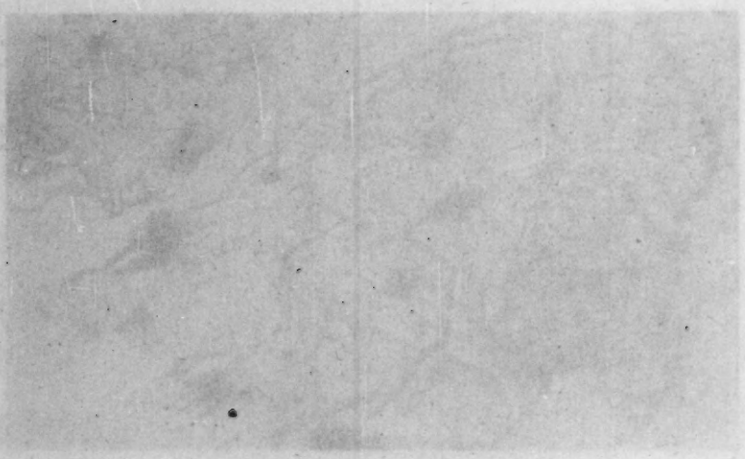

but some acids are present, among which hydrogen chloride, hydrogen fluoride and boric acid may be mentioned in particular. Although these acids are poor in amount in the emanation from the low-temperature fumaroles, they must have once been fairly abundant, as inferred from incrustations around the fumaroles.

Sulphur, sassoltie, gypsum, alunogen, halotrichite, free and rouge-coated silica are the main products fron the fumaroles.

Further investigations are desirable for the elucidation of the mode of formation of these products, especially of the free silica.

25. 米代川にそう一部水準路線の測量（第二報）

地震研究所　宮村攝三
地球物理學教室　岡田悖

（昭和 24 年 9 月 20 日發表—昭和 24 年 12 月 3 日受理）

著者の一人は數年まえ，大塚博士がいわゆる「活動している皺曲構造」[1] の一例としてあげた，米代川下流にそう一部水準路線について，定期的測量によつて，その「活動」をあとづけようとくわだてた．そして，第 1 回を 1942 年 9 月に實施し，その結果を報告した[2]．なお，翌年すこし測量を補足延長し，また今回 1949 年 7 月第 2 回を實施した．

測量區間は地理調査所水準點 (G. S. B.–B. M.)[3] Nr. 5849 より Nr. 5855 までで，なお各鎖部に 3 點づつ震研の假設標石 (E. R. I.–B. M.)[4] をおいてある．G. S. B.–B. M. Nr. 5849 を Nr. 1 とし，G. S. B.–B. M., E. R. I.–B. M. にとうし番號をつけてよぶ．（圖および表參照）假設標石は前報告にしるしたごとくにして，地下にうづめてあつたが，數年をへたとき，標柱は細がつたのでほとんどくさつて，なくなり，野帖にひかえた點の記も，地物の變化によつて無效のものが多く，ほりあてるのに困難であつた．そのため時間の關係でついに發見できなかつたものも二三あつた．そこで，今度はつぎの測量のために，木柱は徑 10 cm の太いものとし，第 1 圖のごとく標石のあたまうえには 40 cm² くらいの厚板をかぶせ，ほりあてに便にした．また假設點の案內略圖は第 2 圖にしるした．

1943 年 8 月には Nr. 17—Nr. 24 を測量した．1949 年には Nr. 1—Nr. 24 の全區間を測量した．これらの結果，および過去の測量との比較を第 I～III 表，および第 3 圖にしめす．たゞし，第 3 圖において，橫軸は皺曲軸にほゞ直交する直線をめのこでひいて，それに投影した位置をとつてある．

測量器械は 1943 年 1949 年ともにツァイス製一等水準儀をもちい，標尺は 1949 年は前年とおなじウィルド製インヴァール標尺，1949 年はツァイス製インヴァール標尺(841,

---

1) 大塚彌之助「活動している皺曲構造」地震 (Zisin) **14** (1942), 46—63.
Yanosuke Otuka, Active Rock Folding in Japan, *Proc. Imp. Acad., Tokyo.* **18** (1942), 518—522.

2) 宮村攝三「米代川にそふ一部水準路線の測量」震研彙報 (*Bull. E. R. I.*) **21** (1943), 197—205. (mit deutscher Zusammenfassung.)

3) G. S. B.—B. M. Geographical Survey Bureau-Bench Mark.

4) E. R. I.—B. M. Earthquake Research Institute-Bench Mark.

842 號）をもちいた.

まず 1942, 43 年—1949 年の變動で注意されることは，E. R. I.–B. M. の變化が G. S. B.–B. M. の變化に對し，いちじるしい沈下をしめしていることである．これは，それらの

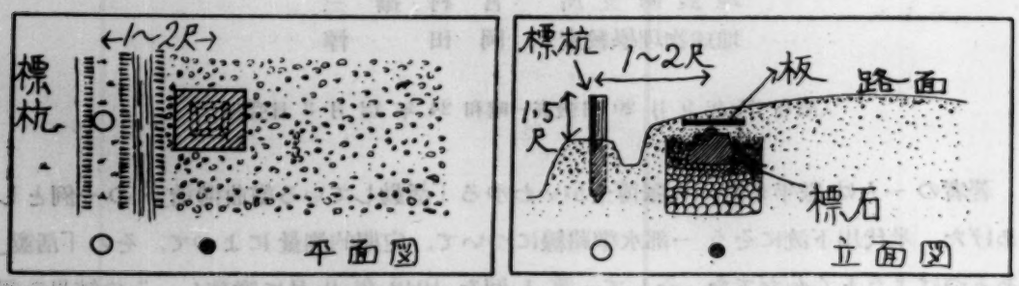

第 1 圖 假設標石埋設狀況略圖 Fig. 1. E. R. I.–B. M.

位置および埋設の施工が適當でなかつたため，この期間全體にわたつて徐々にそれだけうごいたのか，第 1 回の測量が埋設後まもなかつたため，この期間の初期にのみそれだけの沈下をしたのか，いづれかの疑いがあるわけである．もし次回の再測にも同樣の沈下があ

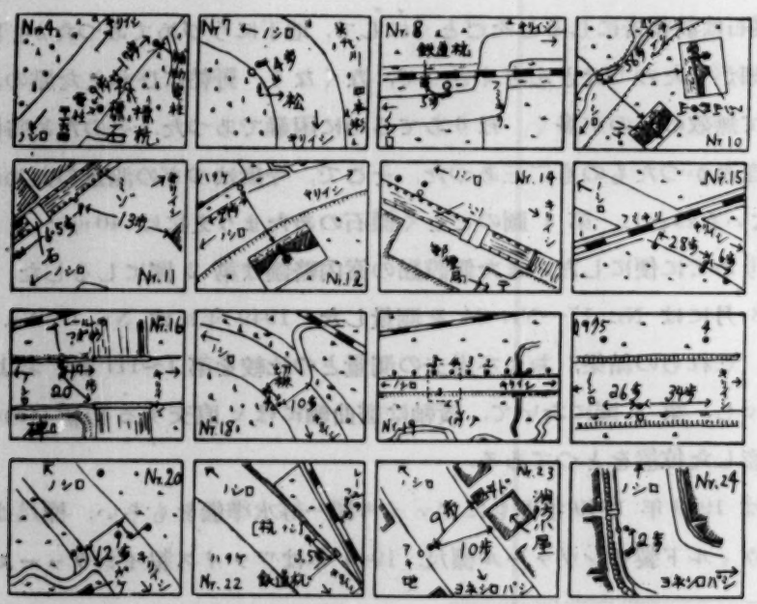

第 2 圖 假設標石所在案內圖 Fig. 2. E. R. I.–B. M.

らわれゝば，前者の場合になるから適當な位置に，もつとしつかりと，いけかえなくてはならない．道路にこだわらず，冲積地をさけて埋設すべきであろう.

したがつて，今回はなお G. S. B.–B. M. の變動だけを問題にするのが妥當である．まづ全體の傾向をみると，1902—1938, 1938—1942 では，東にむかつて隆起し，陸地內

部の曲隆をしめしていたのが，1942—1949 では逆に西あがりとなり，いわゆる日本各地の横断水準線でみられる内陸曲隆の傾向と反對になつてきた．變動の速度も，1 年あたりの變動量としてしめしたものでみられるように，東あがりのときの倍くらいになつている．この期間に，この地方ではなんらいちぢるしい地震等はなかつたので，今後が注目される．

第 I 表　1942 年（一部は 1943 年），1949 年における各水準點の水準差とその變化および震研水準點 No. 5（地理調査所水準點 No. 5850）を不動とせる變動量

Tabelle I. Niveilmentergebnisse der ganzen Route.

Festpunkten (E. R. I.—B. M.) Nr.	水準差 Höhendifferenzen 1942 (1943)	水準差 Höhendifferenzen 1949	水準差の變化 Veränderungen der Höhendifferenzen 1942—1949 (1943—1949)	水準點の變動 Veränderungen der Festpunkten 1942—1949 (1943—1949)
	m	m	mm	mm
1				—
2	—	+17,9499	—	—
3	—			—
4	—			—
5	—	− 3,2608	—	0,0
6	−12,1619	−10,1398	− 5,7	—
7	+ 2,0278			− 5,7
8	− 3,2014	− 3,2100	− 8,6	−14,3
9	− 0,4131	− 0,4215	− 8,4	−22,7
10	− 0,2627	− 0,2794	−16,7	−39,4
11	+ 2,1023	+ 2,0970	− 5,3	−44,7
12	− 2,0904	− 2,0711	+19,3	−25,4
13	+ 1,3451	+ 1,3478	+ 2,7	−22,7
14	+ 1,4857	+ 1,4772	− 8,5	−31,2
15	+ 0,2212	+ 0,1885	−32,7	−63,9
16	+ 0,2820	+ 0,3167	+34,7	−29,2
17	+ 2,2237	+ 2,2298	+ 6,1	−23,1
18	(− 1,7174)	− 1,7215	(− 4,1)	−27,2
19	(− 2,3792)	− 2,3917	(−12,5)	−39,7
20	(+ 1,3301)	+ 1,3284	(− 1,8)	−41,5
21	(+ 3,0327)	+ 3,0362	(+ 3,5)	−38,0
22	(− 1,3354)	− 0,0112	(− 7.6)	—
23	(+ 1,3318)			−45,6
24	(− 0,4834)	− 0,4968	(−13,4)	−59,0

つぎに，變曲活動とむすびつけて，かんがえられるような，こまかい變化では，1902—1938 において大塚博士がしめされた傾向は，1938—1942 の短期間では，むしろ逆のようになつていた．そして，これについての意見はすでにのべた[3]．1942—1949 においても，

活動褶曲の傾向はやはり明瞭でない．この期間はすでに 1902—1938 の約 1/3 の年月にあたるので，のこる期間に同一の傾向にもどりうるかどうかは，むしろうたがわしい．しかし，かりに第3圖において破線でしめしたような大體の傾斜をとりさると，1902—1938 はもちろん，1938—1949 もわずかに褶曲進行の傾向をしめすといえないでもない．（それ

第 II 表 地理調査所水準點の間の水準差變化とその年速度

Tabelle II. Veränderungen der Höhendifferenzen zwischen die Festpunkten von G. S. B.

E.R.I.-B.M. Nr.	G.S.B.-B.M. Nr.	1902—1938		1938—1942 (1938—1943)		1942—1949 (1943—1949)		1938—1949	
		mm	mm/Jahr	mm	mm/Jahr	mm	mm/Jahr	mm	mm/Jahr
1	5849	+ 7.8	+ 0.2	—	—	—	—	− 3.6	− 0.3
5	5850	−40.5	− 1.1	+ 5.5	+ 1.4	−22.5	− 3.2	−17.0	− 1.5
9	5851	+50.4	+ 1.4	− 2.4	− 0.6	+ 0.1	+ 0.0	− 2.3	− 0.2
13	5852	+10.6	+ 0.3	+ 1.9	+ 0.5	− 0.5	− 0.1	− 1.5	+ 0.1
17	5853	−16.8	− 0.5	(+ 5.8)	(+ 1.2)	(−14.5)	(− 2.4)	− 9.0	− 0.8
21	5854								

でも 1938—1942 はやはり逆である）．しかし，これはすこし無理のようだ．むしろ 1902—1938 の結果を大塚博士のごとく，活動褶曲の例とすることの方があぶないのではないかと思われる．現在の地殻變動の性質が，洪積世の運動をとびこえて，時間的單元のことなる第三紀の運動にむすびつく場合はすくないのではないか．それだけに大塚博士の發見

第 III 表 地理調査所水準點の No. 5850 を不動とせる變動とその年速度

Tabelle III. Veränderungen der Festpunkten von G. S. B.

E.R.I.-B.M. Nr.	G.S.B.-B.M. Nr.	1902—1938		1938—1942 (1938—1943)		1942—1949 (1943—1949)		1938—1949	
		mm	mm/Jahr	mm	mm/Jahr	mm	mm/Jahr	mm	mm/Jahr
1	5849	− 7.8	− 0.2	—	—	—	—	+ 3.6	+ 0.3
5	5850	0	0	0	0	0	0	0	0
9	5851	−40.5	− 1.1	+ 5.5	+ 1.4	−22.5	− 3.2	−17.0	− 0.2
13	5852	+ 9.5	+ 0.3	+ 3.1	+ 0.8	−22.4	− 3.2	−1.93	− 0.2
17	5853	+20.5	+ 0.6	+ 5.0	+ 1.3	−22.8	− 3.3	−17.8	− 0.2
21	5854	+ 3.7	+ 0.1	(+10.8)	(+ 2.2)	(−37.6)	(− 6.3)	−26.8	− 0.2

は注目すべきこととかんがえられたわけだが，どうもこの米代川附近の場合はそうではないらしい．今後の再測がこれをあきらかにするだろう．水準變化，段丘，褶曲と三つの異質的時代をしめす地殻變動のつながりはもつと實證的に研究されることが必要であろう．したがつて，他の活動褶曲の例についても，水準測量がくりかえされ，また地形，地質の調査もさらにくわしくおこなわれることが希望される．さらにまたこの活動褶曲が堆積や

撓曲に關する理論から檢討されることも希望される.

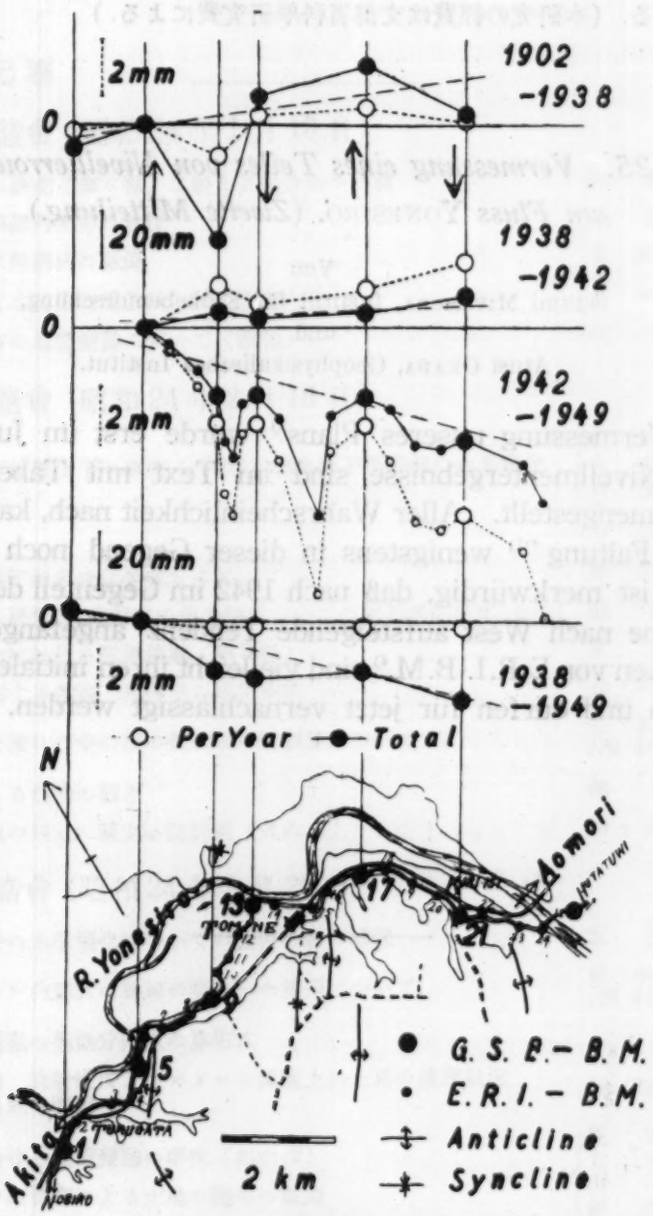

第 3 圖 水準路線と測量結果
Fig. 3. Nivellierroute und Vermessungsresultate

おわりに，1943 年の測量には當時の地球物理學科學生松本誠一，立石哲夫，岩保勘三郎，宮崎正衛の諸氏，1949 年の測量には山本郡地方事務所土木課藤田甚作，大塚鐵雄，信田博の諸氏が協力された．また秋田縣土木部長池田德治氏，山本郡地方事務所長小林捷夫氏，富根村長工藤幹氏，富根村山内嘉市氏等からはそれぞれ非常な御援助をうけたので，

こゝにしるして感謝の意を表したい．なお今村學郎博士が關心をもつて議論してくださつたことを感謝する．（本研究の經費は文部省科學研究費による．）

---

25. *Vermessung eines Teiles von Nivellierroute am Fluss* YONESIRO. (*Zweite Mitteilung.*)

Von
Setumi MIYAMURA, Institut für Erdbebenforschung,
und
Atusi OKADA, Geophysikalisches Institut.

Zweite Vermessung unseres Plans[2] wurde erst im Juli, 1949 ausgeführt. Die Nivellmentergebnisse sind im Text mit Tabellen I～III und Fig. 3. zusammengestellt. Aller Wahrscheinlichkeit nach, kann Dr. OTUKA-sche "tätige Faltung"[1] wenigstens in dieser Gegend noch nicht bestätigt werden. Es ist merkwürdig, daß nach 1942 im Gegenteil der vorigen Frist eine allgemeine nach West aufsteigende Tendenz angefangen hat. Allgemeine Einsinken von E.R.I.-B.M.[4] sind vielleicht ihren initialen Depressionen zuzuschreiben und dürfen für jetzt vernachlässigt werden.

——— 所　　報 ———

○談話會記事

第 252 回談話會（昭和 24 年 1 月 18 日）

1.	表面波の研究（第 4 報）二層ある場合のラヴ波	佐藤泰夫
2.	東京大學構內深井の水位	佐藤泰夫
3.	噴火と氷河構成の關係	長岡半太郎
4.	古代の日本建築耐震講法の調査報告	齋田時太郎
5.	四國地方の地盤變動に就いて（概報）	河角廣

第 253 回談話會（昭和 24 年 2 月 15 日）

1.	四國地方地盤沈下の研究（序報）　德島縣下平野部の水準變化と地形	宮村攝三 吉川虎雄 貝塚爽平 町田貞 谷津榮壽
2.	宮城縣鳴子温泉の化學成分に就いて	野口喜三雄
3.	捕獲岩の研究（火山岩中の包裏物についての岩石學的研究）その1	森本良平
4.	日立鑛山における電氣探鑛（第 3 報）	岸上冬彦
5.	氷河に關する各論　水蒸氣の噴出機構	長岡半太郎
6.	不定常な流れの中の球の抵抗の一近似値について	谷本勉之助 （西村所員紹介）
7.	脈動による建物の動き	池上良平
8.	津波流速の判定に關する諸問題（其の 2）	那須信治

第 254 回談話會（昭和 24 年 3 月 29 日）

1.	德島平野の水準變化についての先月の話の補遺	宮村攝三
2.	ニュートン內挿式の曲面の場合への擴張について	谷本勉之助 （西村所員紹介）
3.	二變數函數の偏微分係數の算術式	同
4.	氷河各論　放射性によるマグマの温度上昇と其の液態狀況並に水蒸氣の噴出	長岡半太郎
5.	油壺に於ける地殼變動の研究（其の 2） 潮汐の負荷による土地の變形の觀測	笠原慶一 力武常次 山田重平 萩原尊禮
6.	油壺に於ける地殼變動の研究．右に對する理論的考察	力武常次 笠原慶一 山田重平 萩原尊禮

追　加

四國地方地盤變動第一回調査豫報

1.	概　　報	河角廣
2.	海岸測量（愛媛縣）	高橋龍太郎
3.	〃　（香川．德島縣）	那須信治

4. 海岸測量（高知縣）　岸上冬彦
5. 驗潮場に於ける地盤變動調査　表俊一郎
6. 〃　越川善明
7. 四國水準點變化と地質との關係（豫報）　森本良平
8. 松山市附近における土地伸縮傾斜觀測計畫　萩原尊禮・力武常次

第 255 回談話會（昭和 24 年 4 月 19 日）

1. 二重數値積分について　谷本勉之助（西村所員紹介）
2. 砂利を傳わる彈性波の模型的考察（2）　高橋健人（佐藤所員紹介）
3. 建築土木材料の內部摩擦に就いて（其の 1）　下鶴大輔
4. 土地の脈動の傳播性に關する研究　池上良平・岸上冬彦
5. 氷河を構成する水蒸氣及び黃土を噴出する孔道　長岡半太郎
   (1) 1783 年（天明 3）氷島 Laki 山と淺間山との噴火狀況比較
   (2) 熔岩のみの孔道と水蒸氣及び黃土を噴出する孔道との區別
6. 建築物に於ける震動勢力の地下逸散の問題（續報）　金井清・吉澤靜代
7. 組立式鐵筋コンクリート實在建物の振動實驗結果（第 2, 3 報）　金井清・鈴木富三郎・田中貞二
8. 日本に於ける破壞的地震を受けた度數の分布　金井清・吉澤靜代
9. 都市震害の研究（1）東京の地盤と震度　河角廣・佐藤泰夫
   （2）橫濱の地盤と震害　表俊一郎
10. 餘震域について　坪井忠二
11. 地震域について　坪井忠二

第 256 回談話會（昭和 24 年 5 月 17 日）

1. 二變數函數の階差法について　谷本勉之助
2. 昭和 21 年の南海道大地震の餘震域について　村內必典（萩原所員紹介）
3. 地震探鑛より知られる地盤の狀態と震害との關係（名古屋市の例について）　表俊一郎・神田祐太郎
4. 氷河を構成する水蒸氣及び黃土とを噴出する孔道（前回の續）　長岡半太郎
   (1) 1783 年（天明 3）氷島 Laki 山と淺間山との噴火狀況比較
   (2) 熔岩のみの孔道と水蒸氣及び黃土を噴出する孔道との區別
5. 驗潮記錄より知らるゝ四國地方の地盤變動　河角廣・表俊一郎・越川善明
6. 土の物理的性質に關する實驗法（其 1）　那須信治

第 257 回談話會（昭和 24 年 6 月 21 日）

1. 回轉對稱系の應力函數の一般性の證明について　谷本勉之助（西村所員紹介）
2. 東京下町に於ける地盤の良否に就いて　北澤五郎（河角所員紹介）
3. 都市の震害（第 2 報）　河角廣
   (1) 東京下町の試錐硬度と震害
   (2) サンフランシスコの地質と震度
4. 氷河論の續き
   地質構造と氷河との直接關係　長岡半太郎
5. 組立式鐵筋コンクリート實在建物の振動實驗結果（第 4 報）　金井清・田中貞二・鈴木富三郎
6. 捕獲岩の研究（その 2）近畿二上山柘榴石黒雲安山岩中の珪質捕獲岩について　森本良平
7. 油壺に於ける地殻變動の研究（その 4）岩石の彈性率について　力武常次
8. 油壺に於ける地殻變動の研究（その 5）
   超不變鋼による土地伸縮計について　萩原尊禮・齋藤貞夫

第 258 回談話會（昭和 24 年 7 月 19 日）

1. 回轉對稱の彈性體系の各種の應力函數について　谷本勉之助
2. 愛媛縣高縄半島における精密水準測量成果　第 1 報　平能金太郎・相田勇
3. 愛媛縣下地盤沈下調査概報　第 2 報　高橋龍太郎・下鶴大輔・羽鳥德太郎
4. 四國地方地盤變動調査
   香川縣德島縣海岸第二次調査　那須信治
   高知縣地盤變動第二次調査　岸上冬彦・池上良平
5. 氷河各論
   黄土（Loess）と氷河との連係並にその地質的分布　長岡半太郎
   氷河の殘せる痕跡
6. 近い地震の P 波走時の異常について　越川善明
7. 木造學校建物（新規格）の振動實驗結果　金井清・鈴木富三郎・長田甲斐男
8. 非木造建築物の震害　金井清
9. 日本に於ける破壞的地震を受けた度數の分布　第 2 報　金井清・吉澤靜代
10. 本邦大地震の時間空間的分布について　河角廣

第 259 回談話會（昭和 24 年 9 月 20 日）

1. ブラウン管による彈性波速度測定裝置（其の 1）　山崎良雄
2. 福井地震の地震計計測結果（第 3 報告）　越川善明
3. 昭和 24 年 7 月 12 日安藝海の地震の通信調査　河角廣・佐藤泰夫
4. レーリー波を發生しない震源　佐藤泰夫

5. 我が國における（1930～1943）年間の顯著地震の統計的研究 — 岸上冬彥・小高美江子
6. 地震による建物破壞機構に關する一考察 — 金井清
7. 回轉對稱の彈性體系の各種の應力函數について — 谷本勉之助
8. 米代川にそう一部水準路線の測量（第2報） — 宮村攝三・岡田惇
9. 相模原水道貯水槽の漏水問題について — 野口喜三雄
10. 淺間火山地獄谷ガスの化學組成の變化と火山活動 — 野口喜三雄・西條八束・坂口豐
11. 氷河論
氷河地帶の豫備歪曲・噴火山と噴氣孔の對稱
ラツコリスの存在・熔岩對チルライトレス堆のアキシヤリチー
段丘と絕壁 — 長岡半太郎
12. 地電位差分布の異常について（其の 1） — 佐久間修三
13. 深さが直線的に變化する海に於ける津浪の傳播 — 力武常次
14. 灣内および灣外に於ける津浪の波形 — 力武常次
15. 地球内部の電氣的性質と溫度分布 — 力武常次

第 260 回談話會（昭和 24 年 10 月 18 日）

1. 曲面の表面積の算術評價について — 谷本勉之助
2. 東京大學構内深井戸の化學成分の垂直分布 — 野口喜三雄・西條八束
3. 隅田川赤羽水門に於けるキテイ颱風による河水組成の變化 — 野口喜三雄・上野精一
4. 燒山（新潟縣）の地質と最近の爆發 — 市村毅平・森本良造・津屋弘達
5. 氷河論の續き
黄土の噴出・黄土（レス）堆の軸性・段丘と絕壁
チエルモーセンと黄土 — 長岡半太郎
6. 地電流變化と地下の電氣的性質 其の 1 — 力武常次
7 福井地震斷層の運動について — 那須信治

第 261 回談話會（昭和 24 年 11 月 15 日）

1. 實在建物の耐震度檢定に關する問題 — 金井清
2. 實在鐵筋コンクリー建物の振動試驗結果 — 鈴木富三郎・長田甲斐男・金井清
3. 最上層の砂層と震害 — 北澤五郎
4. 有珠昭和新山の噴出ガス及び昇華物の分析 — 津屋弘達・白井俊明
5. 燒山噴出昇華物の分析 — 津屋弘達・市村毅・白井俊明
6. 14 世紀の擬似氷河
歐洲の寒冷・河川の凍結・裏海の增水・ロプ，ノルの
氾濫・支那の山崩れ — 長岡半太郎

7. 異方性彈性體內のレーリー波　佐藤泰夫
8. 長い周期の地震計の取扱いについて　岸上冬彦
9. 地域別に見た津浪の危險率（東南海地方）　高橋龍太郎・羽鳥德太郎

第262回談話會（昭和24年12月20日）

1. 二變數函數の變型ベッセル型內挿式について　谷本勉之助
2. 東京大學構內深井の水位　佐藤泰夫
3. 地殼の均衡について　坪井忠二
4. 脈動の傳播性の研究（第2報）　池上良平・岸上冬彦
5. 有珠山の活動に伴つた地震の2,3の性質　水上武・高橋智子
6. 有珠山の活動に伴つた地形變動　水上武・佐久間修三・岡田惇厚
7. 燒山噴火の調査報告　佐久間修三・水上武・宮崎務
8. 第3紀の概況　長岡半太郎
   中世紀より第3紀の變遷
   第3紀の火山活動と山岳の生成
9. 金井式の擴張について　高橋龍太郎
10. 今治，尾道間內海諸島の地盤沈下　高橋龍太郎・下鶴大輔・羽鳥德太郎
11. 高縄半島精密水準測量成果　高橋龍太郎・平能金太郎・相田勇

BULLETIN
OF THE
EARTHQUAKE RESEARCH INSTITUTE
TOKYO UNIVERSITY

VOL. XXVII

1949

東京大學
地震研究所彙報

第 27 號

昭和 24 年

BULLETIN

OF THE

EARTHQUAKE RESEARCH INSTITUTE

TOKYO UNIVERSITY

VOL. XXVII

1949

東京大學

地震研究所彙報

第 27 號

昭和 24 年

Contents.

Vol. XXVII.

Parts 1—4. January—December, 1949.

Page

1. Y. SATÔ, Boundary Conditions in the Problem of Generation of Elastic waves. (in English) 1
2. T. TAKAHASHI and Y. SATÔ, On the Theory of Elastic Waves in Granular Substance. (I). (in English) 11
3. T. RIKITAKE, A Note on the Temperature-Distribution within the Earth. (in English) 17
4. Y. KOSHIKAWA, Magnetic Survey in the Area of Topographical Deformation of Volcano Usu. (in English) 21
5. N. NASU, Block Movement along the Seismic Fault (1). (Fukui Fault and Others) (in English) 27
6. T. HAGIWARA, T. RIKITAKE, K. KASAHARA and J. YAMADA, Observations of the Deformation of the Earth's Surface at Aburatsubo, Miura Peninsula. Part II. (in English) 35
7. T. HAGIWARA, T. RIKITAKE, K. KASAHARA and J. YAMADA, Observations of the Deformation of the Earth's Surface at Aburatsubo, Miura Peninsula. Part III. (in English) 39
8. R. MORIMOTO, A Petrological Note on the Granitic Rocks near the Cape Ashizuri, Shikoku Island, Japan (II). (in English) . 45
9. S. OMOTE, On the Coda Waves of Earthquake Motions. (Part 4.) (in Englisn) 49
10. S. OMOTE, Earthquake Damages in Yokohama City Due to the Great Kwanto Earthquake of September 1, 1923. (in English) 57
11. S. OMOTE, The Relation between the Earthquake Damages and the Structure of the Ground in Yokohama. (in English) . . 63
12. T. AKIMA, A Torsional Pendulum Low-pass Filter Applied to the Study of the Earthquake Waves. (Part 2) (in English) . . . 69
13. R. IKEGAMI and F. KISHINOUYE, A Study on the Propagation of Microseismic Waves. (in English) 75
14. R. IKEGAMI, On the Vibrations of a Building caused by Microseisms. (in English) 81
15. D. SHIMOZURU, Study on the Coefficient of Internal Friction of Materials used in Civil Engineerings and Architectural Structures. (1st Report) (in English) 85
16. K. KANAI, T. TANAKA and T. SUZUKI, Vibration Experiments with the Actual Buildings. (in English) 91

17. K. KANAI, Relation between the Earthquake Damage of Non-wooden Buildings and the Nature of the Ground. (in English) 97
18. N. NASU, Field Determination of the Elastic Property of Soil Layers (1). (in English). 101
19. T. ICHIMURA, R. MORIMOTO and H. TSUYA, A Brief Note on the Recent Explosive Activity of Volcano Yakeyama. (in English) 107
20. H. TSUYA, T. ICHIMURA and T. SHIRAI, Hydrated Aluminium-Sulphate Minerals from New Fumaroles on Volcano Yakeyama, Niigata Prefecture. (in English) 115
21. S. SAKUMA and T. MINAKAMI, Minor Activity of Volcano Yakeyama in 1949. (in English) 117
22. T. MINAKAMI, Recent Activities of Volcano Usu (III). Earthquakes at the Stage of Paroxysmal Eruption. (in English) 123
23. T. MINAKAMI, Recent Activities of Volcano Usu (IV). Earthquakes Followed by the Birth and Development of Lava Dome. (in English) 129
24. H. TSUYA and T. SHIRAI, Gases and Deposits from Fumaroles on the New Dome "Showa-Shinzan", Volcano Usu, Hokkaido, Japan. (in English). 135
25. S. MIYAMURA and A. OKADA, Vermessung eines Teiles von Nivellierroute am Fluss Yonesiro. (Zweite Mitteilung.) (im Japanischen). 141

目　次

第 27 號

第1~4冊 昭和24年1~12月

論文及報告　　頁

1. 彈性波發生の問題における境界條件 (英文)……佐藤泰夫 1
2. 粒狀物體を傳はる彈性波の論理 (I) (英文)……高橋健人・佐藤泰夫 11
3. 地球内部の溫度分布について (英文)……力武常次 17
4. 有珠火山地變地域における地磁氣測量 (英文)……越川善明 21
5. 地震斷層の運動 (其一) (福井斷層及び其他) (英文)……那須信治 27
6. 油壺に於ける地殼變動の觀測　第二報 (英文)……萩原尊禮・力武常次・笠原慶一・山田重平 35
7. 油壺に於ける地殼變動の觀測　第三報 (英文)……萩原尊禮・力武常次・笠原慶一・山田重平 39
8. 四國足摺岬の花崗岩類 (II) (英文)……森本良平 45
9. 地震動の尾部について (其の 4) (英文)……表俊一郎 49
10. 關東大地震による横濱市内の震害分布 (英文)……表俊一郎 57
11. 横濱市内の震害分布と地盤との關係 (英文)……表俊一郎 63
12. 捩り振子を應用した低域濾波器による地震波の研究 (英文)……秋間哲夫 69
13. 土地の脈動の傳播に關する研究 (英文)……池上良平・岸上彦多 75
14. 脈動による建物の振動について (英文)……池上良平 81
15. 建築土木材料の内部摩擦係數の測定 (其の一) (英文)……下鶴大輔 85
16. 實在建物の振動實驗結果 (英文)……金井清・田中貞二・鈴木富三郎 91
17. 非木造建物の震害と地盤の性質との關係 (英文)……金井清 97
18. 土壤層の彈性的性質に關する野外測定 (其の一) (英文)……那須信治 101
19. 最近の燒山火山爆發の調査概報 (英文)……村本毅・市森遠平・津屋弘遠 107
20. 新潟縣燒山火山噴氣孔で採集された水酸化硫酸アルミニウム鑛物 (英文)……津屋弘毅・市白井俊明 115
21. 燒山火山の 1949 年の小活動 (英文)……佐間修三・水上武 117
22. 有珠火山の最近の活動 (III) 爆發的噴火の期間に發生した地震 (英文)……水上武 123
23. 有珠火山の最近の活動(IV) 熔岩丘の成長に伴つた地震(英文)……水上武 129
24. 北海道有珠昭和新山の噴氣孔ガス及び昇華物 (英文)……津屋弘遠・白井俊明 135
25. 米代川にそう一部水準路線の測量 (第二報) (邦文)……宮村攝・岡田惇 141

目　次

論文名索引

Index to Vol. XXVII.

Page

AKIMA, T., (12) A Torsional Pendulum Low-Pass Filter Applied to the Study of the Earthquake Waves. (Part 2) (in English) 69

HAGIWARA, T., RIKITAKE, T., KASAHARA, K. and YAMADA, J., (6) Observations of the Deformation of the Earth's Surface at Aburatsubo, Miura Peninsula. Part II. (in English). 35

HAGIWARA, T., RIKITAKE, T., KASAHARA, K. and YAMADA, J., (7) Observations of the Deformation of the Earth's Surface at Aburatsubo, Miura Peninsula. Part III. (in English) 39

ICHIMURA, T., MORIMOTO, R. and TSUYA, H., (19) A Brief Note on the Recent Explosive Activity of Volcano Yakeyama. (in English) . 107

ICHIMURA, T., TSUYA, H. and SHIRAI, T., (20) Hydrated Aluminium-Sulphate Minerals from New Fumaroles on Volcano Yakeyama, Niigata Prefecture. (in English) 115

IKEGAMI, R., (14) On the Vibrations of a Building caused by Microseisms (in English). 81

IKEGAMI, R. and KISHINOUYE, F., (13) A Study on the Propagation of Microseismic Waves. (in English). 75

KANAI, K., (17) Relation between the Earthquake Damage of Non-wooden Buildings and the Nature of the Ground. (in English). . 97

KANAI, K., TANAKA, T. and SUZUKI, T., (16) Vibration Experiments with the Actual Buildings. (in English) 91

KASAHARA, K., HAGIWARA. T., RIKITAKE, T. and YAMADA, J., (6) Observations of the Deformation of the Earth's Surface at Aburatsubo, Miura Peninsula. Part II. (in English) 35

KASAHARA, K., HAGIWARA, T., RIKITAKE, T. and YAMADA, J., (7) Observations of the Deformation of the Earth's Surface at Aburatsubo, Miura Peninsula. Part III. (in English) 39

KISHINOUYE, F. and IKEGAMI, R., (13) A Study on the Propagation of Microseismic Waves. (in English). 75

KOSHIKAWA, Y., (4) Magnetic Survey in the Area of Topographical Deformation of Volcano Usu. (in English). 21

MINAKAMI, T., (22) Recent Activities of Volcano Usu (III). Earthquakes at the Stage of Paroxysmal Eruption. (in English) . . . 123

MINAKAMI, T., (23) Recent Activities of Volcano Usu (IV). Earthquakes Followed by the Birth and Development of the Lava Dome. (in English) 129

MINAKAMI, T. and SAKUMA, S., (21) Minor Activity of Volcano Yakeyama in 1949. (in English). 117

MIYAMURA, S. und OKADA, A., (25) Vermessung eines Teils von

Nivellierroute am Fluss Yonesiro. (Zweite Mitteilung.) (im Japanischen) 141
MORIMOTO, R., (8) A Petrological Note on the Granitic Rocks near the Cape Ashizuri, Shikoku Island, Japan (II) (in English). 45
MORIMOTO, R., ICHIMURA, T. and TSUYA, H., (19) A Brief Note on the Recent Explosive Activity of Volcano Yakeyama. (in English). . 107
NASU, N., (5) Block Movement along the Seismic Fault (1). (Fukui Fault and Others) (in English). 27
NASU, N., (18) Field Determination of the Elastic Property of Soil Layers (1). (in English) 101
OKADA, A. and MIYAMURA, S., (25) Vermessung eines Teils von Nivellierroute am Fluss Yonesiro. (Zweite Mitteilung.) (im Japanischen) 141
OMOTE, S., (9) On the Coda Waves of Earthquake Motions. (Part 4.) (in English) 49
OMOTE, S., (10) Earthquake Damages in Yokohama City due to the Great Kwanto Earthquake of September 1, 1923. (in English). . 57
OMOTE, S., (11) The Relation between the Earthquake Damages and the Structure of the Ground in Yokohama. (in English) 63
RIKITAKE, T., (3) A Note on the Temperature-Distribution within the Earth. (in English). 17
RIKITAKE, T., HAGIWARA, T., KASAHARA, K. and YAMADA, J., (6) Observations of the Deformation of the Earth's Surface at Aburatsubo, Miura Peninsula. Part II. (in English) 35
RIKITAKE, T., HAGIWARA, T., KASAHARA, K. and YAMADA, J., (7) Observations of the Deformation of the Earth's Surface at Aburatsubo, Miura Peninsula. Part III. (in English) 39
SAKUMA, S. and MINAKAMI, T., (21) Minor Activity of Volcano Yakeyama in 1949. (in English). 117
SATÔ, Y., (1) Boundary Conditions in the Problem of Generation of Elastic Waves. (in English) 1
SATÔ, Y. and TAKAHASHI, T., (2) On the Theory of Elastic Waves in Granular Substance. I. (in English) 11
SHIMOZURU, D., (15) Study on the Coefficient of Internal Friction of Materials used in Civil Engineerings and Architectural Structures. (1st Report) (in English) 85
SHIRAI, T., TSUYA, H. and ICHIMURA, T., (20) Hydrated Aluminium-Sulphate Minerals from New Fumaroles on Volcano Yakeyama, Niigata Prefecture. (in English). 115
SHIRAI, T., and TSUYA, H., (24) Gases and Deposits from Fumaroles on the New Dome "Showa-Shinzan", Volcano Usu, Hokkaido, Japan. (in English) 135

SUZUKI, T., KANAI, K. and TANAKA, T., (16) Vibration Experiments with the Actual Buildings. (in English) 91
TAKAHASHI, T. and SATŌ, Y., (2) On the Theory of Elastic Waves in Granular Substance. I. (in English) 11
TANAKA, T., KANAI, K. and SUZUKI, T., (16) Vibration Experiments with the Actual Buildings. (in English) 91
TSUYA, H., ICHIMURA, T. and MORIMOTO, R., (19) A Brief Note on the Recent Explosive Activity of Volcano Yakeyama. (in English) . 107
TSUYA, H., ICHIMURA, T. and SHIRAI, T., (20) Hydrated Aluminium-Sulphate Minerals from New Fumaroles on Volcano Yakeyama, Niigata Prefecture. (in English). 115
TSUYA, H. and SHIRAI, T., (24) Gases and Deposits from Fumaroles on the New Dome "Showa-Shinzan", Volcano Usu, Hokkaido, Japan. (in English) 135
YAMADA, J., HAGIWARA, T., RIKITAKE, T. and KASAHARA, K., (6) Observations of the Deformation of the Earth's Surface at Aburatsubo, Miura Peninsula. Part II. (in English) 35
YAMADA, J., HAGIWARA, T., RIKITAKE, T. and KASAHARA, K., (7) Observations of the Deformation of the Earth's Surface at Aburatsubo, Miura Peninsula. Part III. (in English) 39

第 27 號 索 引

頁

秋間　哲夫　(12) 捩り振子を應用した低域濾波器による地震波の研究（英文）…… 69
萩原尊禮・力武常次・笠原慶一・山田重平　(6) 油壺に於ける地殻變動の觀測　第二報（英文）…… 35
萩原尊禮・力武常次・笠原慶一・山田重平　(7) 油壺に於ける地殻變動の觀測　第三報（英文）…… 39
市村　毅・森本良平・津屋弘達　(19) 最近の燒山火山爆發の調査概報（英文）……107
市村　毅・津屋弘達・白井俊明　(20) 新潟縣燒山火山噴氣孔で採集された水酸化硫酸アルミニユム鑛物（英文）……115
池上　良平　(14) 脈動による建物の振動について（英文）…… 81
池上良平・岸上冬彥　(13) 土地の脈動の傳播に關する研究（英文）…… 75
金井　清　(17) 非木造建物の震害と地盤の性質との關係（英文）…… 97
金井　清・田中貞二・鈴木富三郎　(16) 實在建物の振動實驗結果（英文）…… 91
笠原慶一・萩原尊禮・力武常次・山田重平　(6) 油壺に於ける地殻變動の觀測　第二報（英文）…… 35
笠原慶一・萩原尊禮・力武常次・山田重平　(7) 油壺に於ける地殻變動の觀測　第三報（英文）…… 39
岸上冬彥・池上良平　(13) 土地の脈動の傳播に關する研究（英文）…… 75
越川　善明　(4) 有珠火山地變地域における地磁氣測量（英文）…… 21
水上　武　(22) 有珠火山の最近の活動 (III) 爆發的噴火の期間に發生した地震（英文）……123
水上　武　(23) 有珠火山の最近の活動 (IV) 熔岩丘の成長に伴つた地震（英文）……129
水上　武・佐久間修三　(21) 燒山火山の 1949 年の小活動（英文）……117
宮村攝三・岡田　惇　(25) 米代川にそう一部水準路線の測量（第二報）（邦文）……141
森本　良平　(8) 四國足摺岬の花崗岩類 (II)（英文）…… 45
森本良平・市村　毅・津屋弘達　(19) 最近の燒山火山爆發の調査概報（英文）……107
那須　信治　(5) 地震斷層の運動（其一）（福井斷層及び其他）（英文）…… 27
那須　信治　(18) 土壤層の彈性的性質に關する野外測定（其の一）（英文）……101
岡田　惇・宮村攝三　(25) 米代川にそう一部水準路線の測量（第二報）（邦文）……141
表　俊一郎　(9) 地震動の尾部について（其の四）（英文）…… 49
表　俊一郎　(10) 關東大地震による横濱市内の震害分布（英文）…… 57
表　俊一郎　(11) 横濱市内の震害分布と地盤との關係（英文）…… 63
力武　常次　(3) 地球内部の溫度分布について（英文）…… 17
力武常次・萩原尊禮・笠原慶一・山田重平　(6) 油壺に於ける地殻變動の觀測　第二報（英文）…… 35
力武常次・萩原尊禮・笠原慶一・山田重平　(7) 油壺に於ける地殻變動の觀測　第三報（英文）…… 39
佐久間修三・水上　武　(21) 燒山火山の 1949 年の小活動（英文）……117

佐藤　泰夫　(1) 彈性波發生の問題における境界條件 (英文)…… 1
佐藤泰夫・高橋健人　(2) 粒狀物体を傳はる彈性波の理論 (I) (英文)…… 11
下鶴　大輔　(15) 建築土木材料の內部摩擦係數の測定 (其の一) (英文) …… 85
白井俊明・津屋弘達・市村　毅　(20) 新潟縣燒山火山噴氣孔で採集された水酸化硫酸アルミニユム鑛物 (英文) ……115
白井俊明・津屋弘達　(24) 北海道有珠昭和新山の噴氣孔ガス及び昇華物 (英文)……135
鈴木富三郎・金井　清・田中貞二　(16) 實在建物の振動實驗結果 (英文)…… 91
高橋健人・佐藤泰夫　(2) 粒狀物体を傳はる彈性波の理論 (I) (英文)…… 11
田中貞二・金井　清・鈴木富三郎　(16) 實在建物の振動實驗結果 (英文)…… 91
津屋弘達・市村　毅・森本良平　(19) 最近の燒山火山爆發の調査概報 (英文)……107
津屋弘達・市村　毅・白井俊明　(20) 新潟縣燒山火山噴氣孔で採集された水酸化硫酸アルミニユム鑛物 (英文) ……115
津屋弘達・白井俊明　(24) 北海道有珠昭和新山の噴氣孔ガス及び昇華物 (英文)……135
山田重平・萩原尊禮・力武常次・笠原慶一　(6) 油壺に於ける地殼變動の觀測　第二報 (英文) …… 35
山田重平・萩原尊禮・力武常次・笠原慶一　(7) 油壺に於ける地殼變動の觀測　第三報 (英文) …… 39

昭和25年5月25日印刷
昭和25年6月5日發行

編輯兼發行者　東京都文京區本富士町壹番地
東京大學地震研究所

印刷者　東京都中央區銀町弐丁目參番地
佐柳信一

印刷所　東京都新宿區市ヶ谷谷町二十一番地
中央製本印刷株式會社
市ヶ谷工場

賣捌所　岩波書店
東京都千代田區神田一ツ橋通町

丸善株式會社
東京都中央區日本橋通二丁目

Sold by

MARUZEN Co. Ltd.,

Chūō-ku, Nihonbasi, Tōkyō.

Price of this copy ; 650.00 Yen. (Postage exclusive.)

BULLETIN OF
THE EARTHQUAKE RESEARCH INSTITUTE
TOKYO UNIVERSITY

Vol. XXVII, Parts 1—4. Jan.—Dec., 1949.

Contents.

Papers and Reports. Page

1. Y. Satô, Boundary Conditions in the Problem of Generation of Elastic Waves. (in English). 1
2. T. Takahashi and Y. Satô, On the Theory of Elastic Waves in Granular Substance. (I). (in English) 11
3. T. Rikitake, A Note on the Temperature-Distribution within the Earth. (in English) . 17
4. Y. Koshikawa, Magnetic Survey in the Area of Topographical Deformation of Volcano Usu (in English) 21
5. N. Nasu, Block Movement along the Seismic Fault (1). (Fukui Fault and Others) (in English). 27
6. T. Hagiwara, T. Rikitake, K. Kasahara and J. Yamada, Observations of the Deformation of the Earth's Surface at Aburatsubo, Miura Peninsula. Part II. (in English). 35
7. T. Hagiwara, T. Rikitake, K. Kasahara and J. Yamada, Observations of the Deformation of the Earth's Surface at Aburatsubo, Miura Peninsula. Part III. (in English). 39
8. R. Morimoto, A Petrological Note on the Granitic Rocks near the Cape Ashizuri, Shikoku Island, Japan (II). (in English). 45
9. S. Omote, On the Coda Waves of Earthquake Motions. (Part 4.) (in English). . . 49
10. S. Omote, Earthquake Damages in Yokohama City Due to the Great Kwanto Earthquake of September 1, 1923. (in Enlish) 57
11. S. Omote. The Relation between the Earthquake Damages and the Structure of the Ground in Yokohama. (in English) 63
12. T. Akima, A Torsional Pendulum Low-pass Filter Applied to the Study of the Earthquake Waves. (Part 2) (in English) 69
13. R. Ikegami and F. Kishinouye, A Study on the Propagation of Microseismic Waves. (in English). 75
14. R. Ikegami, On the Vibrations of a Building caused by Microseisms. (in English) . 81
15. D. Shimozuru, Study on the Coefficient of Internal Friction of Materials used in Civil Engineerings and Architectural Structures. (1st Report) (in English) . . . 85
16. K. Kanai, T. Tanaka and T. Suzuki, Vibration Experiments with the Actual Buildings. (in English) 91
17. K. Kanai, Relation between the Earthquake Damage of Non-wooden Buildings and the Nature of the Ground. (in English). 97
18. N. Nasu, Field Determination of the Elastic Property of Soil Layers (1). (in English) . 101
19. T. Ichimura, R. Morimoto and H. Tsuya, A Brief Note on the Recent Explosive Activity of Volcano Yakeyama. (in English) 107
20. H. Tsuya, T. Ichimura and T. Shirai, Hydrated Aluminium-Sulphate Minerals from New Fumaroles on Volcano Yakeyama, Niigata Prefecture. (in English) 115
21. S. Sakuma and T. Minakami, Minor Activity of Volcano Yake-yama in 1949. (in English) 117
22. T. Minakami, Recent Activities of Volcano Usu (III). Earthquakes at the Stage of Paroxysmal Eruption. (in English). 123
23. T. Minakami, Recent Activities of Volcano Usu (IV). Earthquakes Followed by the Birth and Development of Lava Dome. (in English). 129
24. H. Tsuya and T. Shirai, Gases and Deposits from Fumaroles on the New Dome "Showa-Shinzan", Volcano Usu, Hokkaido, Japan. (in English) 135
25. S. Miyamura and A. Okada, Vermessung eines Teiles von Nivellierroute am Fluss Yonesiro. (Zweite Mitteilung.) (im Japanischen). 141

Institute Notes.